Characterizing The Role of The Chloride/Bicarbonate Exchanger AE1 in Modulating Tight Junction Properties in Renal Collecting Duct Cells

by

Rawad Lashhab

A thesis submitted in partial fulfillment of the requirements for the degree of

Doctor of Philosophy

Department of Physiology

University of Alberta

Abstract

The human kidneys maintain acid/base balance and electrolyte homeostasis. In the collecting ducts, acid secretion and bicarbonate reabsorption are facilitated by type-A intercalated cells (type-A IC). Type-A IC cells express the acid-secreting vacuolar H^+-ATPase pump at the apical membrane, and the kidney anion exchanger 1 (kAE1) at the basolateral membrane to reabsorb bicarbonate. Mutations in the gene encoding kAE1 protein lead to distal renal tubular acidosis (dRTA), a disease where patients suffer from hypokalemia, hyperchloremia, metabolic acidosis and a defective urine acidification among other symptoms. Type-A IC cells also express the tight junction (TJ) protein claudin-4 which facilitates paracellular Cl^- reabsorption, and With-no-lysine kinases 1 and 4 (WNK1 & WNK4), two kinases that regulate claudin-4 phosphorylation.

A membrane yeast two-hybrid assay performed by Dr. Reinhart Reithmeier (University of Toronto) revealed a physical interaction between kAE1 and claudin-4. We therefore hypothesized that this interaction contributes to acid/base balance and electrolyte homeostasis.

First, we confirmed the physical interaction and colocalization between the two proteins in mouse inner medullary collecting duct (IMCD) cells and colocalization in mouse kidney sections. Upon inducibly expressing kAE1 protein in IMCDcells, the transepithelial electrical resistance (TEER) of the monolayer significantly decreased and thepermeability to Na^+ and Cl^-increased. These effects were dependent on kAE1 activity. When endogenous claudin-4 was knocked down, kAE1 expression had no further effect on TEER and TJ properties, indicating that kAE1 modulates TJ properties via claudin-4 protein.

Next, we investigated the mechanism(s) by which kAE1 modulates claudin-4 function. Interestingly, kAE1 expression increased phoshorylation of claudin-4, WNK4 and SPAK (a

downstream effector of WNK4). This effect was abolished using kAE1 E681Q inactive mutant, indicating that kAE1 activity is crucial for triggering these phosphorylation events. WNK463, a pharmacological inhibitor of WNKs including WNK4 resulted in a similar decrease in TEER as that of kAE1 expression. However, the combination of WNK inhibition and kAE1 expression resulted in an additive decrease in TEER rather than abolishing kAE1 effect upon WNK inhibition. Interestingly, claudin-3 abundance was reduced upon kAE1 expression and both claudin-3 and -4 decreased upon kAE1 expression and WNK inhibition. Therefore, although our findings indicate that kAE1 expression induces phosphorylation of claudin-4, WNK4 and SPAK, a definitive conclusion on the role of WNK4 in kAE1's impact on TJ properties could not be drawn.

Finally, we assessed the effect of dRTA causing-mutants kAE1 S525F and R589H on TJ properties. Both mutants are targeted to the basolateral membrane and carry high mannose and complex oligosaccharide. However, they differ in their exchange activity rate. While kAE1 R589H mutant has a similar exchange rate as kAE1 WT, kAE1 S525F mutant is less active than kAE1 WT. Interestingly, assessing their effect on TEER, we found that functionally defective kAE1 S525F mutant had a lower impact on TEER, whereas fully active kAE1 R589H had a similar impact on TEER to kAE1 WT. These results indicated that kAE1 effect on TJ properties is proportional to its functional activity and is likely mediated by WNK4, SPAK and claudin-4 phosphorylation.

Preface

Unless otherwise stated, all findings and outcomes in this study are the original work of Rawad Lashhab.

Chapter 1

Sections (1.3.1.1, 1.3.1.1.2, 1.3.3, 1.6.1, & 1.6.2) of chapter 1 have been published as part of the following review:

Lashhab, R., Ullah, A. K. M. S. & Cordat, E. Renal Collecting Duct Physiology and Pathophysiology. *Biochem. Cell Biol.* **97**, 234–242 (2018).

Chapter 3

Lashhab, R. *et al.* The kidney anion exchanger 1 affects tight junction properties via claudin-4. *Sci. Rep.* **9**, 3099 (2019).

Rawad Lashhab participated in the design and performed the majority of the experiments, and contributed in manuscript preparation and editing. Alina Rumley helped in obtaining preliminary data of this project. Dr. Denis Arutyunov and Midhat Rizvi helped in generating and characterizing mIMCD3 kAE1 E681Q cells. Charlotte You initiated the project by generating the constructs used in this study. Dr. Henrik Dimke performed the immunohistochemistry assay on murine kidney sections (Figure 3.5 D). Drs. Nicolas Touret and Xing-Zhen Zhen Chen participated in experiment design and in performing immunofluorescence experiments. Drs. Richard Zimmermann and Martin Jung provided the nitrocellulose membrane for the peptide spot assay used in section 3.3. Dr. Todd Alexander participated in experiment design and editing of the manuscript. Dr. Emmanuelle Cordat supervised and coordinated the research, and prepared the manuscript.

Chapter 4

Lashhab, R. *et al.* kAE1 expression affects WNK4 and SPAK phosphorylation and affects tight junction properties via a claudin-4 phosphorylation dependent pathway. in preparation (2021).

Rawad Lashhab prepared the manuscript and performed all the experiments, except the immunoblots in Figure 4.9 A were performed by Jared Bouchard and Midhat Rizvi, the left and center panels of Figure 4.9 B were obtained by Dr. Ensaf Almomani, and the functional assay (Figure 4.9 C) was performed by Rawad Lashhab, Shahid Ullah and Daphne Fernandes. Dr. Todd Alexander participated in experiment design. Dr. Emmanuelle Cordat supervised and coordinated the research, and participated in the manuscript preparation and editing.

Acknowledgments

First and foremost, my thanks and praises are to Allah who provided me with the power, motivation and guidance to fulfil this achievement in my life.

My sincere thankfulness, heartfelt appreciation and countless gratitude go to whom who gave me the opportunity to work under her supervision. To whom who helped me develop myself as a scientist and tremendously expand my skills not only in science but all aspects of life. To whom who was supportive, encouraging, inspiring and compassionate throughout the years. To my supervisor, Dr. Emmanuelle Cordat, you've been a big help through this project and your invaluable contribution has kept it going. Thank you, BOSS.

I would like to express my deepest indebtedness and boundless gratefulness to my supervisory committee members Drs. Eytan Wine and Todd Alexander for their intellectual input that helped develop my project. A special thanks to Dr. Todd Alexander for all the help and support during my program, your continuous help has been indispensable.

I would like to thank my friends in our lab during the course of my program, previous and current students and lab managers. Special thanks goes to Shahid Ullah and Denis Arutyunov, thank you for all kind of support you guys provided.

I would also like to thank all members of the Physiology department, students, administrative and academic staff for the like-home feeling environment you have established. Special thanks to Dr. Gregory Funk for his support during his time as an Associate Chair – Graduate Studies.

I would like to extend my gratitude to the funding agency that funded my program: the Libyan-North American Program – Canadian Bureau for International Education “CBIE”, and the International Research Training Group “IRTG”.

Finally, I dedicate my thesis to my first teachers in life, my parents. No words can describe my gratitude and appreciation toward you, may Allah grant you the highest place in Jannah. To my partner in life “Asmae”, thanks for being there in each step of this journey. You have as much as I do in this achievement, WE did it. To my stress-relieve recipe, my triple “R” 3 princesses and prince, Rodainah, Rahaf, Roaa & Mohammad. May Allah guide you to the right path and grant you success in your lives.

Table of Contents

List of Tables

List of Figures

List of Supplementary Figures

List of Abbreviations

aPKC	Atypical protein kinase C
Aqp2	Aquaporin 2
ASDN	Aldosterone sensitive distal nephron
ATP	Adenosine Tri-Phosphate
BK	Big conductance potassium channel
CA II	Carbonic anhydrase II
CCD	Cortical collecting duct
CD	Collecting duct
CNT	Connecting tubule
CO_2	Carbon dioxide
CPE	Clostridium perfringens enterotoxin
CRL	Cullin-ring E3 ligase
Cul3	Cullin 3
DCT	Distal convoluted tubule
dRTA	Distal renal tubular acidosis
eAE1	Erythrocyte anion exchanger 1
ECL	Extracellular loops
ENaC	Epithelial sodium channel
ERK 1/2	Extracellular signal-regulated protein kinases 1/2
GAPDH	Glyceraldehyde-3-phosphate dehydrogenase
HCO_3^-	Bicarbonate

H_2CO_3	Carbonic acid
HPO_4^{2-}	Hydrogen Phosphate
ICs	Intercalated cells
IMCD3	Inner medullary collecting duct cells
JAMs	Junctional Adhesion Molecules
JG	Juxtaglomerular
kAE1	Kidney anion exchanger 1
kDa	Kilodalton
KLHL3	Kelch-like family member 3
KS-WNK1	kidney-specific WNK1
L-WNK1	Long WNK1
LLC-PK1	Lilly Laboratories Cell-Porcine kidney 1
mAChRs	Muscarinic acetylcholine receptors
MDCK	Madin-Darby canine kidney
mIMCD3	Mouse inner medullary collecting duct
NBCe1	Electrogenic Na^+/HCO_3^- cotransporter 1
NCC	Na^+/Cl^- cotransporter
Ncoa7	Nuclear receptor coactivator 7
NHE3	Na^+/H^+ exchanger
NH_3	Ammonia
NH_4^+	Ammonium
OMCD	Outer medullary collecting duct cells
P_{Cl^-}	Absolute permeability to Cl^-

pCO_2	CO_2 partial pressure
PCs	Principal cells
PDZ	PSD-95/DLG-1/ZO-1 (post-synaptic density protein (PSD95), Drosophila disc large tumor suppressor (Dlg1), and zonula occludens-1 protein (zo-1))
PGE2	Prostaglandin E2
pH	Potential of hydrogen or power of hydrogen
PHA II	Pseudohypoaldosteronism type II
PKA	Protein kinase A
PLA	Proximity ligation assay
P_{Na+}	Absolute permeability to Na^+
pRTA	Proximal renal tubular acidosis
PT	Proximal tubule
RBCs	Red blood cells
ROMK	Renal outer medullary potassium channel
SDS-PAGE	Sodium dodecyl sulfate polyacrylamide gel electrophoresis
SLC	Solute carriers
SPAK/OSR1	Ste20-related proline alanine rich kinase/oxidative stress responsive kinase 1
TAMPs	Tight Junction-Associated Marvel domain-containing proteins
TEER	Trans-epithelial electrical resistance
TMDs	Trans-membrane domains
TJs	Tight junctions
type-A ICs	Type-A intercalated cells
type-B ICs	Type-B intercalated cells

V-H^+ ATPase	Vacuolar-type H^+ ATPase
WNK	With-no-lysine (K) kinase
ZO-1	Zonula occlud

1. Chapter 1: General introduction

1.1 Thesis overview

The objective of this thesis is to investigate the relationship between kAE1 (a basolateral membrane protein) and claudin-4 (a tight junction protein). In this thesis, we report a novel physical and functional interaction between a basolateral membrane protein and a tight junction protein. The first insight into their interaction was provided by Dr. Reinhart Reithmeier (University of Toronto) screening for kAE1 interactome by membrane yeast two-hybrid assay.

The main objective of this thesis is to investigate the role of this interaction in acid-base balance and electrolyte homeostasis. The first chapter starts with a general introduction on body homeostasis, followed by anatomical information on the urinary system. I then discuss hormonal regulations of electrolyte homeostasis and how the kidneys, along with other systems, maintain blood pH and acid base balance. The subsequent sections introduce tight junction components, WNK kinase family, SLC4A gene family, concluding with a discussion of associated diseases.

The material and methods used in this thesis are described in Chapter 2. The third Chapter presents evidence of physical interaction between the two proteins and how kAE1 function modulates tight junction properties via claudin-4. The fourth Chapter investigates the mechanism by which kAE1 modifies claudin-4 function. The fifth Chapter summarizes the findings from the previous two chapters, discusses the limitations of our study, proposes a model and concludes with future directions to further develop this project.

1.2 Introduction

The human body is composed of several multi-organs systems that coordinate with each other to perform the daily life tasks of a healthy human, all of which are aimed to maintain body homeostasis of pH, water and electrolytes[1]. The same concept is true of all members of the Animalia kingdom. The nervous and endocrine systems control and regulate the function of different organs for optimum body homeostasis. The arms of control and regulation extend to subcellular level by controlling gene expression of different proteins. On the other hand, the respiratory and digestive systems are responsible for providing oxygen and nutrients, respectively, needed for energy production and body thriving. They also help in body homeostasis by eliminating carbon dioxide and undigested food from the body. The circulatory system is involved in delivering and transferring nutrients, water, oxygen and hormones across the body, and transferring the waste generated by metabolic processes and excessive electrolytes to the urinary system for excretion. The urinary system in turn, especially the kidneys, plays a significant role in body homeostasis, not only by its excretion property, but also by its involvement in hormonal regulation, and the reabsorption of important electrolytes including Na^+, Cl^-, Ca^{2+}, HCO_3^- and Mg^{2+} and the secretion of H^+ and K^+. The synchronized regulation of reabsorption and secretion allows the kidneys to regulate blood pressure by controlling blood volume and electrolyte concentrations, and to sustain normal blood pH mainly through H^+ secretion and HCO_3^- reabsorption[1].

For this thesis, we will be focusing on the urinary system and its role in maintaining acid-base balance and electrolyte homeostasis.

1.3 Urinary system

The urinary system is composed of several organs; two kidneys connected to one ureter. The ureters function is to deliver urine made by kidneys to the bladder. The bladder functions as a storage place where the urine is collected before excretion through the urethra[2].

During fetus development, the urinary system undergoes three development stages[2]: the pronephros, the mesonephros and the metanephros. The pronephros resides at the far edge of the urogenital ridge but it neither has a direct rule in kidney formation nor in its function[3]. However, the pronephros is involved in the reproductive system development and considered as the Wolffian duct precursor. The second stage is the mesonephros, which is located in the middle of the urogenital ridge. Although it does not contribute to the kidney formation, the mesonephros may have some filtration properties during embryonic stages[3]. Nevertheless, the main role for the mesonephros in mammals is to form the adrenal gland and gonads[4]. The last stage reveals the beginning of the future kidney formation, the metanephros[5]. The metanephros forms from the interaction of a ureteric bud, at the start of the urogenital ridge, with special mesenchymal cells called “metanephric mesenchyme cells”. The metanephric mesenchyme cells condense on top of the ureteric bud and induce a subsequent branching that ultimately leads to the collecting ducts formation[5]. In return, the formed branches signal a reciprocal induction that leads to further metanephric mesenchyme cells condensation that form the renal vesicle. The renal vesicle undergoes several morphological changes that lead to the nephron formation, starting from the glomerulus and ending with the distal nephron[5].

1.3.1 The kidney

The kidneys are bean-shaped organs situated in the back of the abdominal cavity on both sides of the vertebral column[5]. They are located behind the abdomen peritoneum and surrounded

by a protective layer of fibrous connective tissue called the renal capsule. Anatomically, the human kidney is composed of two main parts called the cortex and the medulla. The cortex, forming the external part of the kidney, is located between the capsule and the medulla and composed mainly of nephrons which extend to the medulla. The medulla is the innermost part of the kidney underneath the cortex and is arranged into pyramid-shaped structures called renal pyramids. The bases of these pyramids are located at the corticomedullary junction and their tips, which are called papillae, are facing the renal pelvis. Each papilla has 10-25 openings that represent the end of the collecting ducts and are surrounded by cuplike structures called minor calyces. Each two to three minor calyces converge to form a major calyx that join each other to form the renal pelvis which drains the urine from the kidney and continues as the ureter. Together with the renal blood vessels and nerves, the ureter exits from the concave medial side of the kidney that is called the hilum[5].

The kidneys are the core organs of the urinary system in which all the functions, beside transporting the urine, occur[1]. The kidneys play an essential role in (i) ion, pH and water homeostasis, also contributing to hormonal regulation of these processes, (ii) excretion of acids generated by our metabolism and (iii) conservation of key molecules (amino acids, glucose, etc)[5]. The kidneys play different roles in maintaining whole-body homeostasis either directly or indirectly. Some of the direct functions include: regulating appropriate water concentration, maintaining acid-base balance and electrolyte homeostasis, and excreting metabolic waste and foreign chemicals. The indirect functions include the endocrine properties of the kidneys. The kidneys have the ability to produce hormones that indirectly play roles in whole-body homeostasis such as renin, calcitriol and erythropoietin[1].

1.3.1.1 The nephron

Our everyday life and diet generate wastes that our bodies need to excrete, in part through the action of the kidneys. With their complex functional unit called nephron, kidneys provide a sophisticated machinery to specifically filter, excrete, secrete and reabsorb molecules to/from the blood. Blood from the afferent arteriole that enters each renal corpuscle is filtered through fenestrated glomerular endothelial cells, the basement membrane and podocytes foot processes prior to entering the capsular space where it flows into the proximal tubule. Within 24 hours, an average of 180 liters of plasma is filtered by the kidneys[5].

Each kidney contains about 1 million nephrons. Each nephron is composed of a sequence of tubular segments that are defined by transitions in the epithelial cells underlying each segment (**Figure 1.1**)[6–8]. The various series of epithelial segments include the proximal (convoluted) tubule (PT), the loop of Henle (the thin descending limb, thin ascending limb, thick ascending limb), the distal convoluted tubule (DCT), the connecting tubule (CNT) and finally the collecting duct (CD). The type of cells, their tight junction properties as well as the nature and location of solute carriers (SLC) and channels expressed in these cells define the function of each segment. Interestingly, in some sections of the nephron, the transition from one segment to the next occurs in a gradual way, with for example overlapping expression of some key proteins such as the epithelial sodium channel (ENaC) and the sodium/chloride cotransporter (NCC) in the DCT/CD transition[9–11].

The composition of the filtrate in the early part of the proximal tubule is similar to that of the plasma except that it is devoid of blood cells and contains less proteins[12]. As the filtrate flows through the nephron, its composition is modified through reabsorption and secretion. The bulk reabsorption of water, ions and solutes occurs in the PT. Unlike the thin descending limb, the thin ascending limb, the thick ascending limb and the DCT all together contribute to sodium, chloride,

calcium and magnesium reabsorption. Lastly, the CNT and CD are the segments responsible for fine tuning urine composition and urine acidification. The CD tightly regulates the movement of water, sodium, chloride, potassium, bicarbonate and protons using a combination of both transcellular and paracellular pathways involving at least 3 different cell types: principal cells, PCs, type-A and type-B intercalated cells.

This thesis focuses on the structure and function of CD cells, specifically; intercalated cells.

1.3.1.1.1 Principal Cells

Principal cells compose the most prominent cell type of the CD epithelium. During the embryonic development, PCs appear as light cells with scarce organelles when visualized by electron microscopy[13]. They have mitochondria, smooth and rough endoplasmic reticulum, lysosomes, multivesicular bodies and autophagic vacuoles. Their mitochondria content is lower, smaller in size and scattered in the cytoplasm, compared with IC cells' mitochondria[14]. This specific morphological appearance differentiates these cells from other cell types in the CD epithelium. The major role of PCs is to regulate sodium, potassium and water homeostasis[15]. This regulation is accomplished by specific transporters located on their apical surface: the epithelial sodium channel ENaC, the water channel (aquaporin 2) (AQP2), and the renal outer medullary potassium channel (ROMK) (**Figure 1.2).** With intracellular depletion of sodium via the action of basolateral Na^+/K^+ ATPase, ENaC opening permits sodium reabsorption from the luminal fluid resulting in a depletion of positive charges in this compartment. As a result, ROMK action allows secretion of potassium into the luminal fluid. The completion of sodium reabsorption through these cells requires the presence of Na^+/K^+ ATPase pumps at the basolateral membrane. The Na^+/K^+ ATPase propels sodium accumulated inside the cells into the interstitial fluid in exchange for potassium in a $3Na^+/2K^+$ ratio-dependent manner.

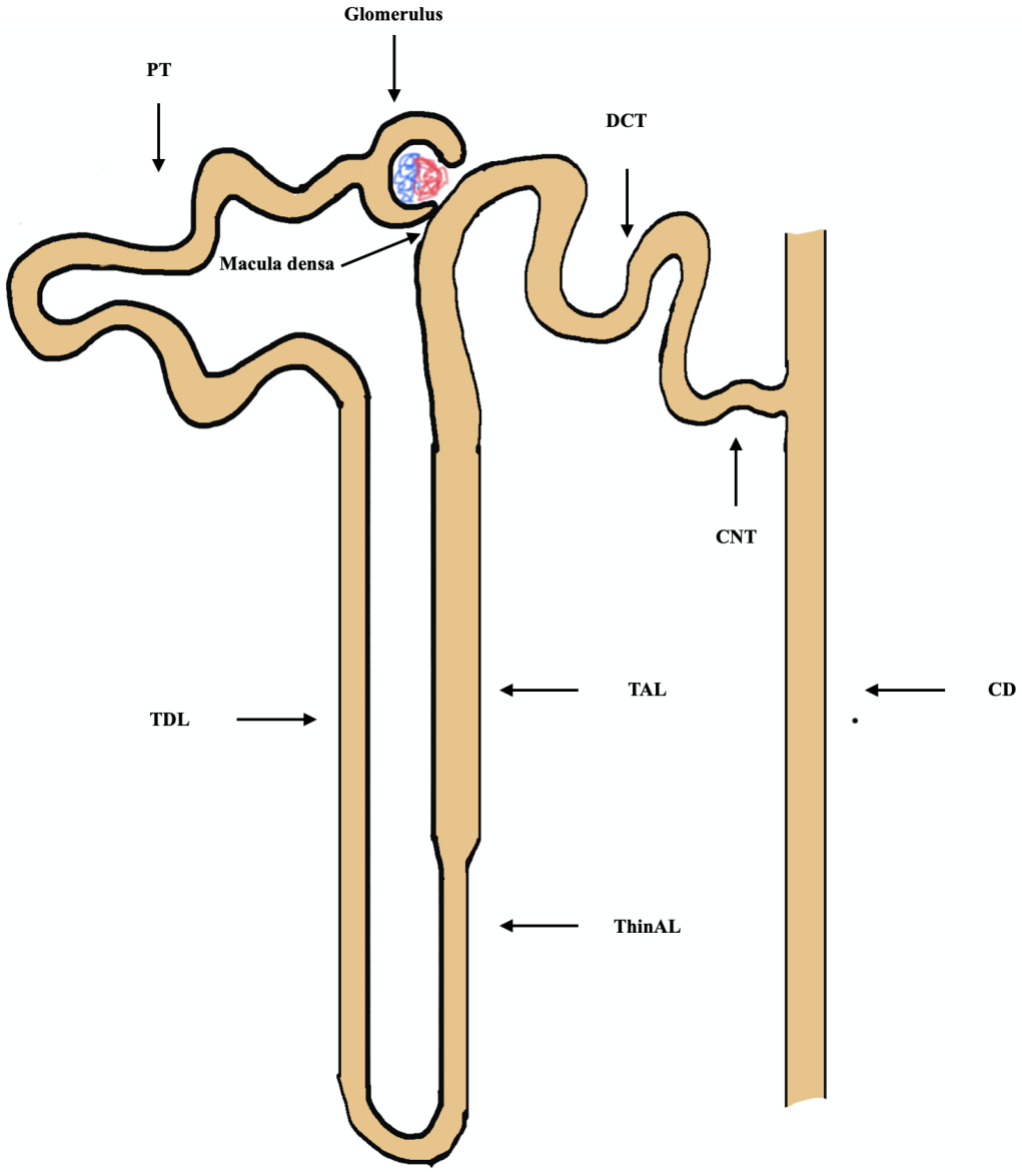

Figure 1.1: The nephron

Schematic model of the nephron anatomy. PT: proximal tubule, TDL thin descending limb, ThinAL: thin ascending limb, TAL: thick ascending limb, DCT: distal convoluted tubule, CNT: connecting tubule, CD: Collecting duct.

ENaC expression level is regulated by several factors including dietary salt content and the action of certain hormones such as aldosterone. More details about the PCs regulation are provided in the "Hormonal regulation" section.

1.3.1.1.2 Intercalated Cells

The other cell types found in the CD are IC or "dark" cells". In comparison with the PCs, IC have a high density of mitochondria, a dark cytoplasm, microprojections at the apical membrane, and lack a primary cilium[16]. All ICs are positive for carbonic anhydrase II (CA II) and V-H^+-ATPase proteins expression. IC can be subdivided into 3 subtypes: type-A, type-B, and non-A, non-B IC. The location of the V-H^+-ATPase in addition to the expression of other key proteins define the IC subtype (**Figure 1.2**)[17,18].

Type-A IC expresses V-H^+-ATPase at the apical membrane and the kidney anion exchanger 1 (kAE1) at the basolateral membrane. These cells significantly contribute to acid/base balance by secreting protons via the apical V-H^+-ATPase, and reclaiming bicarbonate via basolateral kAE1, both ions generated from hydrolysis of CO_2 and water by the CA II. On the other hand, type-B IC expresses basolateral V-H^+-ATPase and pendrin at the apical membrane. In addition to contributing to acid/base balance by secreting bicarbonate and reclaiming protons in case of alkalosis, type-B IC also contribute to electrolyte homeostasis as they are involved in Cl^- reabsorption[17,18].

Although IC can be morphologically, structurally and functionally distinguished from PCs, experimental evidence supports that both cell types originate from the same precursor[19]. Immortalized type-B IC plated at a high density are able to convert to type-A IC and secrete acid instead of alkali[20]. This ability to convert from one cell type to the other is due to the secretion of the extracellular matrix hensin protein by the type-B IC[21]. In support of these findings, a hensin

knock-out mouse model displayed a predominant abundance of type-B IC, the absence of type-A IC in the CD, and development of metabolic acidosis[21].

Lastly, non-A, non-B IC express both V-H^+-ATPase and pendrin at the apical membrane. The function of non-A, non-B IC is still unclear. However, the fact that both V-H^+-ATPase and pendrin are at the apical membrane suggests that these cells are not involved in acid/base balance but instead may be involved in electrolyte homeostasis. It is also thought that these cells may represent a transition state between the other two types depending on die t and plasma pH[18]. A very recent publication showed that the mouse CD contains a third type of cells in addition to PC and IC. These cells have features characteristic of PCs and ICs, as they were positive for both AQP2 and V-H+-ATPase, indicating that they may represent a previously unidentified transitional state between the two main cell types[22]. The distribution of the different IC types in the distal nephron varies among species. In mice, type-A ICs make 40%, 60% and 100% of the IC in CNT, CCD and OMCD/IMCD, respectively. On the other hand, type-B and non-A, non-B IC make 10% and 50%, 20% and 20%, and 0% of the IC in CNT, CCD and OMCD/IMCD, respectively[23,24].

Recent years of research have demonstrated a clear interplay between PC and IC. Indeed, in a similar finding to what was observed in RTA patients[25], mice knockout on the B1 subunit of the V-H^+-ATPase displayed a defective conservation of sodium and chloride due to altered function of ENaC and decreased abundance of pendrin[26]. Thus, a knockout in IC results in functional defects of not only IC but also PC. These animals displayed elevated levels of urinary ATP and prostaglandin E2 (PGE2) originating from type-B IC but acting on PCs in a paracrine process. Therefore, these findings highlight that the function of one cell type is linked to that of its neighbor cells in the CD.

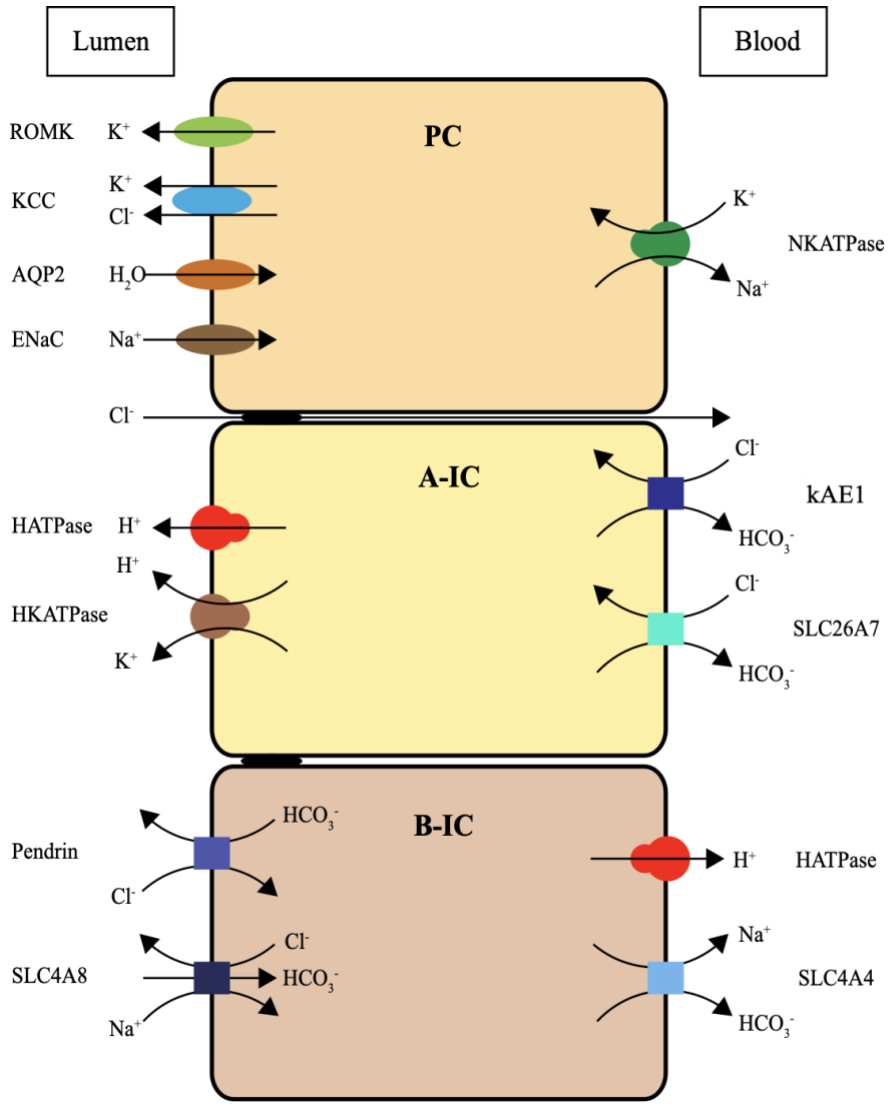

Figure 1.2: Schematic diagram of collecting duct cells.

Schematic model of collecting duct cells and their transporter proteins. PC: principal cells, express apically: ROMK, KCC AQP2 and ENaC; basolaterally: Na^+/K^+ ATPase. A-IC: type-A intercalated cells express apically: V-H^+ ATPase and H^+/K^+ ATPase; basolaterally: kAE1 and SLC26A7. B-IC: type-B intercalated cells express apically: pendrin and SLC4A8; basolaterally: V-H^+ ATPase and SLC4A4.

1.3.2 Hormonal regulation

As an endocrine organ, the kidney synthesizes, regulates and is regulated by several essential hormones in the body. The production of renal hormones is regulated by physiological feedbacks. Additionally, these sophisticated regulatory mechanisms are coordinated by extra-renal hormones that are produced in other organs and act on the kidney to precisely regulate its function. For example, while the kidney secretes hormones such as erythropoietin, calcitriol and renin, other hormones such as aldosterone and parathyroid hormone regulate the kidney's function.

Erythropoietin is secreted in the kidneys by interstitial cells in the peritubular capillaries[1,27]. It stimulates the production and maturation of red blood cells in the bone marrow. These hormone-secreting cells are very sensitive to oxygen levels in the kidney, which is the main factor that controls the production rate of erythropoietin hormone. Under normal conditions, erythropoietin is secreted in amount small enough to replace lost red blood cells and maintain adequate oxygen levels in the body. However, in pathological conditions where there is marked oxygen deficiency, such as severe anemia, heart failure and chronic obstructive pulmonary disease, the hypoxic environment created by these conditions stimulates the renal interstitial cells to produce large amount of erythropoietin. This results in marked increase in red blood cells production to enhance blood oxygen transport capacity[1,27].

Calcitriol (the active form of vitamin D3) is made in proximal tubular cells[1,28]. It is synthesized by converting 25-hydroxyvitamin D3 (calcitriol) to 1-alpha, 25-dihydroxyvitamin D3 (calcitriol) by 1a hydroxylase enzyme. Calcitriol increases calcium levels by enhancing its absorption from the gastrointestinal tract, its reabsorption from the renal tubular urine and its resorption from bones. The activity of 1a hydroxylase enzyme is mediated by parathyroid hormone and regulated by the levels of calcium and the calcitriol. Low calcium and/or calcitriol levels

stimulate the parathyroid hormone secretion, which triggers the renal production of calcitriol with subsequent rapid increase in serum calcium concentration. On the other hand, excessive calcium and/or calcitriol inhibits the release of parathyroid hormone, which subsequently reduces serum calcium levels. Calcium has numerous critical functions in the body and this coordinated system maintains calcium homeostasis[1,28].

A critical regulator of blood pressure and fluid homeostasis, renin is secreted by the juxtaglomerular cells in the kidney[1,29]. The production of renin in these cells is regulated by the renal sympathetic nerves activity, renal blood pressure and sodium concentration in the nephron lumen. Activation of the renal sympathetic nerves led by decreased plasma sodium concentration stimulates the juxtaglomerular (JG) cells to produce renin. Low blood pressure in the kidney is directly sensed by the JG cells and also results in increased renin secretion. The specialized macula densa cells, located at the end of the thick ascending limb, are highly sensitive to the sodium concentration. Low luminal sodium levels activate these cells and result in the release of regulatory factors that diffuse to, and activate the adjacent JG cells to produce renin. As part of the renin-angiotensin system, renin converts angiotensinogen, produced by the liver, to angiotensin-I, which is further converted to angiotensin-II by the angiotensin converting enzyme produced by the lungs. Angiotensin-II ultimately regulates blood pressure by inducing arteriolar constriction and stimulating aldosterone secretion[1,29].

Aldosterone is a mineralocorticoid hormone that is secreted by the adrenal cortex[1,29]. While the above-mentioned hormones are secreted and regulated by the kidney, aldosterone is one of several hormones that regulates the kidney function. As a downstream effector of the renin-angiotensin system cascade, aldosterone production is affected by factors that influence the renin-angiotensin system activation[1,29]. Aldosterone mainly acts on the aldosterone-sensitive distal

nephron, CNT and CD cells. It increases sodium and water reabsorption and potassium secretion by increasing plasma membrane expression of the ENaC[30], Aqp2[31] and ROMK[32]. It also increases phosphorylation of the tight junction protein claudin-4 leading to increased paracellular chloride flux[33]. Additionally, aldosterone increases the activity of the V-H^+-ATPase to increase proton and potassium secretion in response to metabolic acidosis[34].

1.3.3 Blood pH and Acid-base balance

Maintaining acid-base balance is crucial for normal body function[35]. Acid-base balance is defined as a physiological process by which the body stabilizes the extracellular hydrogen ions concentration, $[H^+]$. $[H^+]$ is inversely proportional to the pH value: the higher $[H^+]$ goes, the lower the pH gets[36]. Extracellular pH, including blood, is tightly maintained within 7.35 to 7.45, while intracellular pH varies from 6.3 to 7.4[35]. Failure to maintain blood pH within the normal range affects the optimal function of enzymes, causes protein denaturation and ultimately can lead to death.

Protons are generated through carbohydrates, lipids and proteins metabolism from our daily diet. However, The complete oxidation of these organic components results in energy production: ATP + CO_2+ H_2O[37]. However, incomplete oxidation, ATP hydrolysis and direct ingestion of acids result in either H^+ or HCO_3^- production[37]. Bicarbonate concentration $[HCO_3^-]$ is directly proportional to the pH value, as HCO_3^- binds to free H^+ causing a decrease in $[H^+]$ and an increase in pH[36]. The binding of HCO_3^- to H^+ is a reversible reaction that forms carbonic acid (H_2CO_3). H_2CO_3 in turn can reversibly dissociate to carbon dioxide (CO_2) and water (H_2O):

$$H^+ + HCO_3^- \leftrightarrows H_2CO_3 \leftrightarrows CO_2 + H_2O$$

This reaction is a part of the first line of defense against pH alterations and is called the buffer system. The buffer system can be divided into extracellular and intracellular buffers[36].

Extracellular buffers are mainly based on the above-mentioned equation. In case of acidosis (a decrease in blood pH), the equation moves toward the right lowering [H^+], while in case of alkalosis (an increase in blood pH), the equation shifts toward the left raising [H^+][36]. In contrast, intracellular buffer systems are mainly depending on the intrinsic buffer capacity of the cells, in which the H^+ ions bind to intracellular proteins on either an amine or carboxyl group, or both, to minimize the effect of cytoplasmic free H^+ inside the cells[36,37].

The respiratory system forms the second line of defense against pH changes. The lungs maximize CO_2 excretion in case of acidosis, and minimize it in case of alkalosis[37]. Elevation of the CO_2 partial pressure in the blood, pCO_2, is a result of buffering H^+ by HCO_3^-. Thus, regulation of CO_2 via the lungs is proportional to blood pH homeostasis[37]. The response of the respiratory system to pH alteration is rapid and takes minutes to hours in comparison to the urinary system, which take up to few days to counteract alteration in blood pH[36].

The urinary system is the third line of defense to responds to pH alteration. The kidneys elevate acid excretion as a means to correct acidosis. The urinary system works in cooperation with the respiratory system. In other words, malfunction in one of these systems is compensated by the other. A malfunction in the respiratory system manifests as a respiratory acidosis/alkalosis, while a defect in the urinary system translates into metabolic acidosis/alkalosis[35].

Proximal tubules of the nephron play a significant role in maintaining acid/base balance by reabsorbing almost 80-85% of filtered HCO_3^-[38]. HCO_3^- reabsorption from the lumen to the interstitial fluid undergoes an indirect pathway. The HCO_3^- in the lumen binds to H^+ that is secreted by the PT cells and forms H_2CO_3. H_2CO_3 in turn dissociates to $CO_2 + H_2O$. The CO_2 diffuses into the cell through the plasma membrane and gets reverted to the original state, $HCO_3^- + H^+$[39]. The H^+ gets recycled back to the lumen, either in exchange for Na^+ or direct secretion, to reinitiate

another cycle. In contrast, HCO_3^- is reabsorbed to the interstitial fluid coupled with Na^+[39]. The proteins and enzymes involved in this process include: carbonic anhydrase IV on the brush border of the PT cells which converts HCO_3^- into $CO_2 + H_2O$ in the presence of H^+, Na^+/H^+ exchanger (NHE3) which secretes H^+ in exchange of Na^+[40], V-H^+ ATPase which also contributes to H^+ secretion, CA II that converts CO_2 in the cytosol into HCO_3^+ and Na^+-dependent HCO_3^- cotransporter (NBCe1) which facilitates the final part of reabsorbing the HCO_3^- to the interstitial fluid[41]. The luminal pH at the end of PT drops from 7.4 to 6.7 as a result of HCO_3^- reabsorption and H^+ secretion. Disturbances in this mechanism result in impaired HCO_3^- reabsorption and a disease called proximal renal tubular acidosis (pRTA)[42].

In tubules of the distal nephron (late DCT, CNT and CD), the cells responsible for acid secretion are called type-A IC[43]. In these cells, CO_2 diffuses to the cell and is hydrolyzed via the cytosolic carbonic anhydrase II (CA II) producing H_2CO_3, which in turn dissociates to H^+ and HCO_3^-. The HCO_3^- is absorbed into the interstitial fluid in exchange for Cl^- via the HCO_3^-/Cl^- kidney anion exchanger 1 (kAE1) at the basolateral membrane[44]. On the other hand, H^+ ions are secreted to the lumen via the V- H^+ ATPase[45,46].

In the lumen, the secreted H^+ bind either to ammonia (NH_3) and generate ammonium (NH_4^+), or bind to hydrogen phosphate (HPO_4^{2-}) and generate titratable acid and both are excreted in the urine[42]. This process is highly regulated and a malfunction of any of the 3 main contributors (CA II, kAE1 & V-H^+ ATPase) results in a disease characterized by a low blood pH called distal renal tubular acidosis (dRTA)[42].

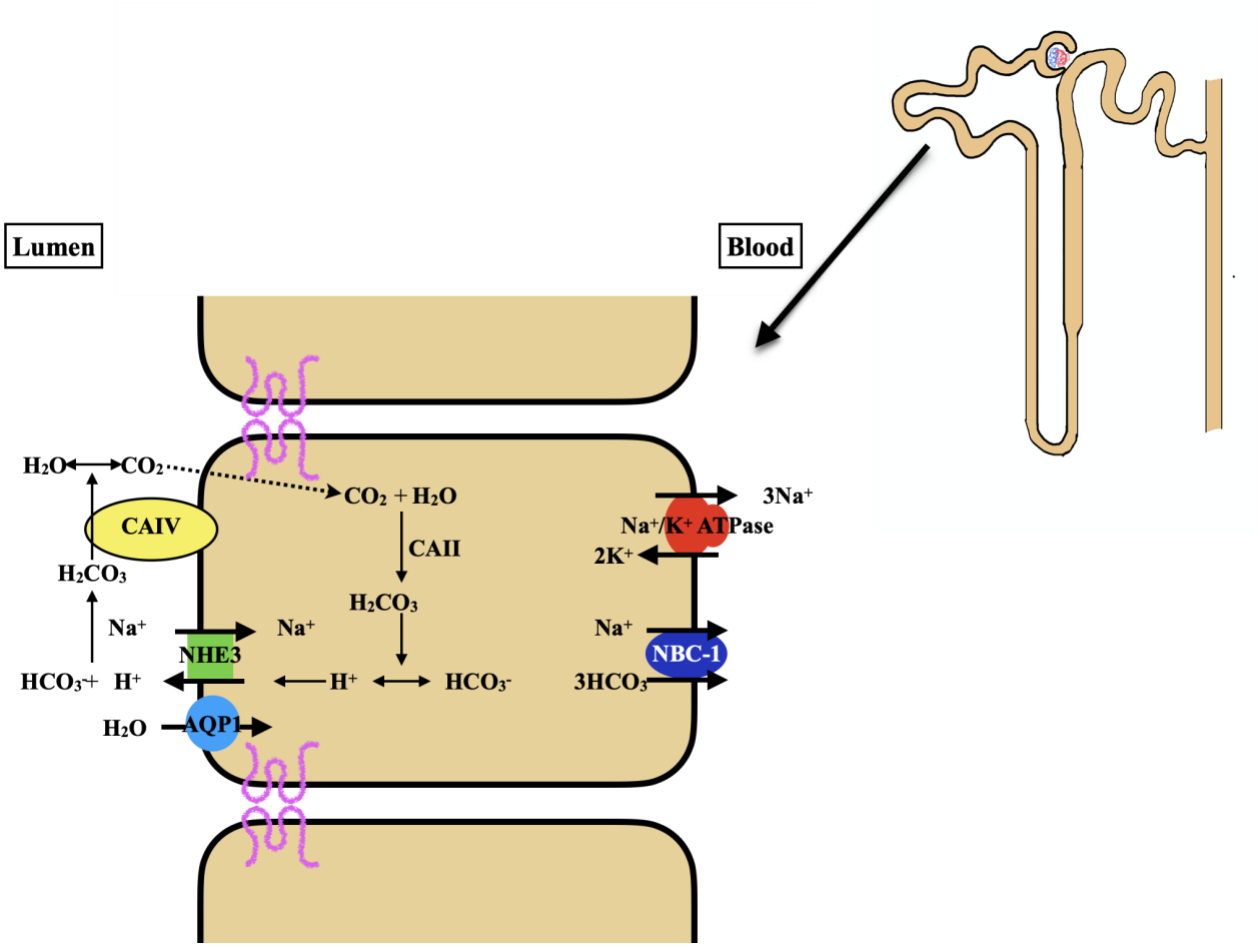

Figure 1.3: Schematic model of HCO_3^- reabsorption process in the PT cells.

In the proximal nephron, proximal tubule cells regulate HCO_3^- reabsorption. In the lumen, protons H^+ associate with HCO_3^- and produce H_2O an CO_2 by carbonic anhydrase IV. CO_2 diffuses into the cells through the plasma membrane where the intracellular carbonic anhydrase II (CAII) catalyzes the CO_2 hydration to produce bicarbonate (HCO_3^-) and a proton (H^+). The proton is secreted into the urine (upper) by the apical Na^+/H^+ exchanger (green). On the other hand, HCO_3^- is reabsorbed into the blood in a mechanism coupled with Na^+ by NBC-1 (blue). Na^+ ions leave the cells via the basolateral Na^+/K^+-ATPase (red). Pink lines between the cells represents cation selective claudin-2.

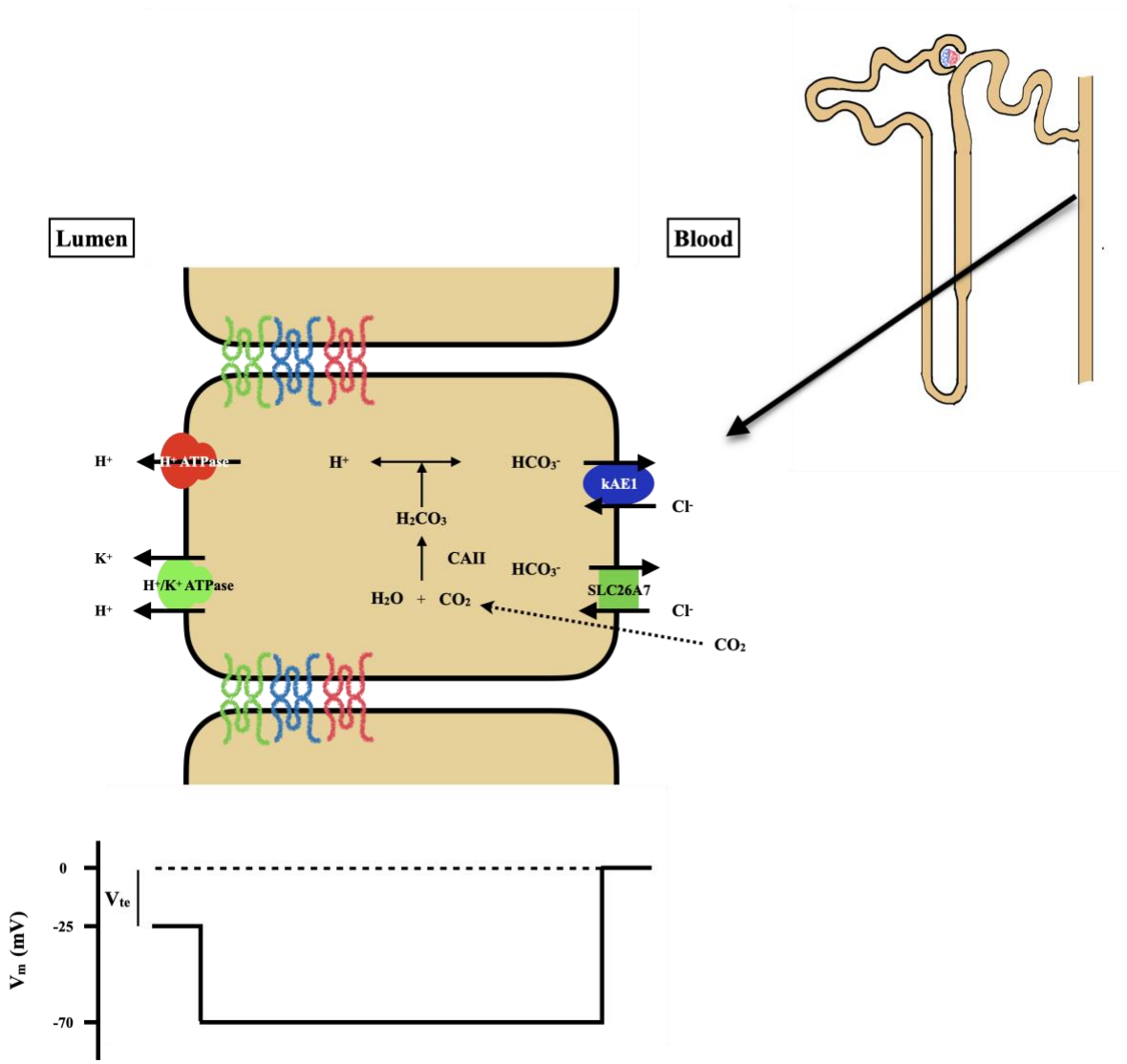

Figure 1.4: Schematic model of the acid secretion process in type-A IC cells

In the distal nephron, type-A IC cells regulate acid secretion. In these cells, CO_2 diffuses into the cells through the plasma membrane where the intracellular carbonic anhydrase II (CAII) catalyzes CO_2 hydration to produce bicarbonate (HCO_3^-) and a proton (H^+). The proton is secreted into urine by apical H^+ (red) and H^+/K^+ ATPases (green), to acidify the urine. On the other hand, HCO_3^- is exchanged into the blood with Cl^- through kAE1 (blue), and SLC26A7 (dark green). Colored and

curved lines between the cells represents anion-selective claudin-4 (green), anion-selective claudin-8 (blue) and non-selective barrier claudin-3 (red). Bottom: diagram representing potential difference across the medullary collecting duct epithelium, V_{te}: transepithelial voltage.

1.4 Tight junctions in Epithelial tissues

In humans, the epithelium forms a layer that cover the body's external surface and lines the internal cavities of different organs, such as the lungs, the gastrointestinal tract and the nephron. As a result, it forms a barrier that separates the internal body compartments from the outside environment. The integrity of the epithelium tissue barrier is maintained by a protein complex called "tight junctions" that connects and seals the space between epithelial cells[47]. In some cases, this barrier can be absolutely impermeable as in the bladder[48]. In other cases, the epithelium has the ability to secrete and absorb ions and organic molecules. These fluxes occur either through, or between the cells of the epithelium and are called transcellular and paracellular pathways, respectively.

Since the plasma membrane is not very permeable to ions and water, specific channels and transporters are required to accelerate their transepithelial movement. The level of expression and localization of these channels and transporters, whether on the apical or basolateral membrane, dictate the amount and direction of the transported molecules, and define the activity as absorption/reabsorption or secretion. Primary and secondary active transport is needed for this type of transport which gives the ability to transport molecules against their electrochemical gradient.

The other type of transport involves the movement of molecules paracellularly where the driving force is the electrochemical gradient of a given molecule. Unlike the transcellular pathway where solutes have to cross 2 barriers, the paracellular pathway only involves 1 barrier through which solutes pass, called tight junctions.

Tight Junctions are complexes of transmembrane proteins, scaffolding proteins and cytoskeleton proteins. For the purpose of this thesis I will focus only on the transmembrane proteins.

There are 3 types of transmembrane proteins in the tight junction protein complex: Junctional Adhesion Molecules (JAMs), Tight Junction-Associated Marvel domain-containing proteins (TAMPs) and Claudins.

1.4.1 Junctional Adhesion Molecules (JAMs)

JAMs belong to the immunoglobulin superfamily[49]. They consist of two extracellular immunoglobulin-like loops, one transmembrane domain and one intracellular domain that contains a PDZ (post synaptic density protein (PSD95), Drosophila disc large tumor suppressor (Dlg1), and zonula occludens-1 protein (ZO-1)) binding motif[50]. They localize to the tight junctions in epithelial and endothelial cells and are also expressed in leukocytes immune cells. In addition to their role in tight junction formation, JAMs are involved in transcytosis of immune cells through tight junctions[49,50].

1.4.2 Tight Junction-Associated Marvel domain-containing proteins (TAMPs)

TAMP*s* consist in four transmembrane-domain proteins and include 3 members: occludin, tricellulin and MarvelD3[51–53]. All 3 proteins share a similar topology of two extracellular loops, one intracellular loop and cytosolic N- and C-termini. However, the MarvelD3 proteins have longer N-terminal and shorter C-terminal domains compared to the other members of the TAMPs family[53]. In terms of localization, occludins are specific to bicellular junctions whereas tricellulins are exclusive to tricellular junctions[52]. Marvel3D proteins co-immunoprecipitate with both occludin and tricellulin[54]. Although TAMPs proteins are part of the tight junction proteins complexes, they are neither essential for the tight junctions formation nor for barrier function[55–57]. In *in vitro* studies, TAMPs proteins were not able to form tight junctions-like strands when transfected into non-tight junction-forming fibroblasts cells[56,57]. This observation was supported by an *in vivo* study where occludin-deficient mice had normal tight junctions appearance[55].

1.4.3 Claudins

Claudins are a family of proteins that are widely expressed in all vertebrates[58] with 26 members currently known in humans[58] and 56 members in the puffer fish[59]. They are made of about 207 to 305 amino acids and their molecular weight ranges between 20 to 28 kDa. Based on their sequence similarity, claudins are classified as classic claudins (1-10,14,15,17 and 19) and non-classic claudins (the rest of claudin family members)[60]. Functionally, claudins are classified based on their ability to increase or decrease the transepithelial electrical resistance when exogenously expressed in epithelial cells[61]. Unlike occludins, claudins have the ability to form TJ strands when transfected into fibroblasts[56]. Claudins have a similar topology with few exceptions. In general, claudins have cytosolic short N-terminal domain, four transmembrane domains, two extracellular loops (ECL1 & ECL2) and a long C-terminal domain (**Figure 1.4**)[58].

ECL1 is bigger in size than ECL2, as it is made of 50 amino acids. A crystal structure of claudin 15 revealed that ECL1 forms 4 out of 5 beta strands formed by the two extracellular loops[62]. It also contains a conserved motif across all kinds of claudins, GLWCC[63]. This motif works as a Hepatitis C virus receptor and is also involved in claudins *trans* interactions and trafficking to the plasma membrane[64]. ECL1 plays a role in paracellular ion selectivity through charged amino acids at specific locations, which create electrostatic forces attracting or repelling ions[65]. For example, lysine at the 65th position in claudin-4 makes it an anion selective pore and/or cation barrier. On the other hand, aspartate at 64th position in claudin 15 makes it a cation selective pore and/or anion barrier[65].

ECL2 is smaller in size and plays a role in trans-interactions with claudins from the opposite cell[66]. It also carries the binding site for Clostridium perfringens enterotoxin (CPE) in CPE-binding claudins. In fact, claudin-3 and claudin-4 have been previously identified as CPE receptors[67,68].

The length of the C-terminus varies among claudins but they all, except claudin-12, -22, -25 and -27, carry a PDZ binding domain that is involved in claudins interaction with scaffolding proteins ZO-1, -2 and -3[69]. The C-terminus plays a critical role for claudins trafficking and degradation, and is involved in several posttranslational modifications. Truncating the C-terminus of several claudins, including claudin-1, -5, -6 and -16, lead to endoplasmic reticulum retention indicating its role in claudins trafficking to the tight junctions[70–72]. Swapping the C-terminal of claudin-4 with that of claudin-2 enhanced claudin-4 membrane stability and prolonged its half-life to a comparable level as in claudin-2[73].

Claudins undergo several posttranslational modifications such as palmitoylation and phosphorylation[58,74,75]. The addition of fatty acids to cysteine residues through palmitoylation has been reported to occur in claudin-14[76]. Mutating these cysteine residues to alanine eliminated the ability of claudin-14 to reach the TJs[76]. Hence, claudins palmitoylation may play a crucial role in claudins targeting to the TJs.

The C-terminus of claudins harbors several phosphorylation sites that are not conserved but are unique in number and location to each claudin[75,77]. Claudins phosphorylation can be regulated by several kinases. The phosphorylation of different sites in different claudins can promote different regulatory effects[77]. The regulatory effects of claudin phosphorylation vary from promoting or inhibiting claudins assembly at the TJs, to modulating their permeability function. For instance, phosphorylation of claudin-16 by protein kinase A (PKA) at Ser217 induces claudin-16 localization to the TJs and prevents its rapid degradation[78]. In contrast, phosphorylation of claudin-3 at Thr192 by PKA results in disruption of the TJs caused by the removal of claudin-3 from the TJs[79]. On the other hand, WNK4 modulates the

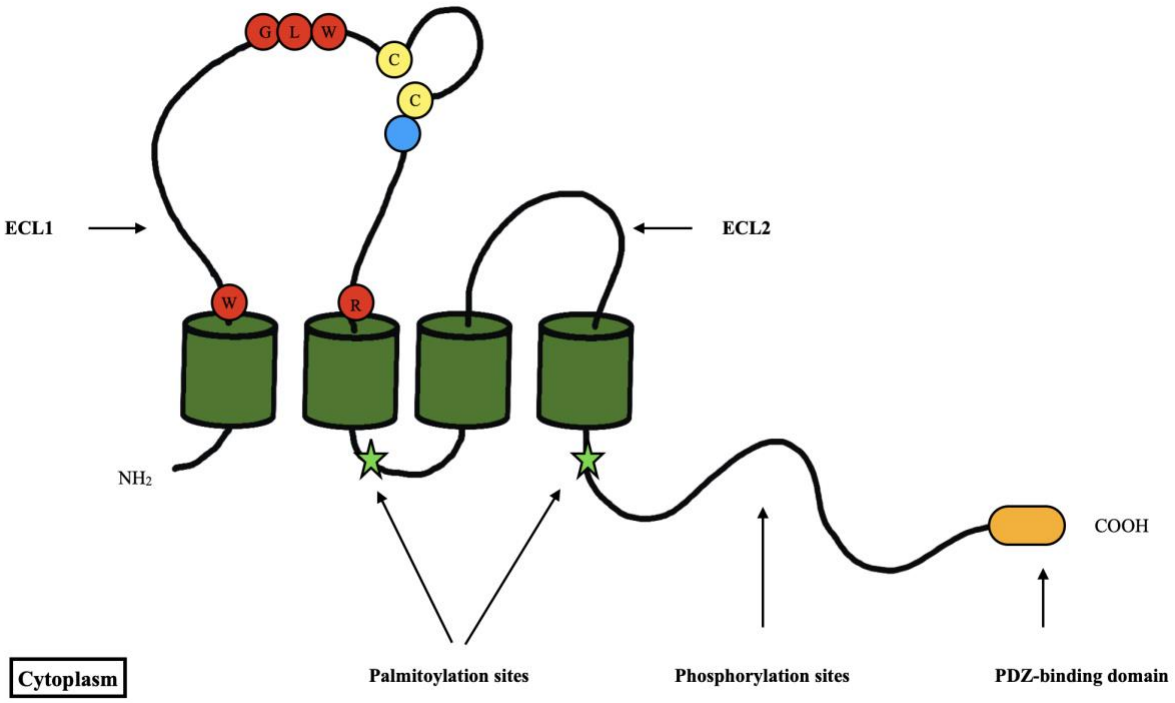

Figure 1.5: Model of claudin protein topology.

Schematic model of claudin's general topology. Claudins have a short N-terminus, 4 transmembrane domains (green barrels), 2 extracellular loops (ECL1 & 2) (red circles: signature amino acids, blue circle: ion binding site), and a cytosolic C-terminus that carries several phosphorylation sites and a PDZ-binding domain (orange) (except for claudin-12, -22, -25 and -27). Claudins can also be palmitoylated (green stars). Modified from[58].

permeability function of claudins 1-4 and -7 causing an increase in Cl^- permeability via their phosphorylation, specifically Ser206 in claudin-7[80,81].

For the purpose of this thesis, I will focus on claudin 4 and its role in the collecting ducts.

1.4.3.1 Claudin-4

Claudin-4 is expressed in various tissues, including the intestine, the lungs, the skin and the kidneys, more specifically in the aldosterone-sensitive distal nephron (ASDN). Claudin-4 is one of the a "classic" claudins and is either considered an anion selective pore or a cation barrier. On the ECL1, claudin-4 carries a positively charged lysine at the 65th position (Lys65) that is responsible for claudin-4 anion selectivity[65]. Substituting the positively charged Lys65 to the polar residue threonine (Lys65Thr) inverted claudin-4 ion selectivity into a cation selective pore when expressed in inner medullary collecting duct IMCD3 cells[82]. In other words, it became a cation selective pore rather than a barrier.

Physiologically, claudins have been classified as pores or barriers based on experiments predominantly relying either on heterologous overexpression or RNA silencing[83,84]. The interpretation of these experiments' outcome is therefore subjective to the cell lines investigated and the background expression of the endogenous claudins in these cells[58]. For example, overexpression of claudin-4 in the cation selective cell line MDCK II, resulted in increased transepithelial electrical resistance and decreased Na^+ permeability[83]. In comparison, claudin-4 overexpression in LLC-PK1 cells, an anion selective cell line, only caused an increase in the transepithelial electrical resistance without affecting the cell line ion selectivity[83].

Claudins are known to oligomerize[61]. However, claudin-4 can only form a homotypic interaction with another claudin-4 on the opposite cell but does not form homodimers in the same cell[85]. However, claudin-4 interacts with claudin-8 in a heteromeric interaction which is crucial for

claudin-4 localization to the TJs[82]. Knocking down claudin-8 in IMCD3 cells results in delocalization of claudin-4 away from the TJs and a decrease in chloride paracellular conductance[82]. Although claudin-4 may not play a role in claudin-8 localization to the TJs in IMCD3 cells, claudin-4 knockout mice showed a reduction of claudin-8 expression at the TJs of the ASDN[82,86].

The TJs formation of the renal nephrons in claudin-4 total-knockout mice was not affected, mostly because of a compensatory claudin-3 enrichment at the TJs[86]. However, these mice developed hyperplasia of the ureteral urothelium leading to urinary tract obstruction and hydronephrosis. In terms of ion permeability, these mice showed normal renal handling for most ions except for a slight but significant increase in Ca^{2+} and Cl^- fractional excretion. The mortality rate of claudin-4 knockout mice was significantly higher at the age of 20 months compared to their wild type littermates, (41% compared to 6% respectively), typically due to hydronephrosis [86].

At the ASDN, claudin-4 facilitates paracellular Cl^- reabsorption called "Cl^- paracellular shunt", while concomitantly promoting transcellular Na^+ reabsorption through ENaC in principal cells[87]. Collecting duct-specific claudin-4 knockout mice were generated using a Cre-loxP recombination strategy[87]. Since the principal cells are the predominant cells at the ASDN, the AQP2 promoter was used to induce claudin-4 knockout exclusively in this segment. The loss of Cl^- paracellular shunt leads to impaired Cl^- reabsorption and hypochloremia. Consequently, increased luminal Cl^- concentration inhibited ENaC activity and resulted in renal loss of Na^+ and water and hypotension. Lastly, decreased blood Cl^- concentration in these mice was compensated by an efflux of intracellular HCO_3^- leading to metabolic alkalosis[87].

Altogether, these findings emphasize the important role claudin-4 plays in the ASDN in acid/base balance and electrolyte homeostasis.

1.4.3.2 Regulation of claudin-4

As claudins are the main components of the TJ proteins complex that regulate the paracellular pathway, several physiological factors affect claudins' expression, function and degradation, thereby regulating the paracellular ionic flux. The level of regulation ranges from transcriptional regulation to post-translational modification[58]. For the purpose of this thesis I will focus on the regulation of claudin-4 by phosphorylation.

Claudin-4 has been reported to be phosphorylated by several kinases at different sites on its C-terminal tail[77]. Since claudin-4 is widely expressed throughout the body tissues, different cell lines have been used to study the effect of claudin-4 phosphorylation.

In MDCK cells, the receptor tyrosine kinase EphA2 interacts with claudin-4 and phosphorylates Tyr208 at the PDZ binding domain of the claudin-4 C-terminus[88]. This phosphorylation causes the dissociation and removal of claudin-4 from the TJ protein complex. A similar observation was detected in other cell lines, however, with different kinases. In ovarian cancer cells OVCA433 cells, claudin-4 colocalizes with the protein kinase C at the TJs[89]. Upon stimulation, claudin-4 is phosphorylated by protein kinase C at Thr189 and Ser194 that leads to delocalization of claudin-4 from the TJs and defective barrier function. In rat salivary epithelial SMG-C6 cells, activation of muscarinic acetylcholine receptors (mAChRs) also stimulates the phosphorylation of claudin 4 at Ser195 through the extracellular signal-regulated protein kinases 1 and 2, ERK 1/2[90]. Subsequently, claudin 4 is internalized, ubiquitinated and eventually degraded.

On the other hand, in keratinocyte HaCat cells, claudin-4 phosphorylation induces its targeting to the TJ and increases TEER[91]. In these cells, claudin-4 is phosphorylated by the atypical protein kinase C aPKC at Ser195. Mutating the serine 195 to alanine suppresses TJs formation induced by aPKC[91].

1.5 WNK kinases

With-no-lysine (K) kinase family consists of four members (1-4). They are distinguished from other kinase families by the presence of a cysteine instead of the conserved catalytic lysine required for ATP binding near the N-terminus in other protein kinases, such as lysine 72 in PKA[92].

WNK1 is a ubiquitous kinase. It is highly expressed in testis, heart, lungs and kidneys[93]. WNK1 kinase is a large protein that contains a kinase domain near its N-terminus[94] and an auto-inhibitory domain that has the ability to interact with the N-terminus and inhibits its kinase activity[94,95]. WNK1 has the ability to auto-phosphorylate itself on serine 382 to self-activate[95]. Interestingly, two isoforms of WNK1 have been detected: the long, ubiquitous isoform of WNK1, which is referred to as the "long WNK1" (L-WNK1) and in the distal nephron, the short but highly expressed kidney-specific WNK1 (KS-WNK1) isoform[93]. KS-WNK1 lacks the kinase domain at its N-terminus that is present in the L-WNK1, and therefore has no kinase activity[93]. However, KS-WNK1 plays a significant role in L-WNK1 regulation as it inhibits its activity and attenuates its downstream effect[96].

In addition to WNK1, WNK4 has been also detected at the distal nephron of the kidney, however, WNK1 and 4 have different subcellular expression patterns[97]: WNK1 is predominantly cytoplasmic, whereas WNK4 is localized to the TJs of DCT, and in cytoplasm and TJs of CCD.

Both proteins are sensitive to intracellular chloride concentration $[Cl^-]_i$ changes [98]. An increase in $[Cl^-]_i$ inhibits WNK1 and WNK4 activities, however, WNK4 is sensitive to lower $[Cl^-]_i$, changes than WNK1 [98]. Indeed, WNK4 kinase activity is inhibited within the physiological range of $[Cl^-]_i$, 0 to 40 mmol/l, whereas WNK1 kinase activity was suppressed within a higher range of $[Cl^-]_i$, 60 to 150 mmol/l[98]. Crystallographic studies showed that the mechanism by which chloride

ions suppress WNK1 kinase activity is through their binding to the catalytic site of WNK1, which prevents its autophosphorylation[99].

WNK1/4 kinases are highly involved in electrolyte homeostasis in the distal nephron. They regulate the expression of different transporters by inducing distinct regulatory mechanisms. For example, WNK1/4 promote ubiquitination of ENaC channels leading to their degradation[100]. Also, they inhibit ROMK channel function by inducing its clathrin-mediated endocytosis[101]. Another transporter regulated by WNK1/4 is the sodium-chloride cotransporter (NCC)[102], however, WNK1 and 4 have opposite effects on this transporter's regulation. In *Xenopus* oocytes, coexpression of WNK4 with NCC inhibited NCC activity. In contrast, WNK1 coexpression with NCC prevented the inhibitory effect of WNK4 on NCC's activity but had no direct effect on its activity[102].

1.6 WNK4 and Claudin-4

The colocalization of WNK4 and claudin-4 at the TJs of the distal nephron cells raises the question of their relationship. In MDCK II cells, WNK4 physically interacts and phosphorylates claudin-4[80]. Both claudin-4 phosphorylation and physical interaction with WNK4 were lost upon deletion of claudin-4 C-terminus. However, addition of the highly conserved PDZ-binding "YV" motif restored claudin-4's ability to bind to WNK4. Overexpression of WNK4 WT or of the gain-of-function PHA II-causing mutant WNK4 D564A caused different outcomes. They both increased claudin-4 phosphorylation, however, significant decrease in the transepithelial electrical resistance accompanied with an increase in Cl^- paracellular permeability were only observed in WNK4 D564A-expressing cell line. Nevertheless, the magnitude of the WNK4 D564A effect on claudin-4 phosphorylation was greater than the effect of WNK4 WT[80]. WNK4 Q562E and E559K, another two gain-of-function PHA II-causing mutants, had a similar effect on TJ properties when inducibly expressed in MDCK II cells[101]. On the other hand, WNK4 D318A kinase-dead mutant did not show

any effect on TJ properties, indicating that the effect seen on TJ properties caused by WNK4 WT and disease-causing mutants is due to the WNK4 kinase activity and its downstream effectors[101].

1.7 SLC4A gene family

In addition to claudin-4, this Thesis focuses on a second protein, the basolateral kidney anion exchanger 1, kAE1. This transporter belongs to the solute carrier (SLC) transporter proteins family "SLC4A". This family consists of 10 members classified based on their electrogenicity into 3 groups: electroneutral Na^+-independent Cl^-/HCO_3^- exchangers, electrogenic Na^+-dependent HCO_3^-cotransporter and electroneutral Na^+-dependent HCO_3^- cotransporter[103], (**Figure 1.6**).

For the purpose of this thesis I will focus on the electroneutral Na^+-independent Cl^-/HCO_3^- anion exchanger 1 (AE1).

1.7.1 The electroneutral Na^+ independent bicarbonate transporter AE1

The first anion exchanger to be cloned and sequenced was the product of the *SLC4A1* gene, AE1[104–106]. The main physiological function of AE1 is the electroneutral exchange of one Cl^- for one HCO_3^- ion; however, it also has the ability to transport Br^-, F^-, I^-, HPO_3^{2-}, and SO_4^{2-}, but with lower affinity in a respective order[104,107–109]. AE1 consists of two structural domains: a long cytoplasmic 43 kDa N terminal domain, and a 55 kDa membrane domain[110,111] (**Figure 1.7**). A crystal structure of AE1 was recently obtained[112] and is detailed below. The N terminal domain of AE1 provides a hub for multiple interaction sites with cytoskeletal proteins (e.g. ankyrin and protein 4.1 and 4.2)[113,114], and glycolytic enzymes (e.g. GAPDH)[115,116]. (see details in the next paragraph). The membrane domain, on the other hand, carries the transport activity of the protein[110]. AE1 is expressed as two isoforms, the erythrocyte AE1, eAE1, and the kidney AE1, kAE1. eAE1 is expressed in red blood cells (RBC), whereas kAE1 is expressed at the basolateral membrane of type-A IC in the kidneys[117,118].

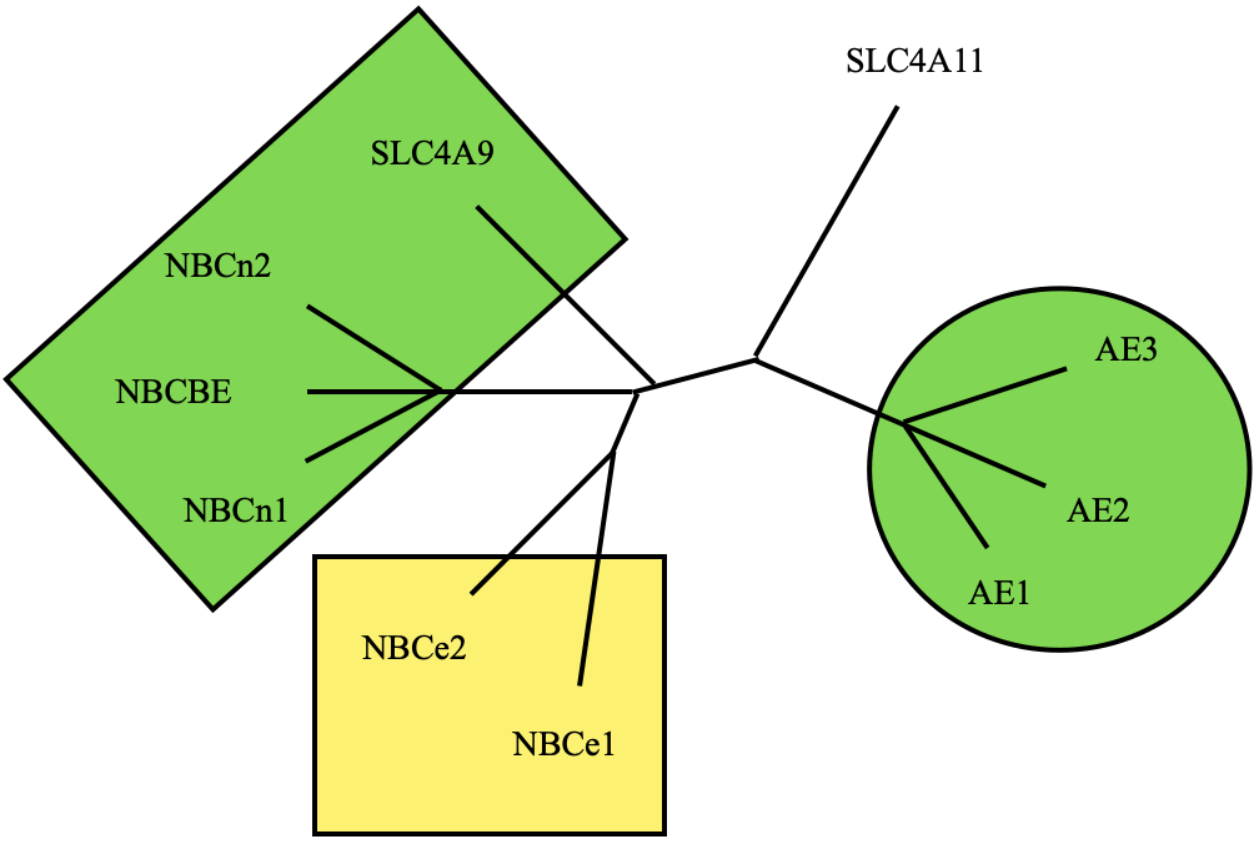

Figure 1.6: Phylogenetic dendrogram of SLC4 membrane transporters.

Clustal Omega software was used to align human SLC4 family members' amino acid sequences to calculate relative phylogenetic distances (https://www.ebi.ac.uk/tools/msa/clustalo/). Green circle includes electroneutral Na^+-independent HCO_3^- transporters, the green rectangle encompasses electroneutral Na^+-dependent HCO_3^- transporters, while the yellow rectangle includes electrogenic Na^+-dependent HCO_3^- transporters. Modified from[119].

1.7.1.1 eAE1

Erythrocyte AE1 accounts for 50% of the RBC plasma membrane proteins, representing approximately 1.2 x 10^6 copies per cell[105]. On SDS-PAGE gels of RBC ghosts lysate, eAE1 is detected as the third band from the top, from which it acquired its "band 3" name[105]. eAE1 is composed of 911 amino acids[105]. The N-terminal domain consists of the first 360 amino acids, whereas the membrane domain consists of the rest of the amino acids sequence which includes a short cytoplasmic C-terminal region composed of 883-911 amino acids[120].

The N-terminal of eAE1 plays multiple roles: (i) it interacts with cytoskeletal proteins such as ankyrin[113], protein 4.1[121] and protein 4.2[114], and glycolytic enzymes such as GAPDH[122]; and (ii) it is essential to maintain flexibility and deformability of RBCs as they transit through capillaries that are smaller than the RBC's diameter[123]. The C-terminal, on the other hand, physically interacts with CAII in RBCs[124]. This interaction increases Cl^-/HCO_3^- exchange rate of eAE1 by 40%[124]. Both eAE1 N- and C-termini interact with a variety of kinases as well that will not be detailed here[125].

As mentioned above, a crystal structure of the AE1 membrane domain (residues 381-887) was recently obtained and revealed that the protein has 14 trans-membrane domains (TMDs) that arrange into two subdomains: a gate domain (TMDs 5-7 & TMDs 12-14), and a core domain (TMDs 1-4 & TMDs 8-11)[112] (**Figure 1.7**). The gate domain provides an oligomerization interface, the core domain encloses the substrate binding and transport site. Arginine 730 in TMD 10 and glutamate 681 in TMD 8 of the core domain are both essential for AE1 Cl^-/HCO_3^- exchange[112].

In RBCs, CO_2 generated by the cellular metabolism diffuses into the RBC through the plasma membrane. CAII hydrolyses the CO_2 into a proton that contributes to the release of O_2 from hemoglobin, and a HCO_3^- that is exchanged with Cl^- into the blood by eAE1 where it contributes to acid/base balance.

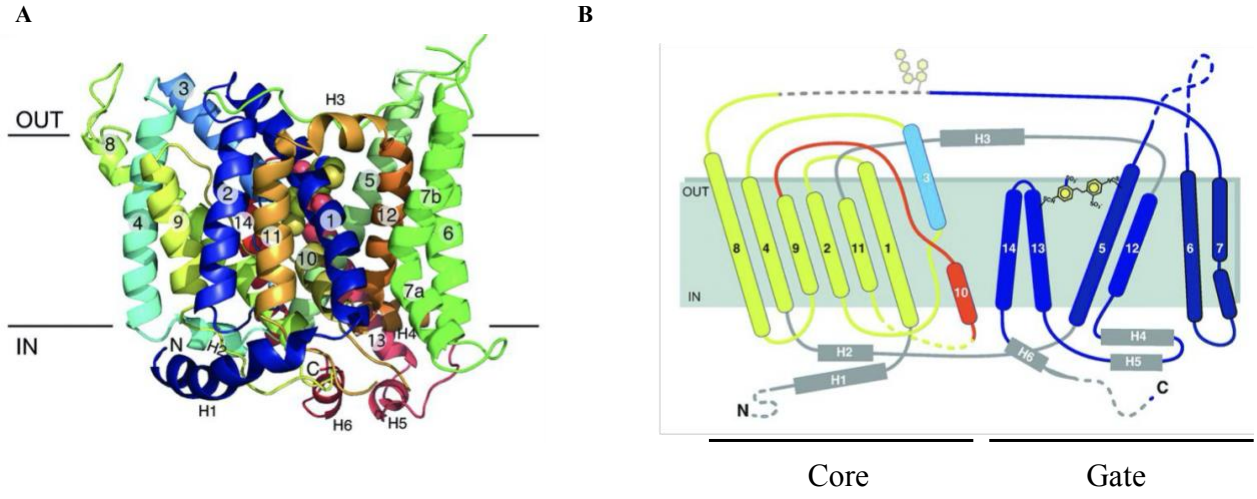

Figure 1.7: AE1 crystal structure

A, View of the structural details in the membrane plane of AE1. **B,** topological model of AE1 crystal structure. Figures used from[112] with permission.

This mechanism is reversed in the lungs. HCO_3^- is exchanged with Cl^- into the RBC where it is converted back to CO_2 by CAII. CO_2 in turn diffuses out of the RBC into the lung from which it is exhaled.

1.7.1.2 kAE1

The 846 amino acid kidney isoform of AE1 (kAE1) differs from the erythrocyte isoform by lacking the first 65 amino acids at the N-terminus of the transporter[118]. kAE1 expression in kidney cells is induced by a promoter sequence within the 3' intron of exon 20 of *SLC4A1* gene[126]. Otherwise, kAE1 is identical to eAE1 in terms of function and likely topological structure.

kAE1 is expressed at the basolateral membrane of type-A IC cells of the CD[124], and to a lower extent in podocyte cells[124]. In type-A IC cells, kAE1 synchronises with v-H^+- and H^+/K^+-ATPase, and CAII to maintain acid/base balance[127]. The acids produced by the cellular metabolism are transported into the blood as a conjugate acid in the form of CO_2, which diffuses into type-A ICs. Subsequently, CAII hydrolyses CO_2 to a proton and HCO_3^-. The proton is secreted into the urine through V-H^+- ATPase and H^+/K^+-ATPase pumps, resulting in urine acidification. HCO_3^-, on the other hand, is expelled into the blood through kAE1 in exchange with Cl^-. The acid secretion and HCO_3^- retrieving by type-A ICs is crucial for whole body pH homeostasis.

1.7.1.2.1 kAE1 interactome

1.7.1.2.1.1 Interactors of the amino-terminal cytosolic domain

The kAE1 cytoplasmic domain contains various protein binding motifs that are critical for its membrane localization and function. In glomerular podocytes, nephrin, which is an essential component in the slit diaphragm protein complex, interacts with kAE1 N-terminal domain and this interaction is mediated by an integrin-linked kinase (ILK)[128,129]. The N-terminus of kAE1 also

contains 3 specific motifs that are required for its interactions with Ankyrin G and its transport to the cell membrane[130].

1.7.1.2.1.2 Interactors of the carboxyl-terminal cytosolic domain

The C-terminus of kAE1 also has specific binding sites that interact with different proteins. Binding of kAE1 via its C-terminus to the CA II enzyme was found to be essential for maintaining the bicarbonate and proton balance[124]. Another protein called Peroxiredoxin 6 binds the C-terminus of kAE1 and regulates its expression, localization, and function in the kidney's intercalated cells[131,132]. Similarly, GAPDH binds to kAE1 C-terminus, but the role of this interaction is not clearly defined. It has been suggested that GAPDH could also regulate membrane trafficking and localization of kAE[133,134]. The membrane localization and abundance of kAE1 are also enhanced via its interaction with the B1 subunit of the Na^+/K^+-ATPase[135]. Adaptor proteins involved in kAE1 membrane trafficking such as AP-1 mu1A, AP-3 mu1 and AP-4 mu1 and clathrin bind to kAE1 C-terminus and regulate its membrane association[136–139]. Finally, PDLIM5 binds kAE1 C-terminus as well as ILK, which, as mentioned above, is a binding partner of kAE1 N-terminus[128,140]. This suggests that PDLIM5 forms a bridge connecting multiprotein complexes at the N- and C-termini of kAE1. These multiprotein complexes are essential to regulate the abundance and membrane localization of kAE1.

1.8 Diseases related to kAE1 & Claudin-4

1.8.1 Distal renal tubular acidosis

Type 1 or distal renal tubular acidosis (dRTA) results from a renal defect in acid secretion[141] and consequently in a loss of bicarbonate reabsorption in tubules of the distal nephron[142]. Mutations in the genes encoding either kAE1[143–145], the V-H^+-ATPase[146] or CA II[147] can result in dRTA. dRTA patients carrying dominantly or recessively-inherited mutations develop renal stones,

hypokalemia, hyperchloremia, nephrocalcinosis, metabolic acidosis and a defective urine acidification in addition to facing difficulties to thrive[148]. At this time, 23 point or frameshift mutations in *SLC4A1* gene encoding kAE1 protein are reported to cause dRTA, in a homozygous, heterozygous or compound heterozygous state[149–152]. Investigations in Madin-Darby canine kidney (MDCK) cells showed that dRTA-causing kAE1 mutants were either non-functional or mis-trafficked to the apical membrane, the Golgi or the endoplasmic reticulum[153–155]. Co-expression of dominant dRTA mutants with the WT kAE1 protein (thereby mimicking the situation found in patients with a dominant form of the disease) showed that the mutants affected the trafficking of the WT protein in these cells[155]. In contrast, co-expression of recessive mutants with kAE1 WT, as found in parents of the patients with recessive dRTA, showed that the WT protein rescued the mutant's trafficking. These findings provided a molecular mechanism for development of dRTA.

However, recent *in vivo* findings challenged our understanding of dRTA pathophysiological mechanisms. Indeed, when expressed in mouse inner medullary collecting duct (mIMCD3) or mouse cortical collecting duct M1 cells, the dominant mutant kAE1 R607H (corresponding to the human dominant kAE1 R589H dRTA mutation) showed a normal function and proper targeting of the protein to the basolateral membrane[156]. This mutant was previously reported to be retained in the endoplasmic reticulum in MDCK cells[154,155]. Moreover, in a kAE1 R607H knock-in mouse model that developed dRTA upon acid challenge, the protein was properly targeted to the basolateral membrane, although its expression level was lower compared with wild type mice[156]. In fact, these mice had a lower amount of V-H^+-ATPase and were unable to relocate this protein to the apical membrane upon acid challenge. In fact, the number of type-A IC in these mice was significantly lower in comparison with the WT mice (**Figure 1.8**).

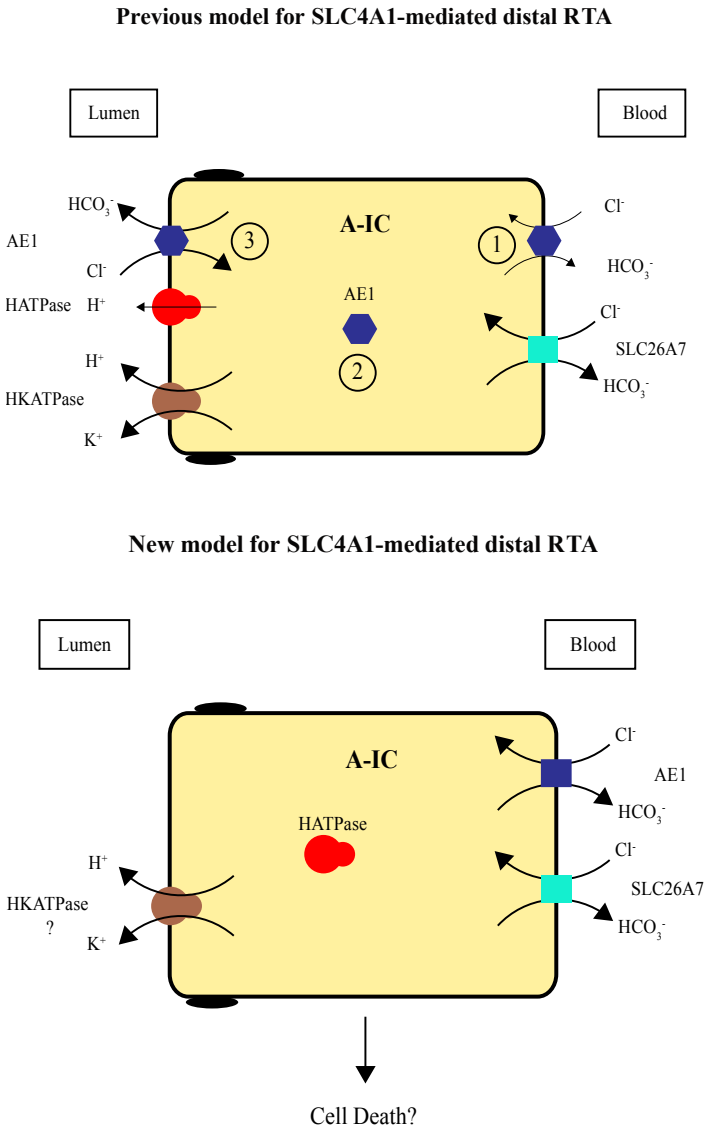

Figure 1.8: Schematic diagram illustrating the previous and the new model for SLC4A1-mediated dRTA.

Top, dRTA-causing SLC4A1 mutant proteins were described as either non-functional (1), intracellularly retained (2), or apically mistrafficked (3) based on MDCK cell studies. Bottom, recent *in vivo* findings showed that a dominant dRTA-causing mutation did not cause mistrafficking of the protein but rather a lack of relocation of the V-H+-ATPase to the apical membrane upon plasma acidification, possibly resulting in a dramatic loss of type-A ICs in the CD.

A recent study investigating the interactome of the V-H^+-ATPase identified the nuclear receptor coactivator 7 as an interactor[157]. A targeted deletion of this protein in mice resulted in incomplete dRTA[158]. These recent findings may be the first step towards deciphering the functional link between basolateral kAE1 and apical targeting of the V-H^+-ATPase. Therefore, our understanding of the pathophysiology associated with dRTA remains obscure and further studies will be necessary to fully understand the molecular mechanisms of this complex disease.

The CA II enzyme is found in the cytosol of the PT cells, loop of Henle and in the ICs of the CD[159]. CA II converts CO_2 and water into bicarbonate and protons in PT cells and IC. Accordingly, the lack or dysfunction of CA II results in an impaired bicarbonate reabsorption and acid secretion[160], defined as Type 3 renal tubular acidosis. Patients with type 3 RTA have acidemia, alkaline urine, osteopetrosis, cerebral calcification and mental retardation. Beside the kidney, the tissues and organs affected in type 3 RTA correlate with tissue-expression of the CA II. A recent study of CA II deficient mice showed that CA II also plays a significant role in urine concentration[161]. In addition to type 3 RTA, these mice had polyuria and polydipsia without altered sodium or calcium reabsorption/excretion indicating that they had a specific defect in water reabsorption.

1.8.2 Pseudohypoaldosteronism type II

Another disease that manifests in CD-originating acid/base dysregulation and involves claudin-4 is pseudohypoaldosteronism type II (PHAII)[162]. This condition originates from defects in the DCT, CNT and CD but for the purpose of this review, we will focus on the role of the CD. Patients with PHA II present symptoms of increased blood pressure, hyperkalemia and hyperchloremic acidosis[162]. PHA II is either caused by a deletion in the first intron or missense mutations in the genes encoding WNK1 or WNK4, respectively. Both deletion or mutations lead

to an increase in WNK activity. WNK1/WNK4 are both expressed in IMCD cells[163164]. While WNK1 is mainly cytoplasmic, WNK4 is localized to the tight junction in the distal nephron[162]. As mentioned above, both proteins are inhibited by a rise in $[Cl^-]_i$[165] but WNK4 is inhibited at a lower $[Cl^-]_i$ concentration than WNK1. WNK4 normally inhibits ENaC activity, therefore PHAII-causing WNK4 mutations result in increased ENaC conductivity and un-regulated sodium reabsorption[166]. Although there is currently no report of claudin-4 mutations resulting in PHA II, PHA II causing mutations in WNK1/4 encoding genes result in increased claudin-4 phosphorylation and Cl^- paracellular flux[80].

Second, as claudin-8 interacts with claudin-4, one of our protein of interest, a mention of KLHL3 and cullin 3 (Cul3) as two additional proteins whose malfunction causes PHAII is needed[167,168]. These two proteins form the "cullin-ring E3 ligase" (CRL) complex where KLHL3 serves as a substrate adaptor for the Cullin-3-mediated ubiquitylation of several proteins, including WNK1, WNK4 and claudin-8[169,170]. KLHL3 mutations are either dominant or recessive and impair KLHL3 interaction with the target protein, while Cul3 mutations are all dominant and alter the structure and stability of the CRL complex. These mutations result in inappropriate sodium and chloride reabsorption in the CD by at least two pathways. One pathway involves the ubiquitylation of claudin-8 by KLHL3[169,171]. Knocking down claudin-8 in immortalized mouse IMCD cells results in the loss of claudin-4 localization to tight junctions and as a result a decrease in paracellular chloride conductance. PHAII-causing mutations in KLHL3 disrupt its interaction with claudin-8, thereby preventing claudin-8 ubiquitination and degradation, and causing an increase in paracellular chloride flux. The second pathway involves the ubiquitylation of WNK proteins by KLHL3. In a mouse model knocked-in with the PHAII-causing dominant KLHL3 R528H mutation, WNK1 and WNK4 expression level were increased compared to control littermates due

to a loss of interaction with the KLHL3 mutant and impaired WNK1 and 4 ubiquitylation[172]. This disease illustrates the complex interplay between tight junction properties and transcellular ion fluxes.

1.8.3 Claudin-4 in non-kidney related diseases

Several Mendelian diseases have been linked to mutations in genes encoding claudins, including claudin-1 (neonatal sclerosing cholangitis with ichthyosis)[173], claudin-14 (autosomal recessive, non-syndromic deafness, associated with high risk to develop kidney stones and reduced bone mineral density)[174,175], claudin-16 (familial hypomagnesemic hypercalciuria with nephrocalcinosis, "FHHNC")[176], and claudin-19 (FHHNC with ocular involvement)[177]. However, no mutation has been found in claudin-4 gene to cause a Mendelian-inherited disease[58]. Instead, alterations in claudin-4 expression levels have been linked to various diseases. For example, downregulation of claudin-4 expression is associated with several inflammatory diseases such as collagenous colitis[178] and ulcerative colitis[179]. In addition, claudin-4 abundance is also affected in different kinds of human tumors. For example, it can be downregulated in breast cancer[180], gastric carcinoma[181], ovarian carcinoma[182] and bladder carcinoma[183]. On the other hand, it can be upregulated in pancreatic cancer[184] and thyroid carcinoma[185].

1.9 Thesis hypothesis:

Several years ago, our collaborator Dr. Reinhart Reithmeier (University of Toronto) found that that kAE1 interacts with claudin-4 using a membrane yeast two-hybrid assay. Based on this finding*, we hypothesized that kAE1/claudin-4 interaction regulates the acid/base balance and electrolytes homeostasis*.

1.10 Thesis objectives:

1. To confirm kAE1 and claudin-4 interaction in mammalian cells,
2. To study the potential implications of kAE1 expression on claudin-4 (abundance and function),
3. To investigate the mechanism(s) by which kAE1 affects claudin-4 function.

2. Chapter 2: Material & Methods

2.1 Plasmid constructs and antibodies

The pLVX TRE3G kAE1 construct was generated by shuttling human kAE1 cDNA carrying an external hemagglutinin (HA) epitope in position 557 (eAE1 numbering) into pLVX-TRE3G plasmid (Clontech) using MluI restriction sites in 3' and 5' of the open reading frame. The insertion of the HA epitope did not alter kAE1 localization or function (26). The sequence of the full construct was then verified using automated sequencing (The Applied Genomics, Edmonton, AB). This construct has been designated as "kAE1" throughout the manuscript. The kAE1 E681Q, S525F and R589H mutants were generated using the Q5 site-directed mutagenesis kit (NEB) and mutagenesis primers with the sequences indicated in Table 2.1. Three different inducible claudin-4 shRNA-containing lentiviruses were purchased from Dharmacon (Dharmacon SMARTvector Inducible Lentiviral shRNAs, GE Healthcare) that enclosed 3 siRNA hairpin oligonucleotides with sequences shown in Table 2.2. The siRNAs were downstream of the mouse CMV promoter, and were followed by a Turbo RFP reporter to track transduction and expression upon doxycycline induction. Polyclonal rabbit antibodies detecting murine claudin-4 or claudin-3 used for immunoblot or immunoprecipitation was purchased from InVitrogen (Cat # 36-4800 and 34-1700, respectively), monoclonal mouse anti-claudin-4 antibody coupled to AlexaFluor488 (3E2C1) was used for immunofluorescence and was obtained from Thermoscientific (Cat # 329488), polyclonal rabbit anti-claudin-8 antibody was purchased from InVitrogen (Cat # 40-2600), polyclonal rabbit anti-calnexin antibody is a kind gift from Dr. David Williams (U of Toronto). Polyclonal rabbit anti-WNK1, polyclonal rabbit anti-phospho WNK1, polyclonal rabbit anti-WNK4, polyclonal rabbit anti-phospho WNK4, polyclonal sheep anti-SPAK/OSR1

Table 2.1: Primers used to generate kAE1 mutants

kAE1 mutant	Forward primers	Reverse primers
kAE1 E681Q	CATATTCCTGCAGTCTCAGATCAC	AGGATGAAGACCAGCAGAG
kAE1 S525F	GAGATCTTCTTCTTCCTCATTTCCC	CTGGGTATAGCGGGAGATG
kAE1 R589H	ATGATGCTGCACAAGTTCAAG	GGCAAAGAAGAAGGTACC

Table 2.2: shRNA oligonucleotides sequence used to generate claudin-4 knock-down mIMCD3 cells

shRNA #	shRNA sequence
shRNA 1	CAAAGTTACTAGCCCGTAG
shRNA 2	GGACCGCTCACAACGTCAT
shRNA 3	CCGGAGCCGTGTTCATCGT

and polyclonal sheep anti-phospho SPAK/OSR1 antibodies are kind gifts from Dr. Maria Chavez-Canales (U of Mexico), polyclonal rabbit anti-beta catenin antibody (Cat # C2206) was obtained from Sigma-Aldrich, USA. Monoclonal mouse anti-HA antibody was obtained from Covance (Cat # MMS-101R) and subsequently BioLegend (Cat # 901513).

2.2 Cell Culture

2.2.1 mIMCD3 cells inducibly expressing kAE1 WT-HA, kAE1 mutants or EV

70% confluent Lenti-X 293T cells (Clontech) were transfected with 7 μg of either pLVX-Tet3G regulator plasmid, pLVX-TRE3G kAE1 WT-HA (later referred as kAE1), pLVX-TRE3G kAE1 E681Q-HA, pLVX-TRE3G kAE1 S525F-HA, pLVX-TRE3G kAE1 R589H-HA or empty pLVX-TRE3G (pLVX-TRE3G EV) response plasmids using Lenti-X HTX Packaging mix and Xfect Transfection Reagent (Clontech), following the manufacturer's instructions. Cells were incubated at 37 °C in serum-free OptiMEM medium (Gibco) for 48 hours. Supernatants containing the lentivirus were collected and filtered through 0.45 μm filters. 70% confluent mIMCD3 (ATCC, CRL-2123) were then co-infected with lentiviruses containing both regulator (pLVX-Tet3G) and response (pLVX-TRE3G kAE1 WT-HA, pLVX-TRE3G kAE1 mutant, or pLVX-TRE3G EV) plasmids and 8 μg/ml of polybrene (Sigma-Aldrich, USA) for 48 hours. The growth medium was then complemented with 4 μg/ml Puromycin and 2 mg/ml G418 to select infected cells. Expression of kAE1 proteins was optimally detected after incubation with 0.5 μg/ml of doxycycline for 24 hours. Upon doxycycline induction, these cells expressed similar amounts of kAE1 even after multiple passages.

2.2.2 Lentiviruses containing shRNA against claudin-4 in EV or kAE1 expressing cells

To generate claudin-4 knocked down (claudin-4 KD) cells, 3 different claudin-4 shRNA were used. 10^5 mIMCD3 cells were plated on a 6 well plate and transduced with each shRNA-

containing lentiviruses (titer ranging from 4.5 to 6.5 10^7 TU/ml) to reach a MOI of 6, in the presence of 8 µg/ml of polybrene in serum-free OptiMEM medium for 48 hours at 37°C. Transduction medium was replaced by an antibiotic free medium for 24 hours followed by incubation with a selection medium containing 4 µg/ml of Puromycin. Claudin-4 shRNA expression was optimally induced with 5 µg/ml Doxycycline for 48 hours. To generate the mIMCD3 cell line with both inducible knockdown of claudin-4 and expression of kAE1 protein or empty vector, we co-infected claudin-4 KD cells with lentiviruses that either contained regulator (pLVX-Tet3G) and response (pLVX-TRE3G kAE1 WT-HA or pLVX-TRE3G EV) plasmids for 48 hours at 37°C. We therefore generated 2 cell lines: "claudin-4 KD/EV", which upon induction with doxycycline are knocked down for claudin-4, and "claudin-4 KD/kAE1", which upon doxycycline induction express kAE1 and are knocked down for claudin-4. The cells were subsequently grown in a selection medium containing 4 µg/ml Puromycin and 2 mg/ml G418. Expression of kAE1 proteins and claudin-4 knockdown were induced using 5 µg/ml of Doxycycline for 48 hours.

2.3 Functional Assay

70 % confluent IMCD3 cells expressing kAE1-HA were grown on 11 X 7.5 mm glass coverslips and treated as previously described (91). Briefly, after three washes of the coverslips with serum-free OptiMEM medium (Gibco), the cells were incubated with 10 µM BCECF-AM (Sigma-Aldrich, USA) for up to 1 hour at 37°C. Coverslips were then placed in fluorescence cuvettes at room temperature and the cells were perfused with Ringer's buffer (5 mM glucose, 5 mM potassium gluconate, 1 mM calcium gluconate, 1 mM magnesium sulphate, 10 mM HEPES, 2.5 mM NaH_2PO_4, 25 mM $NaHCO_3$, pH 7.35-7.45) containing 140 mM chloride. Intracellular alkalinization was then induced by replacing the perfusing solution with a chloride free Ringer's buffer containing 140 mM gluconate. Finally, we calibrated the BCECF-AM intracellular fluorescence by perfusing the cells

with buffers at pH 6.5, 7.5, or 7.0 supplemented with 100 μM nigericin sodium salt (Sigma-Aldrich, USA). A Photon Technologies International (PTI) (London, Ontario, Canada) fluorescence spectrometer was used to read the fluorescence emissions generated by the samples. Excitation wavelengths of 440 and 490 nm and emission wavelength of 510 nm were used. The transport rates were calculated using linear regression of the initial rate of intracellular alkalinization (first 60 seconds), normalized to pH calibration measurements. All measurements were done using FeliX software (Photon Technology International, USA).

2.4 Immunoblotting and immunoprecipitation

Confluent or sub-confluent mIMCD3 cells expressing kAE1-HA were lysed in RIPA lysis buffer (0.3 M NaCl, 20 mM Tris/HCl pH 7.5, 2 mM EDTA, 2 % Deoxycholate, 2 % Triton X-100, 0.2 % SDS, pH 7.4) supplemented with Complete EDTA-free protease inhibitors (Roche), and PhoSTOP phosphatase inhibitor (Roche) where indicated. The total protein concentration was measured using a BCA assay (Pierce, Rockford, IL, USA). 20 or 60 (where indicated) μg of proteins were loaded on a SDS-PAGE gel and kAE1, claudin-3, claudin-4, claudin-8, WNK4, phospho-WNK4, SPAK, phospho-SPAK and β-actin proteins in the lysates were detected by immunoblotting with mouse anti-HA, rabbit anti-claudin-4, rabbit anti-WNK, rabbit anti-pWNK4, sheep anti-SPAK, sheep anti-pSPAK or mouse anti-β-actin antibodies overnight at 4 °C as indicated in Table 2.3, followed by secondary antibodies coupled to horseradish peroxidase (HRP) for 1 hour at room temperature. Enhanced chemiluminescence (ECL prime western blotting detection reagent from GE Healthcare, Wauwatosa, WI, USA) and a BioRad Imager were used to detect proteins. Relative band intensities were determined using ImageLab software (BioRad). For immunoprecipitations, the lysate was incubated with 3 μl of rabbit anti-claudin-4 or anti-claudin-3 antibody for 2 hours on a rocker at 4°C, followed by 30 μl of protein G-coupled sepharose beads (GE Healthcare) for an additional

hour at 4°C. Eluted proteins were separated by SDS-PAGE and claudin-4, claudin-3 or kAE1 proteins immunoblotted using either a mouse anti-claudin 4, mouse anti-claudin-3 or a mouse anti-HA antibody, respectively.

Table 2.3: List of primary antibodies used in immunoblot assays

Protein	Antibody	Species	Concentration/1% milk in µl TBST
kAE1 (WT, E681Q, S525F, R589H)	Anti-HA	rat	1/2000
Claudin-3	Anti-claudin-3	rabbit	1/1000
Claudin-4	Anti-claudin-4	rabbit	1/1000
Claudin-8	Anti-claudin-8	rabbit	1/1000
β-actin	Anti-β-actin	mouse	1/10000
WNK4	Anti-WNK4	rabbit	2/1000
pWNK4 S1196	Anti-pWNK4	rabbit	1/1000
SPAK	Anti-SPAK	sheep	2µg/ml
pSPAK S373	Anti-pSPAK	sheep	2µg/ml

2.5 Ussing Chambers experiments

Confluent mIMCD3 cells stably expressing kAE1-HA in an inducible manner were grown on 0.45 μm semi-permeable Transwell filters (Costar, Cat # 07200225) for 10 days. 24 hours prior to the beginning of the experiment, kAE1 protein expression was induced by incubation of the cells with 0.5 μg/ml of doxycycline. Where indicated, 4 μM of WNK 463 inhibitor was added to the growth medium 24 hours prior to beginning of the experiment. 0.1 mM of amiloride were applied apically and 0.1 mM of bumetanide were applied basolaterally and the beginning of the experiment where indicated. The filters were then mounted in Ussing chambers and bathed at 37°C in solution A containing: 145 mM NaCl, 1 mM $CaCl_2$, 1 mM $MgCl_2$, 10 mM glucose, and 10 mM HEPES, pH 7.4. The current was first clamped using a DVC 1000 I/V clamp (World Precision Instruments, Sarasota, FL) and electrodes filled with 3 M KCl. Data were recorded as a trace using PowerLab (ADInstruments, Colorado Springs, CO) and Chart 4.0 software. 90 μA pulses were applied across the epithelial monolayer and a dilution potential was induced by replacing solution A bathing the basolateral membrane with an iso-osmotic solution containing 80 mM NaCl (Solution B: 80 mM NaCl, 130 mM mannitol, 1 mM $CaCl_2$, 1 mM $MgCl_2$, 10 mM glucose, and 10 mM HEPES, pH 7.4) allowing us to calculate transepithelial electrical resistance (TEER), absolute permeabilities of the epithelium to sodium and chloride and ion permeability ratios using the Goldman-Hodgkin Katz and Kimizuka Koketsu equations, as described previously[186,187].

2.6 Proximity Ligation Assay

Confluent mouse IMCD3 cells expressing kAE1 WT-HA proteins were seeded on 12 mm glass cover slips and incubated with or without 0.5 μg/ml Doxycycline for 48 hours before the experiment day. The assay was performed according to the manufacturer's instructions (Olink Bioscience, Sweden). Briefly, the cells were washed with 1 X PBS, fixed with 4 % PFA, quenched

with 50 mM NH_4Cl, permeabilized with 0.1 % Triton-X 100 and washed twice with buffer A (10 mM Tris, 150 mM NaCl, 0.05 % Tween 20, pH 7.4; provided by the company, Olink Bioscience, Sweden). In a pre-heated humidified chamber, the cells were then blocked with 40 µl of the blocking solution (provided by the company; Olink Bioscience, Sweden) at 37° C, prior to addition of 40 µl mouse anti HA and rabbit anti claudin-4 antibodies (1/500 in provided antibody diluent) for 1 hour at 37°C. After washes, the two minus anti-mouse and the plus anti-rabbit PLA probes were added to each sample for 1 hour at 37° C in the humidity chamber, followed by the ligation-ligase mixture for 30 minutes and finally with the amplification-polymerase mixture in the humidity chamber for 100 minutes. After 3 washes with 1/100 of provided buffer B supplemented with DAPI, the coverslips were mounted on glass slides. Samples were examined using a 60 X oil objective with a WaveFX confocal microscope (Quorum Technologies, Canada).

2.7 Immunohistochemistry

PBS/heparin-perfused 129S6/SvEvTac mouse kidneys were paraffin-embedded and sectioned every 2 µm prior to formalin-fixation as previously described (93). Sections were then rehydrated using Tissue-Clear (Tissue-Tek, Dakura sections) and subsequently incubated in graded ethanol solutions into water and next submitted to heat induced antigen retrieval with a TEG solution (10 mM Tris, 0.5 mM EGTA, pH = 9.0). Sections were next incubated with 0.6 % H_2O_2 and 50 mM NH_4Cl in PBS to block endogenous peroxidases enzymes and free aldehyde groups. Sections were incubated with mouse anti-AE1 antibody (kind gift from Dr. Sebastian Frische) in 0.1 % Triton X-100 in PBS at 4°C followed by anti-mouse Cy3 secondary antibody and mouse anti-claudin-4 antibody coupled to Alexa488 prior to mounting with Aquamount. The kidney sections were observed using an Olympus IX81 microscope equipped with a Nipkow spinning-disk optimized by Quorum Technologies (Guelph, ON, Canada) and a 63 X oil objective.

2.8 Immunofluorescence

Sub-confluent or polarized mouse IMCD3 cells expressing kAE1-HA proteins were incubated with or without 0.5 µg/ml Doxycycline for 24 hours prior to fixation with 4 % paraformaldehyde (Canemco Supplies) in PBS followed by incubation with 100 mM glycine in PBS (pH 8.5) to quench non-specific fluorescence. After cell permeabilization with 0.2 % Triton X-100 in PBS and blocking with 1 % BSA, the kAE1 proteins were detected with a mouse anti-HA primary antibody (Covance) followed by an anti-mouse antibody coupled to Cy3 (Jackson Immunoresearch Laboratories), while endogenous claudin-4 was detected with a mouse anti-claudin-4 antibody coupled to Alexa488. Nuclei were stained with DAPI. Coverslips were finally mounted onto glass slides using DAKO mounting solution and examined using an Olympus IX81 microscope equipped with a Nipkow spinning-disk optimized by Quorum Technologies (Guelph, ON, Canada) and a 63 X oil objective.

2.9 Cell Surface Biotinylation

Polarized mouse IMCD3 cells expressing kAE1 WT-HA proteins were incubated with or without 0.5 µg/ml Doxycycline for 24 hours prior to two incubations with EZ-Link Sulfo-NHS-SS-Biotin reagent (1 mg/ml) (Pierce) at 4 °C for 15 min in borate buffer (10 mM Boric acid, 145 mM NaCl, 7.2 mM KCl, 1.8 mM $CaCl_2$, pH 9). The excess of biotin was quenched 3 times (10 minutes each) with 100 mM glycine in PBS. The cells were lysed in 300 µl RIPA lysis buffer (10 mM Tris-HCl, 150 mM NaCl, 1 mM EDTA, 1 % Triton X-100, 0.1 % SDS, 1 % deoxycholate, 1 µg/ml aprotinin, 2 µg/ml leupeptin, 1 µg/ml pepstatin A, and 100 µg/ml PMSF, pH 7.5). An aliquot (30 µl) of the lysate was kept as total lysate (T) and the remaining was incubated with streptavidin agarose resin (100 µl, Thermo Scientific) for 1 hour at 4 °C. An aliquot (30 µl) of unbound proteins (U) was saved. The same volume (30 µl) of "T" and "U" fractions were loaded on SDS-PAGE gel and

samples were immunoblotted with a mouse anti-claudin-4 antibody. Relative band intensities were determined using the Image Lab software (BioRad). The results are expressed as unbound/total (U/T) ratios.

2.10 Real-time quantitative PCR

Total mRNA was isolated from claudin-4 KD/kAE1 mIMCD3 cells incubated with doxycycline for 48 hours or kept in control conditions, using EZ-10 DNAaway RNA Mini-Preps Kit, (BIOBasic Canada Inc, ON, Canada). DNAse I treatment was next performed, followed by reverse transcription of 5 µg RNA using SuperScript II transcriptase and random primers obtained from IDT (Integrated DNA Technologies, San Diego, CA). The cDNA was next used to determine claudin-4 and the internal control actin mRNA levels using primers from Thermo Fisher/ABI (claudin-4 primers and probe: Cat # Mm00515514-s1; actin primers and probe: Cat # Mm01205647-g1). To determine the mRNA levels of WNK1 or 4 and the internal control actin, the cDNA from the previous step was used with primers from IDT (Integrated DNA Technologies, San Diego, CA), (WNK1 primers and probe: Cat # Mm.PT.58.9776943, WNK4 primers and probe: Cat # Mm.PT.58.28970884, actin primers and probe: Cat # Mm01205647-g1). Expression levels were determined by qPCR on an ABI Prism 7900 HT sequence detection System (Applied Biosystem, Foster City, CA).

2.11 Immobilized iron affinity electrophoresis

Cell lysates were prepared as described above except of slight modifications. The lysis buffer contains phosphatase inhibitors, 1 X TBS were used instead of PBS for washing prior lysing the cells, and the SDS-PAGE gels were slightly modified as they did not include a stacking gel but only a resolving gel with 10 % acrylamide. After full polymerization and removal of the combs, 35 µl / well of 10 % resolving gel without 20 mM $FeCl_3$ was added to the bottom of half of the

wells and 35 µl / well of 10 % resolving gel with 20 mM $FeCl_3$ was added to the bottom of the remaining half of the wells and left to polymerize. Each sample was loaded twice on the same gel, once in a $FeCl_3$-containing well and once in a $FeCl_3$-free well, where the $FeCl_3$-free wells functioned as controls. Standard immunoblot technique described previously was followed. The total or non-phosphorylated Claudin-4 proteins were detected using rabbit anti-Claudin-4 antibodies.

2.12 Statistical Analysis

All experiments were independently repeated a minimum of three times. Results are expressed as mean values ± standard error of the mean (SEM) and "n" indicates the number of independent experimental repeats. Statistical comparisons were either made using unpaired Student t-test or one-way ANOVA where appropriate, $P < 0.05$ was considered significant.

3. Chapter 3: The kidney anion exchanger 1 affects tight junction properties via claudin-4

3.1 Introduction

Type A IC cells in the distal nephron are essential to maintain a balanced plasma pH. These cells secrete protons generated by cytosolic carbonic anhydrase II into the lumen while transporting bicarbonate back into the blood. This physical separation of acids and bases is mediated by the apical V-H^+-ATPase and the basolateral kidney anion exchanger 1 (kAE1).

kAE1 is a 14 transmembrane segments dimeric glycoprotein with cytosolic amino- (N) and carboxyl (C)-terminal ends[112]. The kAE1 transmembrane domain is sufficient for the exchange of Cl^- and bicarbonate ions and encompasses the binding site for stilbene derivatives. It also carries the N-glycosylation site at position 642 (numbering as per the erythroid isoform). The N-terminus is truncated by the first 65 amino acids present in the erythroid form of the protein, while a short C-terminus is conserved in both erythroid and renal isoforms[188]. This cytosolic domain interacts with various proteins including carbonic anhydrase II[189], adaptor protein 1A&B[136,137,139], glyceraldehyde phosphate dehydrogenase[134], peroxiredoxin 6[131], and contains a putative type I PDZ binding domain [190], which interacts with PDLIM5[140].

Defects in the genes encoding carbonic anhydrase II, the V-H^+-ATPase or basolateral kAE1 can lead to distal renal tubular acidosis (dRTA)[42]. This disease is characterized by a metabolic acidosis, hypokalemia, hyperchloremia, nephrocalcinosis and renal failure if untreated. Interestingly, Sebastian and colleagues observed that even after sustained correction of the metabolic acidosis, RTA patients fail to conserve Na^+ and Cl^- ions[191]. Using MDCK cells as a model for intercalated cells, dRTA originating from mutated SLC4A1 gene that encodes for kAE1 was proposed to arise either from an inactive mutant, from mis-trafficking of this protein to either intracellular compartments, or to the apical membrane[192–197]. However, recent evidence obtained from human biopsies[198] and mice knocked in with the dominant dRTA mutation R607H

(equivalent of the R589H in humans), which developed incomplete dRTA, suggests that the origin of the disease is much more complex than so far anticipated[199]. Indeed, in type-A intercalated cells from homozygous R607H knocked-in mice, the mutated protein was found to be functional and located at the basolateral membrane, while apical V-H^+-ATPase failed to relocate to the luminal membrane upon acidic conditions, thus giving rise to incomplete dRTA. These recent findings highlight the fact that the molecular and cellular mechanisms leading to dRTA are still poorly understood.

In an effort to decipher how intercalated cells maintain normal plasma pH homeostasis, we focused our efforts on the intriguing and un-explained finding from Toye and colleagues who showed that kAE1 expression in MDCK I cells results in a leaky epithelium to apically applied fluorescently labelled biotin molecules[194]. These findings support that expression of kAE1 somehow affects tight junction permeability. Taking into account this latter report together with the renal loss of Na^+ and Cl^- in RTA patients[191], we hypothesized that defective kAE1 function as seen in dRTA patients results in a tighter collecting duct epithelium, and may result in urinary loss of Na^+ and Cl^-.

In this manuscript, we report the characterization of the tight junction properties of mouse inner medullary collecting duct (mIMCD3) cells inducibly expressing kAE1. We provide evidence that the increased leakiness of kAE1-expressing mIMCD3 cells is mediated by an effect on claudin-4, a paracellular pore to Cl^- ions that is expressed in principal cells and intercalated cells of the collecting duct and which physically interacts with kAE1 protein.

3.2 Results

3.2.1 kAE1 expression results in decreased transepithelial electrical resistance

In MDCKI cells, Toye and colleagues reported that stably expressing kAE1 protein resulted in an increased leakiness of the epithelial monolayer to fluorescently labelled biotin when added to the luminal side of the monolayer[194]. To further assess the effect of kAE1 in epithelial properties, we infected mIMCD3 cells with lentiviruses containing kAE1 cDNA whose expression was inducible upon incubation with doxycycline. This strategy also allowed us to avoid the progressive loss of kAE1 expression seen when it is constitutively expressed[197,200]. Upon induction, we observed that kAE1 protein was located at the basolateral membrane, and carried complex oligosaccharides (**Figure 3.1 A & B**), supporting a similar processing as in other cell lines and in mouse kidney as previously described[194,197,199]. The protein was functional as we measured the initial rate of intracellular alkalinization of 0.38 ± 0.04 ΔpH/min (n=9) compared to 0.04 ± 0.01 ΔpH/min (n=9) in the absence of doxycycline. The initial rate of intracellular alkalinization was significantly higher than that measured in MDCK cells stably expressing kAE1 WT (0.25 ± 0.03 ΔpH/min, n=5) (**Figure 3.1 C**). The data interpretation therefore supports that in this cell line, kAE1 behaves in a similar way to intercalated cells. To assess tight junction properties, cells grown for a minimum of 10 days on semi-permeable Transwell filters were mounted onto Ussing chambers and TEER was measured. While the initial TEER value was 314.5 ± 27.2 ohm*cm^2 (n=4) in mIMCD3 cells in the absence of doxycycline, the TEER significantly decreased to 121.4 ± 18.5 ohm*cm^2 (n=3) upon cell incubation with doxycycline for 24 hours (**Figure 3.1 D**). Of note, this decrease was not due to doxycycline since incubation of non-infected mIMCD3 cells with this chemical did not alter the TEER (**Supplemental Figure**). This result is consistent with kAE1 expression affecting tight

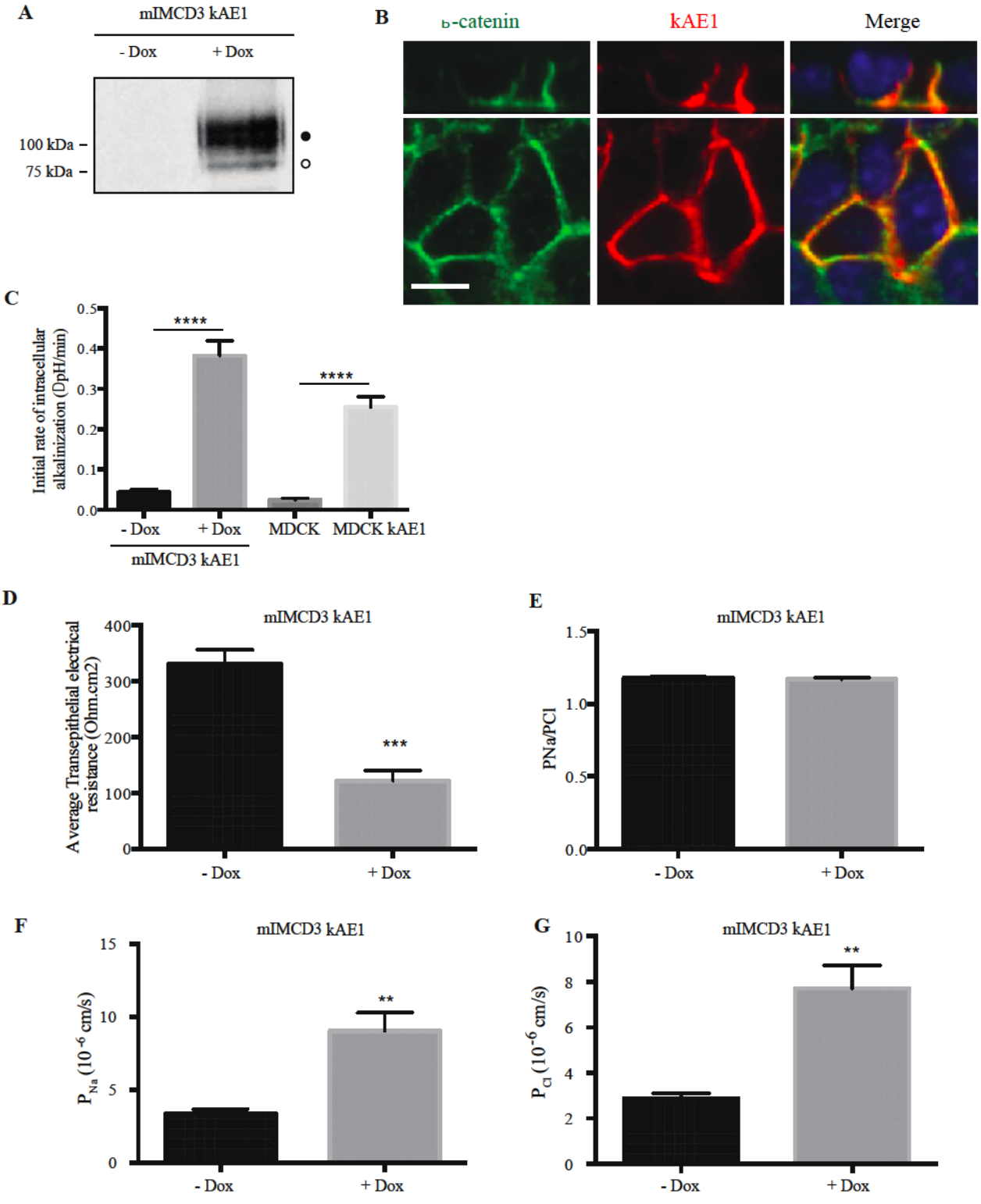
A
mIMCD3 kAE1
- Dox
+ Dox
100 kDa
75 kDa
B
ь-catenin
kAE1
Merge
C
Initial rate of intracellular alkalinization (DpH/min)
0.5
0.4
0.3
0.2
0.1
0.0
****
****
- Dox
+ Dox
MDCK
MDCK kAE1
mIMCD3 kAE1
D
mIMCD3 kAE1
Average Transepithelial electrical resistance (Ohm.cm2)
400
300
200
100
0
***
- Dox
+ Dox
E
mIMCD3 kAE1
PNa/PCl
1.5
1.0
0.5
0.0
- Dox
+ Dox
F
mIMCD3 kAE1
P_Na (10^-6 cm/s)
15
10
5
0
**
- Dox
+ Dox
G
mIMCD3 kAE1
P_Cl (10^-6 cm/s)
10
8
6
4
2
0
**
- Dox
+ Dox

Figure 3.1: Expression of kAE1 in mIMCD3 cells decreases trans-epithelial electrical resistance (TEER) and increases transepithelial Na^+ and Cl^- ion fluxes.

A, mIMCD3 cells expressing kAE1 in an inducible manner were incubated with or without doxycycline for 24 hours, prior to lysis and analysis of protein abundance by immunoblot. Mouse anti-HA antibody was used to detect kAE1 protein. Black and white circles correspond to kAE1 carrying complex and high mannose oligosaccharides, respectively. **B**, mIMCD3 cells expressing kAE1 were grown to full polarization on semi-permeable filters for 10 days and induced with doxycycline for 24 hours prior to immunostaining with either anti-β-catenin antibody (green) or anti-HA antibody (red). The nuclei were stained with DAPI (blue). **C**, 70 % confluent mIMCD3 cells expressing kAE1 were induced with doxycycline for 24 hours prior to loading the cells with BCECF-AM in the presence of NaCl. Upon switching the extracellular solution to one containing Na gluconate instead of NaCl, the initial rate of intracellular alkalinization was recorded for the first 60 seconds and plotted as a function of time (see methods for further details). Error bars correspond to means ± SEM, n=5 at minimum, ****P < 0.0001 versus "mIMCD3 kAE1 – Dox" or "MDCK" condition using one-way ANOVA. **D**, Ussing chambers measurements of TEER showing that kAE1 expression results in decreased TEER but unchanged P_{Na}/P_{Cl} ratio (**E**). However, both absolute permeabilities to Na^+ (**F**) and Cl^- (**G**) increased upon kAE1 expression. Error bars correspond to means ± SEM, n=4 at minimum, **P < 0.01 and ***P < 0.001 versus "– Dox" condition using un-paired t-test.

junction properties by reducing the tightness of the epithelium (193 ohm*cm^2 reduction in the TEER value upon kAE1 expression), and with the former observation from Toye and colleagues[194].

We next measured the dilution potential generated after the basolateral compartment was diluted to approximately 50% of the concentration of Na^+ and Cl^- and we then calculated the absolute permeability to Na^+ and Cl^- using the Hodgkin-Katz equation. Although the Na^+ to Cl^- absolute permeability ratio remained unchanged upon incubation with doxycycline (P_{Na}/P_{Cl} of 1.18 ± 0.01 and 1.17 ± 0.01, n = 3, in the absence and presence of doxycycline, respectively) (**Figure 3.1 E**), the absolute permeabilities to both ions increased. The permeability to Na^+ increased from 3.3 ± 0.3 10^{-6} cm/s to 9.0 ± 0.1 10^{-6} cm/s and that of Cl^- increased from 2.9 ± 0.2 10^{-6} cm/s to 7.7 ± 0.1 10^{-6} cm/s upon doxycycline incubation (**Figure 3.1 F & G**). This result indicates that expression of kAE1 renders the renal epithelium more leaky to both anions and cations.

3.2.2 The function of kAE1 is essential to alter TEER

As erythroid AE1 plays an important scaffolding role in red blood cells[201], we next wondered whether the decrease in tightness of the monolayer was due to the physical presence of the exchanger or to its function in epithelial cells. Since kAE1 interacts with a number of cytosolic proteins[201], it may act as a scaffolding protein that modulates tight junction properties. To test this possibility, we generated an mIMCD3 cell line that expresses the mutant protein kAE1 E681Q, which is unable to perform chloride/bicarbonate exchange[202,203]. As shown in **Figure 3.2 A**, upon incubation of mIMCD3 cells with doxycycline, the kAE1 E681Q mutant was expressed and migrated as two main bands similar to kAE1 WT protein, corresponding to a population of high mannose-carrying and complex-carrying kAE1 E681Q protein[194,197,199]. Although kAE1 E681Q mutant exhibited a higher percentage of high mannose-carrying population than kAE1 WT (47 ± 2 % versus 9 ± 5 %, respectively, n=3), they were similarly localized in

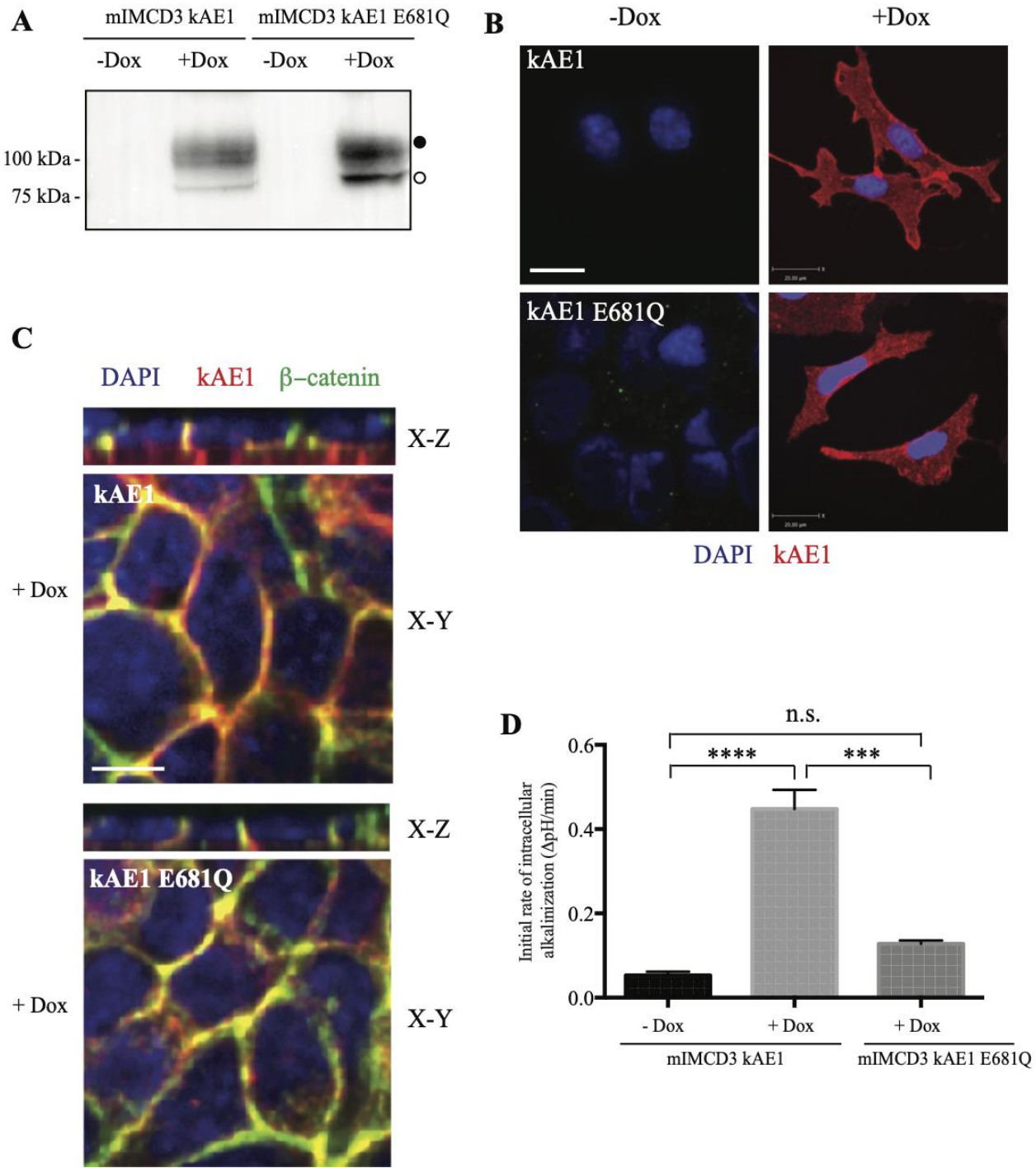
A
mIMCD3 kAE1
mIMCD3 kAE1 E681Q
-Dox
+Dox
-Dox
+Dox
100 kDa -
75 kDa -
B
-Dox
+Dox
kAE1
kAE1 E681Q
DAPI
kAE1
C
DAPI
kAE1
β–catenin
X-Z
kAE1
+ Dox
X-Y
X-Z
kAE1 E681Q
+ Dox
X-Y
D
n.s.
****
***
Initial rate of intracellular alkalinization (ΔpH/min)
0.6
0.4
0.2
0.0
- Dox
+ Dox
+ Dox
mIMCD3 kAE1
mIMCD3 kAE1 E681Q

Figure 3.2: kAE1 E681Q mutant reaches the plasma membrane but is inactive.

A, Immunoblot of mIMCD3 cells either expressing kAE1 WT or E681Q mutant. Both proteins are expressed at comparable levels and both carry complex (black circle) and high mannose (white circle) oligosaccharides**. B,** mIMCD3 cells stably expressing kAE1 WT or E681Q mutant were grown on glass coverslips and incubated with doxycycline to induce kAE1 protein expression. Cells were then immunostained with an anti-HA antibody followed by Cy3 coupled secondary antibody (red). Blue staining corresponds to nuclear localization with DAPI. Bar = 20 μm. **C,** mIMCD3 cells stably expressing kAE1 WT or E681Q mutant and incubated with doxycycline (+ Dox) were grown on semi-permeable filters, fixed, permeabilized and incubated with rabbit anti-β-catenin (green) and mouse anti-HA antibodies (red). Nuclei were stained with DAPI (blue). X-Y shows a middle section through the cells, X-Z shows a side view of the cells. Bar = 10 μm. **D,** Functional assay using pH-sensitive fluorescent probe BCECF on either mIMCD3 cells stably expressing kAE1 WT without doxycycline (mIMCD3 kAE1 - Dox), with doxycycline (mIMCD3 kAE1 + Dox) or kAE1 E681Q with doxycycline (mIMCD3 kAE1 E681Q + Dox). Error bars correspond to means ± SEM, n=3. ***P < 0.001 versus "mIMCD3 kAE1 + Dox" condition, ****P < 0.0001 versus "mIMCD3 kAE1 - Dox" condition, n.s. indicates no significant difference with "mIMCD3 kAE1 – Dox" condition using one-way ANOVA.

non-polarized cells or polarized cells where they both colocalized with the basolateral membrane marker β-catenin (**Figure 3.2 B & C)**. Importantly, we confirmed that kAE1 E681Q mutant's function was not significantly different from the control (mIMCD3 cells not expressing kAE1) but was significantly lower than the kAE1 WT function (**Figure 3.2 D**). We therefore confirmed that this mutant is functionally inactive although expressed at the basolateral membrane. We next performed Ussing chamber experiments and found that expression of the kAE1 E681Q mutant neither altered the TEER nor the absolute permeabilities to Na^+ or Cl^- in mIMCD3 monolayers **(Figure 3.3 A-D)**. These results indicate that the effect of kAE1 protein on the tight junction permeability is dependent on its function rather than solely on its physical presence.

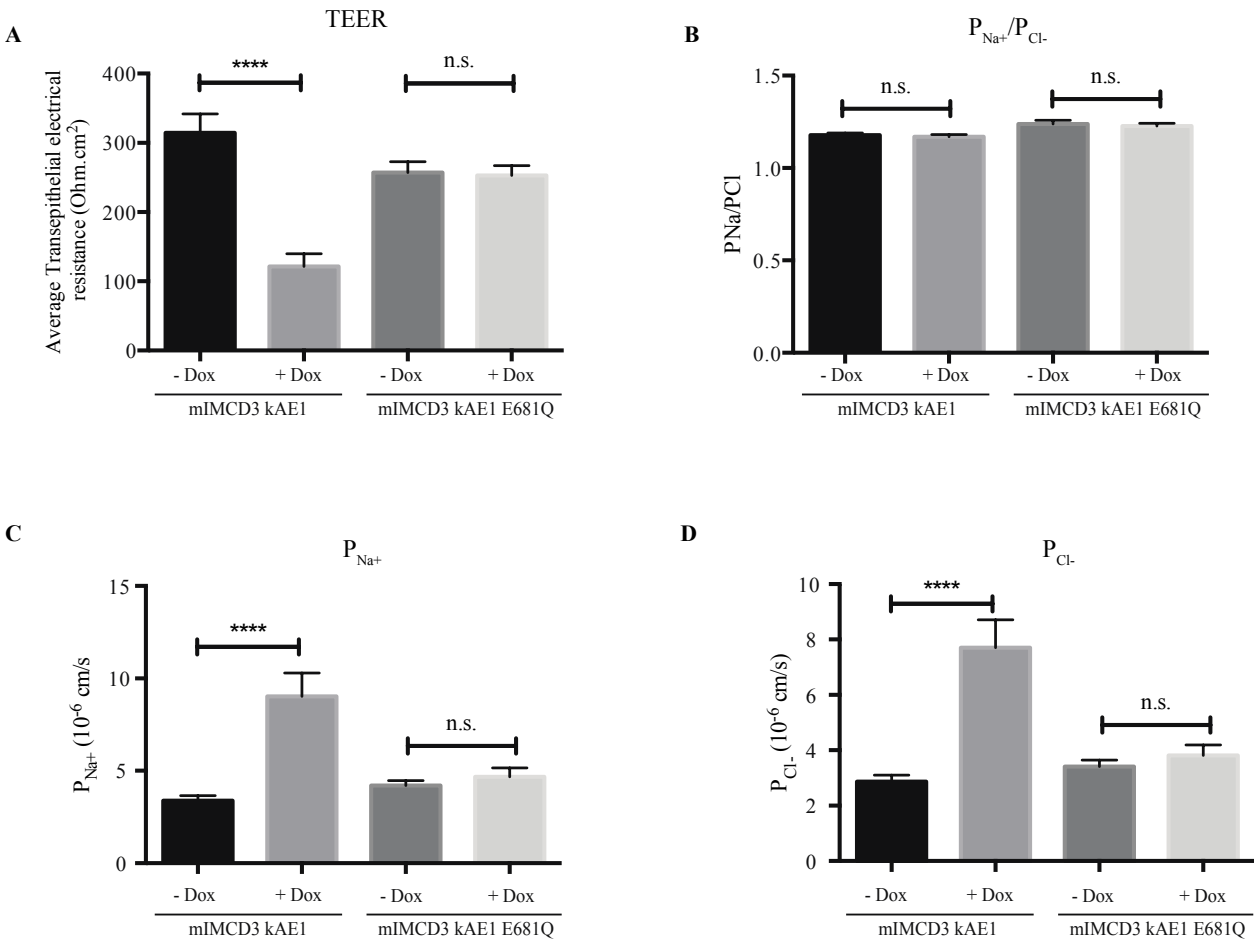

Figure 3.3: The kAE1 E681Q mutant does not affect tight junction properties.

mIMCD3 cells stably expressing kAE1 E681Q mutant were grown on semi-permeable filters for 10 days prior to mounting in Ussing chambers after inducing protein expression (+ Dox). Measurements of TEER (**A**), P_{Na}/P_{Cl} ratio (**B**) and absolute permeability to sodium (**C**) or chloride (**D**) show that kAE1 E681Q mutant expression does not affect tight junction permeability, compared to kAE1 WT (mIMCD3 kAE1). Error bars correspond to means ± SEM, n=7. No significant (n.s.) difference was observed in any of the conditions (One-way ANOVA) for mIMCD3 kAE1 E681Q cells, ****$P < 0.0001$ versus "mIMCD3 kAE1 - Dox" condition.

3.2.3 kAE1 interacts with the tight junction protein claudin-4

To determine by what mechanism kAE1 protein decreases TEER, we performed a membrane yeast two-hybrid assay in collaboration with Dr. Reinhart Reithmeier (University of Toronto, personal communication, February 2013) and found that kAE1 physically interacts with the tight junction protein claudin-4. Claudin-4 is expressed in murine principal cells, intercalated cells[24], MDCK cells[204] and mIMCD3 cells[205] where it forms a paracellular pore to Cl^- ions. To confirm our finding, we performed a co-immunoprecipitation in mIMCD3 cells expressing kAE1 WT. As shown in **Figure 3.4 A**, endogenous claudin-4 co-immunoprecipitated with both high mannose- and complex-containing kAE1 protein (left and middle top panels), indicating that claudin-4 interacts with kAE1 proteins located both in the endoplasmic reticulum, and at the Golgi and beyond. Neither an irrelevant IgG (**Figure 3.4 A**, right top panel) nor a claudin-3 antibody (**Figure 3.4 B**) precipitated kAE1, indicating that the interaction between kAE1 and claudin-4 is specific. Interestingly, the inactive kAE1 E681Q mutant also co-immunoprecipitated with claudin-4 (**Figure 3.4 C**), indicating that the interaction between claudin-4 and kAE1 is not sufficient to regulate tight junction properties. To further confirm our results, we asked whether claudin-4 and kAE1 co-localize by performing a proximity ligation assay (PLA, **Figure 3.4 D**) and an immunostaining on either mIMCD3 cells (**Figure 3.5 A-C**) or a mouse kidney section (**Figure 3.5 D**). The proximity ligation assay was performed on polarized mIMCD3 kAE1 cells using calnexin, a chaperone protein known to interact with newly synthesized kAE1 [206] as a positive control. **Figure 3.4 D** depicts that in contrast to negative controls obtained in absence of doxycycline, induction of kAE1 protein expression resulted in red staining in cells stained with anti-calnexin antibody and more modestly in cells stained with the mouse anti-claudin-4 antibody. This finding confirms that claudin-4 and kAE1 proteins are within 30 to 40 nm distance to each other in polarized mIMCD3 cells. Interestingly, in cells stained for both kAE1 and claudin-4, X-Z sections showed staining at the upper lateral level of the

polarized cells, supporting proximity of both proteins in the tight junction. Immunostaining of claudin-4 and kAE1 was performed on non-polarized and polarized mIMCD3 cells expressing kAE1 (**figure 3.5 A-C).** In contrast with non-polarized mIMCD3 cells that did not express kAE1, claudin-4 appeared enriched at the plasma membrane in kAE1-expressing cells, as indicated by the line scan of both channels in **Figure 3.5 B**. In polarized mIMCD3 cells (**Figure 3.5 C**), however, there was no obvious relocation of claudin-4 to the basolateral membrane as claudin-4 was predominantly junctional, which may reflect that mIMCD3 cells do not polarize as extensively as other renal epithelial cell lines. Importantly, claudin-4 staining was discontinuous and irregular after polarization, possibly reflecting a reduced access of the epitope after polarization of the mIMCD3 cells. This finding supports that only a small fraction of kAE1 and claudin-4 proteins interact with each other, in agreement with the small amount of red dots seen in "claudin-4 & kAE1" panel compared to "CNX & kAE1" panel in our PLA experiment (**Figure 3.4 D)**. To further assess whether the two proteins colocalize, we performed an immunostaining on mouse kidney sections. As shown in **Figure 3.5 D**, claudin-4 (green) was detectable at the tight junctions between cells, including between two kAE1-expressing cells, indicating that claudin-4 is expressed in type-A intercalated cells. Interestingly, claudin-4 was also detectable at the basal membrane of 31 % of kAE1-expressing cells (arrowhead, 40 out of 129 cells observed). This finding supports that claudin-4 is not exclusively junctional but can be present at the basal membrane of some murine intercalated cells as well.

To assess whether kAE1 affected the abundance of claudin-4 at the tight junction/plasma membrane, we next quantified the amount of claudin-4 at the cell surface with or without kAE1 expression. Cell surface biotinylation was performed on mIMCD3 kAE1 cells grown to polarity, and total (T) versus non-biotinylated (U) fractions were compared. As shown in **Figure 3.5 E & F**, there was no significant difference between cell surface abundance of claudin-4 in the presence or absence of kAE1

protein, therefore supporting that kAE1 does not affect plasma membrane/junctional abundance of claudin-4. Together these results support that *(i)* at least a portion of kAE1 protein interacts with claudin-4 and *(ii)* claudin-4 surface abundance is not altered by kAE1 expression.

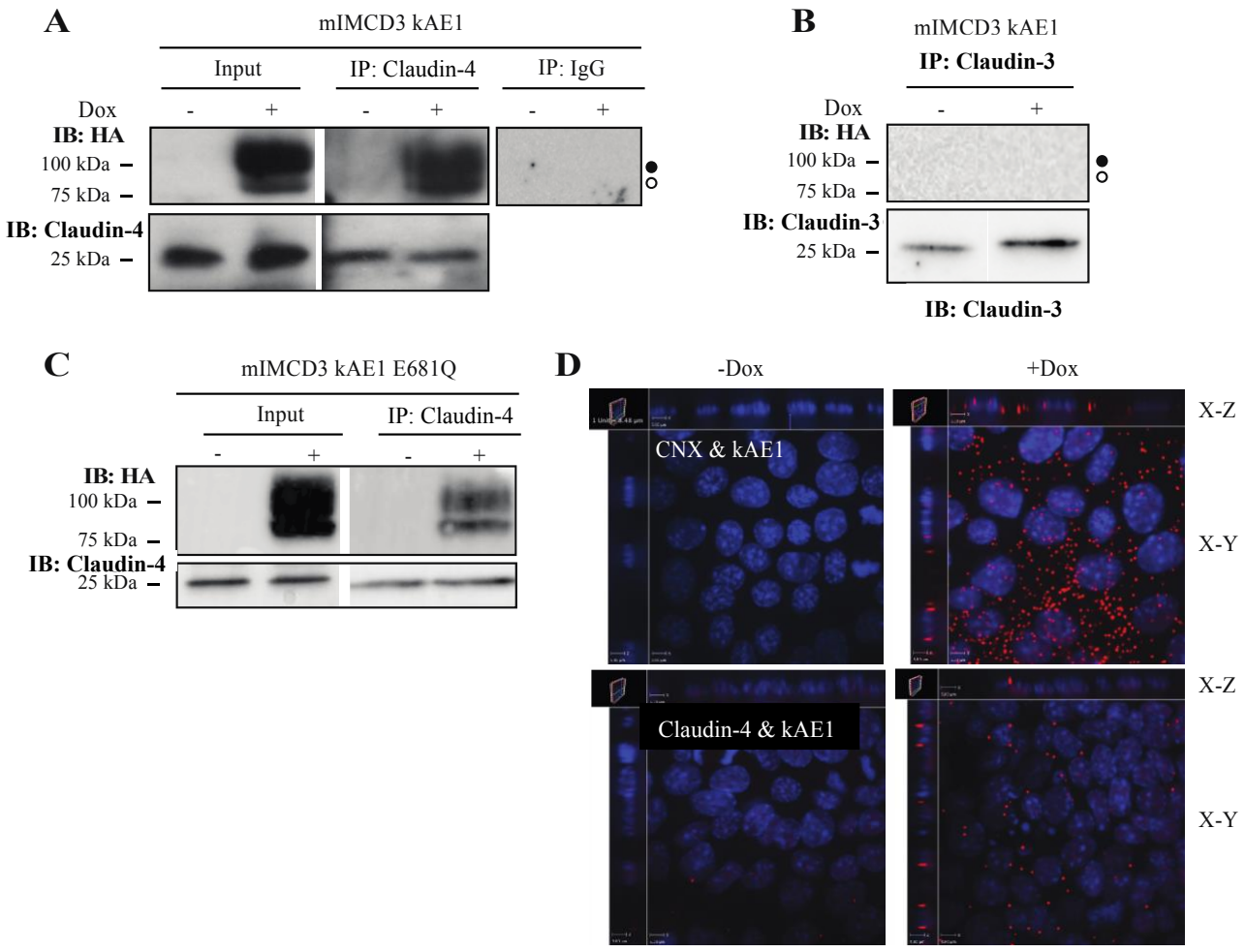

Figure 3.4: kAE1 protein is in close proximity and interacts with claudin-4.

A, Confluent mIMCD3 cells stably expressing kAE1 protein in an inducible manner were grown for 10 days in a 10 cm dish, lysed (Input) and claudin-4 was immunoprecipitated using a rabbit anti-claudin-4 antibody (IP lanes). As a control an irrelevant IgG antibody was used (right panel). Eluted proteins were separated on SDS-PAGE gel prior to immunoblotting with a mouse anti-claudin-4 (bottom blot) or mouse anti-HA (top blot) antibody. Dark circle corresponds to kAE1 carrying complex oligosaccharide, white circle indicates kAE1 carrying high mannose oligosaccharide. **B**, A similar experiment was performed but immunoprecipitating claudin-3. No kAE1 co-immunoprecipitated with claudin-3 (top panel). **C**, The claudin-4 immunoprecipitation was repeated using mIMCD3 kAE1 E681Q cells and shows that claudin-

4 interacts with the mutant. **D**, Proximity ligation assay was performed on mIMCD3 cells stably expressing kAE1 grown for 10 days on semi-permeable filters. CNX, corresponding to calnexin, was used as a positive control[194], claudin-4 corresponds to claudin-4. Cells were examined under a confocal microscope using a 63 X objective and sections (X-Z) or top views (X-Y) are shown. Red signal indicates that the 2 proteins labeled are within 30 to 40 nm of distance from each other. Nuclear staining is shown in blue as DAPI staining.

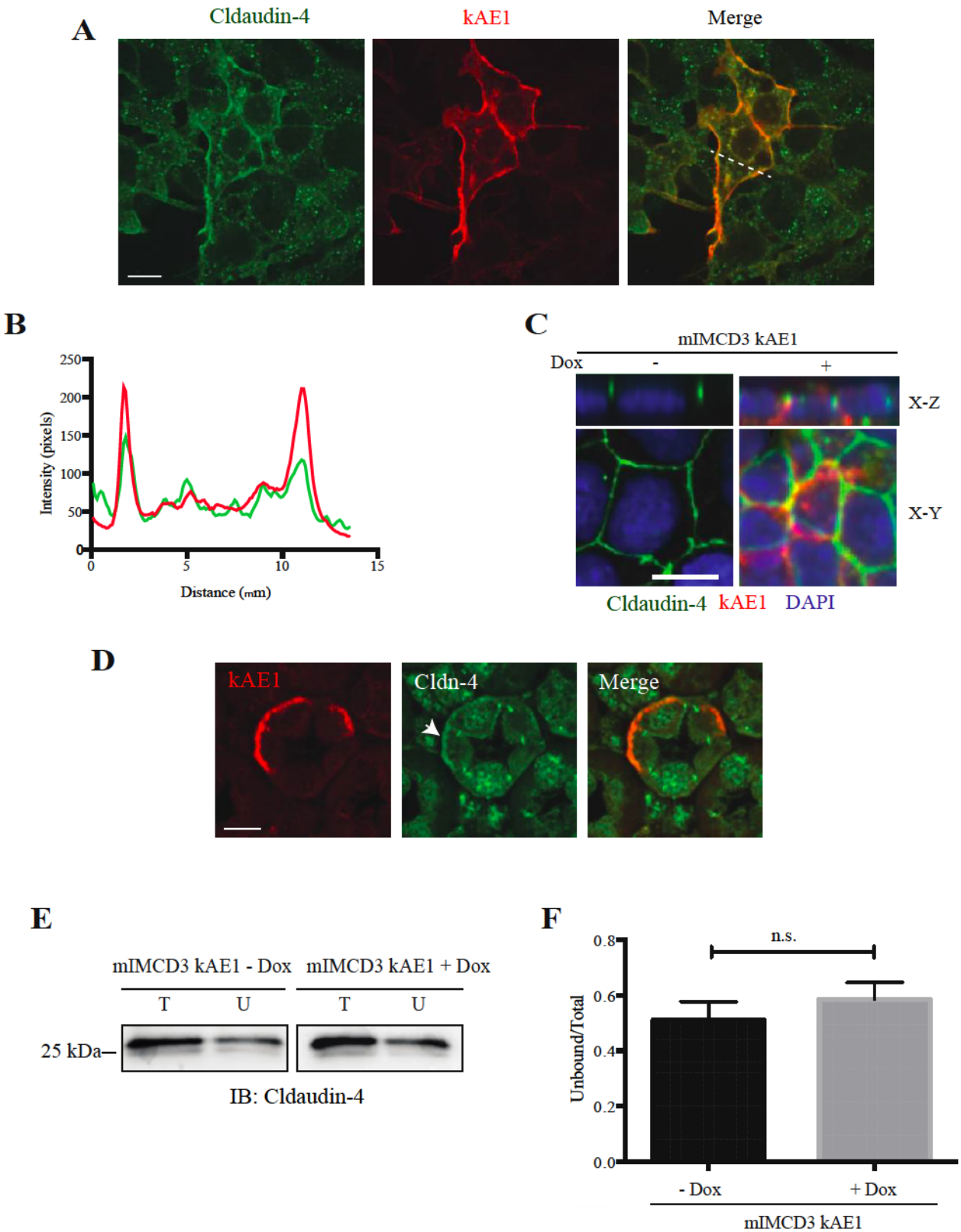
A
Cldaudin-4
kAE1
Merge
B
Intensity (pixels)
Distance (mm)
C
mIMCD3 kAE1
Dox
-
+
X-Z
X-Y
Cldaudin-4 kAE1 DAPI
D
kAE1
Cldn-4
Merge
E
mIMCD3 kAE1 - Dox
mIMCD3 kAE1 + Dox
T
U
T
U
25 kDa
IB: Cldaudin-4
F
n.s.
Unbound/Total
- Dox
+ Dox
mIMCD3 kAE1

Figure 3.5: Claudin-4 colocalizes with kAE1 at the plasma membrane of mIMCD3 cells and in murine intercalated cells.

A, sub-confluent mIMCD3 cells expressing kAE1 were grown on glass coverslips, and incubated with doxycycline to induce kAE1 protein expression. Cells were then immunostained with an anti-HA antibody followed by Cy3 coupled secondary antibody (red) and anti-claudin-4 antibody (green). Bar = 20 μm. **B**, Quantification of fluorescence intensities in the green and red channels along the dotted line shown in A (right panel), highlighting an enrichment of claudin-4 at the plasma membrane in non-polarized mIMCD3 cells. **C**, mIMCD3 kAE1 cells were grown on semi-permeable filter for 10 days prior to immunostaining with anti-HA (red) and anti-claudin-4 (green) antibodies. Nuclei were stained with DAPI (blue). X-Y shows a middle section through the cells, X-Z shows a side view of the cells. Bar = 10 μm. **D**, Mouse kidney sections were immunostained with anti-AE1 antibody (red) and anti-claudin-4 (green). Arrowhead indicates that in addition to its junctional localization, claudin-4 is detectable at the basal membrane of kAE1-positive intercalated cells of the renal collecting duct. **E**, Cell surface biotinylation performed on polarized mIMCD3 kAE1 cells ± Dox. Total (T) and unbound (U) claudin-4 are shown. **F**, quantification of the cell surface biotinylation results (U/T ratios), showing that there is no significant difference in the amount of cell surface claudin-4 upon kAE1 expression in polarized cells. Error bars correspond to means ± SEM, n=7. n.s. indicates no significant (n.s.) difference with "mIMCD3 kAE1 – Dox" condition using un-paired t-test.

3.2.4 The kAE1-induced decrease in TEER is mediated by claudin-4

To assess whether the interaction between kAE1 and claudin-4 was relevant to the decrease of TEER observed in mIMD3 cells upon kAE1 expression, we knocked down endogenous claudin-4 using small hairpin RNA (shRNA). To minimize compensatory up- or down-regulation of other tight junction proteins as previously shown with claudin-4 constitutive knockdown[186], we aimed at preparing cell lines where claudin-4 knockdown was also inducible. However, we were not able to find a commercial shRNA system inducible with a drug other than doxycycline. Therefore, to assess the individual effect of claudin-4 knockdown over that of kAE1 expression, we generated two cell lines: a mIMCD3 cell line which upon doxycycline incubation expressed siRNA that resulted in the knockdown of endogenous claudin-4 (referred to here-after as claudin-4 KD/EV), and a second mIMCD3 cell line in which doxycycline induced both claudin-4 knockdown and kAE1 expression (namely claudin-4 KD/kAE1). **Figure 3.6 A** shows an immunoblot confirming that after 48 hours of incubation of the cells with doxycycline, both kAE1 was expressed (lanes 8 & 9), albeit only to 20 % of the control level (lane 1), and claudin-4 was knocked down by approximately 70 % (lanes 6-9). Quantitative PCR also confirmed the knockdown of claudin-4 mRNA (**Figure 3.6 B**). Despite two separate attempts to generate these cells, we were unable to obtain higher kAE1 expression. As claudin-4 was reported to interact with claudin-8[207], we verified whether claudin-4 knockdown affected claudin-8 abundance. The immunoblot in **Figure 3.6 A** shows that reducing claudin-4 abundance in these cells did not affect claudin-8 expression level.

We next examined the electrophysiological properties of these cell lines in Ussing chambers. In claudin-4 KD/EV mIMCD3 cells, knock-down of claudin-4 was associated with a significant decrease in TEER (271 ± 37 ohm*cm^2 in "– Dox" versus 177 ± 9 ohm*cm^2, in "+Dox", n=4, **Figure 3.6 C**) consistent with a previous report[208]. In contrast to results from **Figure 3.1 D**, when claudin-4 was knocked down,

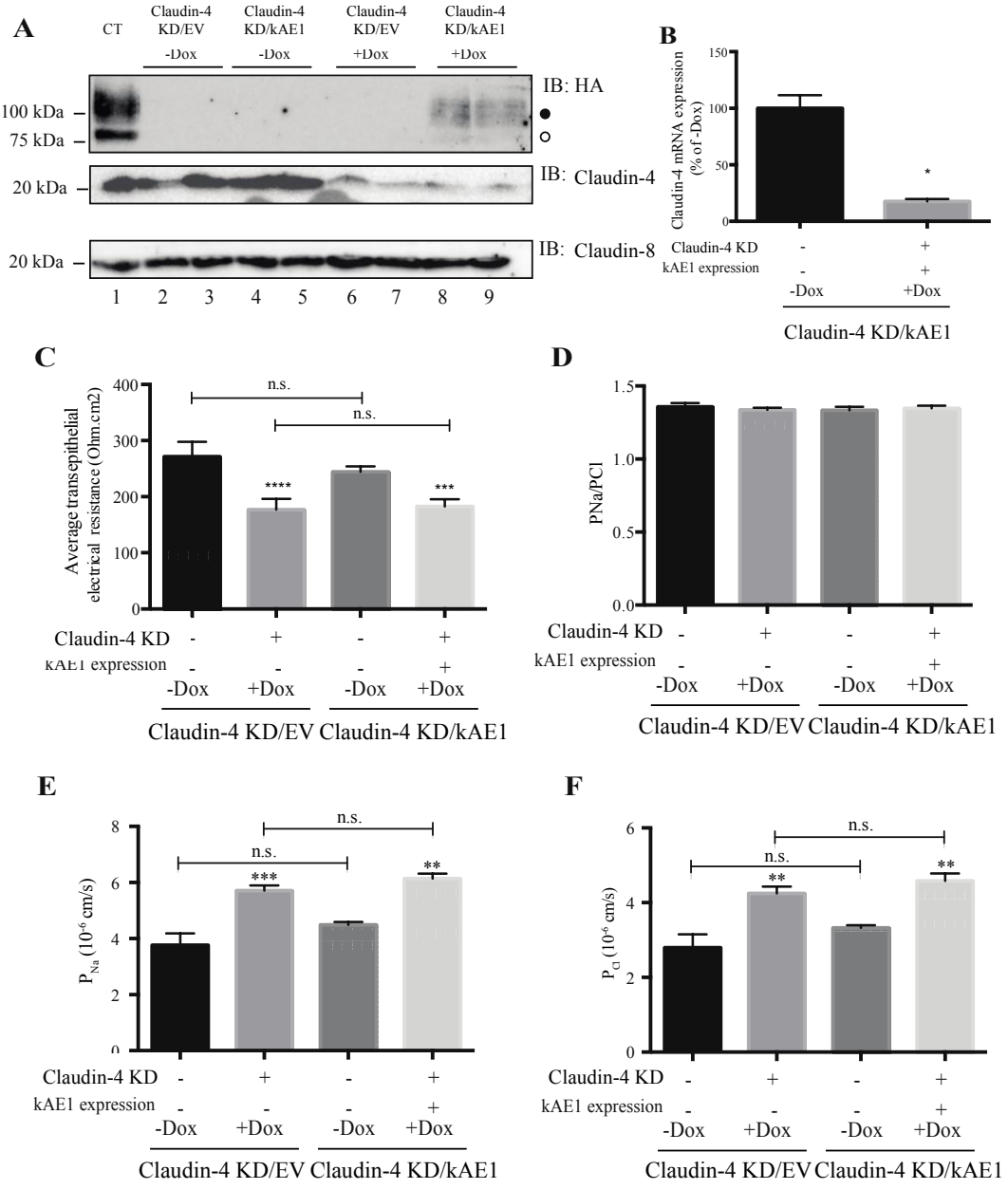

Figure 3.6: Claudin-4 knockdown reduces TEER and increases absolute permeability to both Na^+ and Cl^-.

A, mIMCD3 cells expressing kAE1, claudin-4/EV or claudin-4/kAE1 in an inducible manner were either incubated in presence or absence of doxycycline for 48 hours, prior to lysis and analysis of protein abundance by immunoblot. Mouse anti-HA antibody was used to detect kAE1 protein (upper panel),

rabbit anti-claudin-4 (middle panel) or rabbit anti-claudin-8 (bottom panel) antibodies were used respectively to detect claudin-4 and claudin-8. The dark circle corresponds to kAE1 carrying complex oligosaccharide, and the white circle indicates kAE1 carrying high mannose oligosaccharide. Twenty micrograms of proteins were loaded in every lane. **B**, Quantitative PCR analysis of claudin-4 mRNA abundance in claudin-4 KD/kAE1 incubated in control conditions or with Doxycycline. The results are expressed as a percentage of "claudin-4 KD/kAE1 – Dox" conditions and are normalized to the expression of actin. Error bars correspond to means ± SEM, n=3. *P < 0.05 versus "claudin-4 KD/kAE1 - Dox" condition using un-paired t-test **C**, Ussing chambers data showing an equivalent decrease in TEER in both claudin-4 KD/EV and claudin-4/kAE1 cells incubated with doxycycline. Error bars correspond to means ± SEM, n=4. ***P < 0.001 versus claudin-4 KD/kAE1 cells without doxycycline, ****P < 0.0001 versus claudin-4 KD/EV cells without doxycycline. n.s. indicates non-significant difference (One-way ANOVA). Although P_{Na}/P_{Cl} ratio was unchanged, (**D**) , absolute permeability to both Na^+ (P_{Na}) (**E**) or Cl^- (P_{Cl}) (**F**) were increased upon Doxycycline incubation of claudin-4/EV and claudin-4/kAE1 cells. Error bars correspond to means ± SEM, n=4, ***P < 0.001 versus claudin-4 KD/EV cells without doxycycline, **P < 0.01 versus the same cell line without doxycycline.

kAE1 expression did not significantly affect the TEER (177 ± 9 ohm*cm^2 in "claudin-4/EV" versus 182 ± 6 ohm*cm^2, in "claudin-4/kAE1", n=6). This could be due to the low kAE1 expression in claudin-4 KD/kAE1 cells (20 % of the control cells, **Figure 3.6 A**). To test this hypothesis, we induced 20 % of kAE1 expression and measured TEER in these conditions. Upon incubation of kAE1-expressing mIMCD3 cells with 31 ng/ml of doxycycline [which induced a 20 % kAE1 expression compared to maximal expression (**Figure 3.7 A**)], the TEER significantly decreased to 287 ± 10 ohm*cm^2 compared to 377 ± 25 ohm*cm^2 in absence of Dox incubation (n=4) (**Figure 3.7 B**). This indicates that a 20 % kAE1 expression is enough to induce a 90 ohm*cm^2 decrease in TEER. Given the absence of a decrease in TEER upon 20 % kAE1 expression in claudin-4 knockdown cells, we interpret this result as kAE1 expression no longer reducing TEER in the absence of claudin-4. Together, these data support that the effect of kAE1 on tight junction properties is mediated through claudin-4.

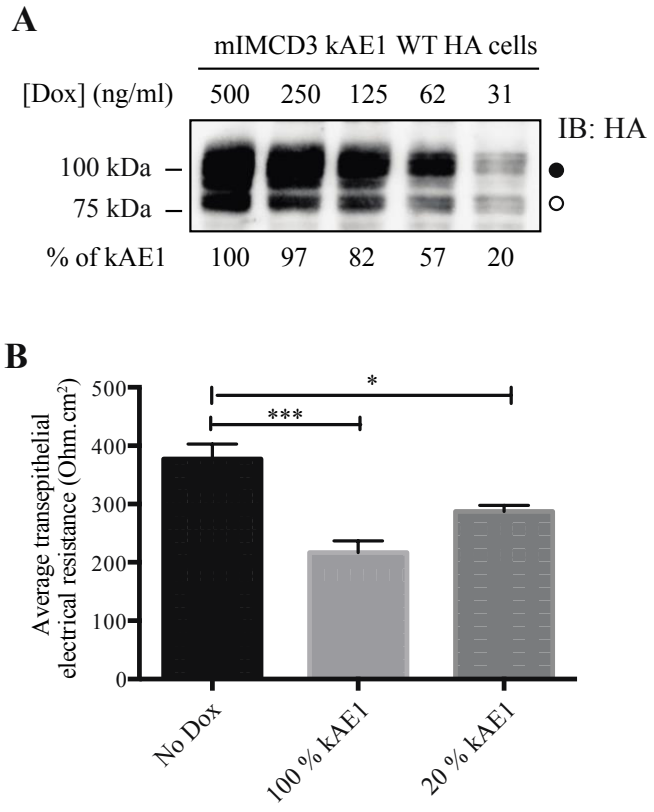

Figure 3.7: 20 % of kAE1 expression is enough to significantly alter tight junctions properties.

A, Immunoblot from mIMCD3 kAE1 cells incubated for 24 hours with various concentrations of doxycycline, and relative quantification of kAE1 abundance in these cells (bottom numbers). Incubation of the cells with 31 ng/ml of doxycycline was determined to induce 20 % kAE1 expression compared to the routine 500 ng/ml doxycycline incubation. The dark circle corresponds to kAE1 carrying complex oligosaccharide, and the white circle indicates kAE1 carrying high mannose oligosaccharide. **B**, Ussing chamber data showing that compared to cells that do not express kAE1 (No Dox), a 20 % kAE1 expression results in significant decrease in TEER. Error bars correspond to means ± SEM, n=4, ***P < 0.001 versus mIMCD3 kAE1 cells without doxycycline, *P < 0.05 versus mIMCD3 kAE1 cells without doxycycline.

3.2.5 kAE1 WT expression acidifies the cytosolic pH, and alkalinize the pH and decreases Cl- concentration of the extracellular basolateral medium

To start deciphering the molecular mechanisms of kAE1 effect on tight junction properties and claudin-4, we addressed whether kAE1 expression in mIMCD3 cells alters cytosolic and/or extracellular ionic concentrations. After growing kAE1 mIMCD3 cells for 8 days on semi-permeable filters and a 24 hour-induction of kAE1 expression with doxycycline, we measured the basolateral growth medium Cl^- concentration and pH. As shown on **Figure 3.8**, we observed a significant alkalization of the pH medium from 6.81 ± 0.01 in "–Dox" to 7.12 ± 0.02 in "+Dox" (n=3) concomitant with a reduction of Cl^- concentration in the basolateral growth medium from 157 ± 6 mM in "– Dox" to 116 ± 6 mM in "+ Dox" (n=3) upon kAE1 expression, supporting that the activity of kAE1 WT alters the basolateral growth medium composition. Additionally, we measured the initial cytosolic pH in cells with or without incubation of doxycycline for 24h and observed a significant acidification of the cytosolic pH in cells expressing kAE1 WT compared to the absence of kAE1 (**Figure 3.8 C**). Of note, the functionally inactive kAE1 E681Q mutant did not significantly change the cytosolic pH (**Supplementary Figure 2**). Together, these results support that the function of kAE1 WT affects cytosolic and extracellular pH and basolateral growth medium Cl^- concentration, which may alter claudin-4 function and thereby mediate the effect on tight junction properties.

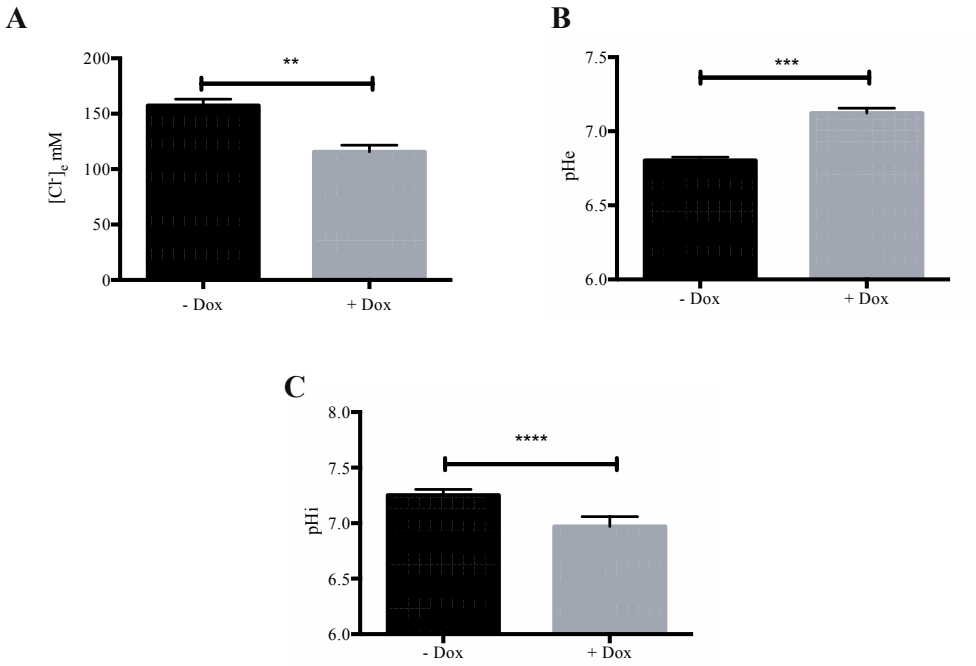

Figure 3.8: kAE1 expression alters cytosolic pH and Cl^- concentration and pH of the basolateral growth medium.

Chloride concentration (**A**) and pH (**B**) of the basolateral growth medium were measured on mIMCD3 kAE1 cells grown for 8 days on semi-permeable filters and kept un-induced or induced with doxycycline for 24 hours. **C**, Initial cytosolic pH was measured for the 20 seconds before switching from a Cl^--containing to a Cl^--free Ringer's perfusion solution in mIMCD3 kAE1 cells kept un-induced or induced for 24 hours with doxycycline. Error bars correspond to means ± SEM, n=3-7, **P < 0.01, ***P < 0.001 and ****P < 0.0001 versus mIMCD3 kAE1 cells without doxycycline.

3.3 Discussion

In this manuscript we provide evidence that kAE1 expression and function alters tight junction permeability in renal epithelial cells. Our results therefore align with the effect of kAE1 expression in polarized MDCK I cells observed by Toye and colleagues[194]. To confirm their results and further investigate this effect, we generated a mIMCD3 cell line stably expressing kAE1 upon doxycycline induction, using the Clontech pLVX-TRE3G inducible expression system. We observed that upon incubation of the cells with doxycycline, kAE1 protein was synthesized, consisting of a high mannose-carrying and a complex-carrying population of proteins at steady state[194,197,199], which predominantly localized to the basolateral membrane and was functional (**Figure 3.1 A**). Using Ussing chambers, we confirmed that inducible expression of kAE1 protein reduced the TEER of renal mIMCD3 epithelial cells. This data indicates that the effect of kAE1 on TEER is not cell type specific as it has now been observed in two distinct cell lines, mIMCD3 (our data) and MDCK I cells (Toye and colleagues)[194]. Although the increased absolute transepithelial permeability to Cl^- might reflect kAE1-induced transcellular Cl^- permeability, kAE1 was not expected to increase transcellular Na^+ permeability as it acts as a chloride-bicarbonate exchanger. We thus propose that the absolute permeability to Na^+ (and possibly that to Cl^-) is increased via the paracellular pathway. Our results further support that the effect of kAE1 on TEER is mediated by the tight junction protein claudin-4.

A four transmembrane domain protein, claudin-4 is expressed in both intercalated and principal cells of the collecting duct[205,209,210], as well as in the thin ascending limb of the loop of Henle[58,205]. This protein acts as an aldosterone-regulated and osmosensitive paracellular Na^+ barrier and Cl^- pore depending on the cell type and clone[211,212]. Claudin-4 contains a PDZ binding site in its cytosolic carboxyl terminal domain, which interacts with PDZ proteins such as MUPP1 or ZO-1 to maintain its location at the tight junction[208]. Aldosterone regulates claudin-4 abundance via threonine phosphorylation, which

leads to a sharp decrease in TEER[212]. Importantly, claudin-4 physically interacts with claudin-8[207], which promotes trafficking of the former to tight junctions. Although claudin-4 total knockout mice develop lethal hydronephrosis at one year of age[210], principal cell-specific claudin-4 knockout leads to hypotension, hypochloremia and metabolic alkalosis caused by a severe renal wasting of Cl^-, without any alteration in claudin-8 abundance[205], in agreement with our results (**Figure 3.6 A**). In contrast, claudin-8 knockout induced mistargeting and intracellular retention of claudin-4 protein[213].

We found that endogenous claudin-4 knockdown in mIMCD3 cells results in a significant decrease in TEER, in agreement with a previous report in the same cell line[208] (**Figure 3.6**). However, our results differ from those of Gong and colleagues who observed that claudin-4 knockdown increased TEER[205,207]. This discrepancy might be either due to a clonal variation of the mIMCD3 cells used, or to the experimental protocol used for measuring TEER, as we did not incubate our cells with transcellular transporter inhibitors in order to preserve kAE1 function. Interestingly, in our claudin-4 KD mIMCD3 cells (claudin-4 KD/EV), both absolute Cl^- and Na^+ permeabilities were increased (**Figure 3.6 E & F**), which may indicate that in our cell line, claudin-4 acts as a Cl^- and Na^+ barrier, or that it works in concert with another claudin providing a Cl^- barrier. Nevertheless, it is notable that either kAE1 expression (**Figure 3.1 F & G**) or claudin-4 KD has a similar effect on TEER, and absolute permeabilities to Na^+ and Cl^-.

To address whether the kAE1 effect on trans-epithelial properties was somehow related to claudin-4 while minimizing compensatory up-/down-regulations of other proteins, we tried to use two inducible systems to express kAE1 while knocking-down claudin-4. As our attempts to find non-doxycycline dependent inducible commercially available shRNA were unsuccessful, we used the claudin-4 KD/EV cell line as a control for the claudin-4 KD/kAE1 cells. Regardless kAE1 failed to

significantly alter TEER in cells knocked down for claudin-4 (**Figure 3.6 C**), inferring that the effect of kAE1 on tight junctions is mediated by claudin-4.

kAE1 expression induced an increased absolute permeability to both Cl^- and Na^+ ions although claudin-4 is reported to only act as a Cl^- pore but not as a Na^+ pore[207]. This un-expected increase in Na^+ permeability may either indicate a disorganization of tight junctions upon kAE1 expression or a more specific effect on tight junction proteins. As claudin-4 physically interacts with claudin-8[207], it is possible that alteration of claudin-4's function results in secondary modification of (an)other claudin(s) function, possibly claudin-8. Although we did not detect a significant change in claudin-8 protein abundance in claudin-4 knockdown cells (**Figure 3.6 A**), it remains possible that kAE1 expression results in alteration of its location or phosphorylation state in these cells. Such an effect of the loss of one claudin on another claudin has been documented for claudin-16 and claudin-19, whose loss of activity causes familial hypomagnesemia with hypercalciuria and nephrocalcinosis (FHHNC)[214,215]. Thus, we propose that kAE1-induced decrease in epithelial tightness is rather due to a specific remodeling of cationic and anionic paracellular pores, which will need to be investigated in future studies.

Results from the proximity ligation assay support that both claudin-4 and kAE1 are within a 30 to 40 nm distance from each other (**Figure 3.4 D**). Interestingly, we observed a signal at the upper level of the lateral membrane, likely corresponding to tight junctions. A proximity ligation assay performed on non-polarized kAE1 expressing mIMCD3 cells also revealed an intracellular signal (**Supplementary Figure 3**), supporting that the interaction occurs before full differentiation and polarization of the epithelial cells. In agreement with this finding, co-immunoprecipitation of claudin-4 shows an interaction with both immature, high mannose-carrying kAE1 as well as mature, complex-carrying kAE1 (**Figure 3.4 A**). As immature kAE1 corresponds to kAE1 protein located in the endoplasmic reticulum (ER), this data is consistent with a physical interaction between the two proteins occurring as early as in the ER.

Interestingly, in claudin-4 knockdown mIMCD3 cells, we were unable to detect kAE1 at an expression level similar to cells expressing claudin-4, despite two independent attempts to generate these cells (**Figure 3.6**). Together with the interaction occurring early in the processing pathway, it is tempting to speculate that claudin-4 possibly plays a chaperone-like effect on kAE1 processing and possibly stability, a hypothesis that will also need to be further investigated.

kAE1 is predominantly a basolateral membrane protein while claudin-4 is primarily junctional in polarized cells. Based on the proximity ligation assay performed on polarized cells, a small portion of kAE1 may be located at the tight junction. Immunolocalization and cell surface biotinylation of claudin-4 in polarized control or kAE1-expressing mIMCD3 cells reveal no striking change in claudin-4 localization or plasma membrane abundance (**Figure 3.5 C, E & F**). Given the colocalization of kAE1 and claudin-4 in mouse kidney sections (**Figure 3.5 D**) and at the cell surface in non-polarized mIMCD3 cells (**Figure 3.5 A**), we were surprised by the lack of obvious colocalization after mIMCD3 cell polarization. This may be due to the poor polarization of these cells, which makes it difficult to assess subtle localization changes by confocal microscopy. Alternatively, it is possible that the claudin-4 epitope becomes less accessible to the antibody upon integration to tight junctions. Finally, these observations may suggest that these cells or their growth conditions do not truly model the *in vivo* environment of renal intercalated cells. The colocalization of claudin-4 and kAE1 at the plasma membrane in non-polarized kAE1-expressing mIMCD3 cells (**Figure 3.5 A & B**) and at the basal membrane of mouse kidney sections (arrowhead, **Figure 3.5 D**) raises the possibility that expression of kAE1 may have relocated a portion of claudin-4 from the tight junction to the basolateral membrane, thereby altering tight junction properties, without changing its overall cell surface abundance (**Figure 3.5 E & F**). The relocation of claudins from tight junction to either the cytosol or the lateral membrane has been previously described in intestinal and pancreatic epithelial cells[216–218], highlighting that their localization

is highly dynamic. A kAE1-dependent partial relocation of claudin-4 may support a fast and possibly reversible modulation of tight junction properties in response to acute homeostatic changes. Alternatively, the alteration of cytosolic concentration of protons (and therefore likely of Cl^-) in the vicinity of claudin-4 due to kAE1 activity (**Figure 3.8**) may result in a change in claudin-4 phosphorylation status and therefore activity[212]. This latter change may allow a fast and reversible change in tight junction properties. This second hypothesis is in line with the loss of effect on tight junction properties upon expression of the functionally dead kAE1 E681Q mutant (**Figure 3.3**).

Our experiments showed that rather than kAE1 playing a scaffolding effect on tight junctions in a similar way as erythroid AE1 links cytoskeleton to plasma membrane in red blood cells[220], its activity appears to be crucial for its effect on tight junctions. Importantly, Toye and colleagues reported that the functional dRTA mutant kAE1 R901X which was mis-trafficked to the apical membrane in MDCK I cells, did not alter the epithelium tightness[194]. This finding indicates that the function of an active Cl^-/bicarbonate transporter in another location than either the basolateral membrane or tight junction is not sufficient to affect renal epithelial tightness. Therefore, our data together with Toye's results suggest that the regulation of tight junction properties by kAE1 is not only dependent on the function of the bicarbonate exchanger but possibly also on the close vicinity with claudin-4, although we don't have additional experimental evidence other than Toye's results supporting the latter at this point. We speculate that at interaction sites between claudin-4 and kAE1 at the level of tight junctions, kAE1's function generates a microenvironment where either or both Cl^- and bicarbonate local concentrations vary acutely, thus resulting in rapid alterations of claudin-4 function. Importantly, claudin-4 interacts with claudin-8 which itself regulates paracellular permeability to acidic and basic ions[221], therefore it is also possible that the claudin-4/kAE1 interaction alters paracellular flux of hydroxyl ions or protons, and plays a role in acid-base homeostasis. Finally, another alternative is that kAE1 expression may relocate

a portion of claudin-4 away from tight junctions in certain conditions, thereby affecting tight junction properties. Interestingly, a study from Sebastian and colleagues reported that RTA patients waste renal Na^+ and Cl^- even with sustained oral administration of potassium bicarbonate[191]. Upon low dietary intake of Na^+, these patients were unable to conserve Na^+ and Cl^-. We speculate that our findings highlighting a role for claudin-4/kAE1 interaction in regulating TEER and ion permeability could possibly account for the reported loss of urinary Na^+ and Cl^- in dRTA patients[191]. We propose that in dRTA patients where kAE1 function is abnormal due to a mutation in the SLC4A1 gene, the functional interaction between kAE1 and claudin-4 is altered, thus resulting in a tighter collecting duct epithelium preventing Na^+ and Cl^- reabsorption[222] and thus loss of urinary ions. This loss of urinary electrolytes would therefore not be improved by sustained correction of metabolic acidosis as it would be caused by a defective ability of kAE1 to reduce the trans-epithelial resistance, a hypothesis that will need to be tested in further studies.

4. Chapter 4: kAE1 expression affects WNK4 and SPAK phosphorylation and affects tight junction properties via a claudin-4 phosphorylation dependent pathway

4.1 Introduction

Fine-tuning of urine composition occurs in the renal collecting ducts. Collecting ducts are composed of a mixture of principal cells and intercalated cells. Principal cells are mainly responsible for transcellular water and Na^+ reabsorption through aquaporin 2 (AQP2) and epithelial Na^+ channel (ENaC), and potassium secretion through the renal outer medullary K^+ channel, ROMK. On the other hand, type-A and type-B intercalated cells work in harmony to sustain systemic acid/base balance. Type-A IC cells express apical V-H^+ ATPase to acidify the urine, and basolateral kidney anion exchanger 1 (kAE1) to reabsorb HCO_3^- to the blood stream in exchange with Cl^-. Conversely, neighbor type-B IC cells express basolateral membrane V-H^+-ATPase to reabsorb H^+, and apical pendrin, to secrete HCO_3^- into the urine. The efficiency of these transcellular fluxes also depends on the paracellular permeability of the epithelium, which is dictated by the tight junctions claudins. In humans, claudins form a 26-member family of transmembrane proteins that are localized in tight junctions[223,224]. They span the membrane 4 times and determine the tight junctions' selective permeability. One common feature shared between principal cells and intercalated cells is that both cell types express claudin-4 protein[225,226]. The main function of claudin-4 in the collecting ducts is to provide a Cl^- paracellular shunt to facilitate Cl^- reabsorption and block paracellular Na^+ back flux to the urine[207].

In the collecting duct, claudin-4 has been indirectly implicated in pseudohypoaldosteronism type II (PHA II), a disease characterised by hypertension, hyperkalemia and hyperchloremic acidosis[80]. The main cause of the disease has been genetically linked to two members of with-no-lysine kinase (WNK) family members, WNK1 and WNK4[227]. A deletion mutation in the first intron of the gene encoding WNK1 or other missense mutations in the WNK4-encoding gene have been found to cause PHA II[227].

WNK1 and 4 are highly expressed in the distal nephron. They regulate salt and potassium homeostasis transcellularly by regulating the membrane expression and activities of epithelial sodium

channel ENaC[100], the Na^+/Cl^- cotransporter NCC[102] and renal outer medullary potassium channel ROMK[101], through downstream effectors Ste20-related proline alanine rich kinase/oxidative stress responsive kinase 1 (SPAK/OSR1 kinases)[228]. WNK4 inhibits these transporters' activity by decreasing their membrane expression. WNK1 has a similar effect on ENaC and ROMK, however, it counteracts the WNK4 inhibitory effect on NCC when co-expressed in *Xenopus* oocytes[229]. Additionally, WNK1 and 4 also regulate the paracellular ionic flux in the distal nephron by increasing claudin-4 phosphorylation[80,230,231]

We have previously reported that the type-A intercalated cell-specific kAE1 expression affects TJ properties via claudin-4[226]. Encoded by *SLC4A1*, the 14 transmembrane domain glycoprotein kAE1 exchanges Cl^- for bicarbonate and when mutated, causes distal renal tubular acidosis (dRTA), a disease characterized by a metabolic acidosis, hyperchloremia, hypokalemia, nephrocalcinosis, ultimately leading to renal failure if untreated. Interestingly, dRTA patients fed a low NaCl diet display an urinary loss of Na^+ and Cl^-, even after normalization of their plasma pH[191]. When expressed in polarized Madin-Darby canine kidney (MDCKI) cells, kAE1 results in a leaky epithelium that becomes permeable to apically applied fluorescent biotin[194]. In our recent publication[226], we investigated this effect by expressing kAE1 wild-type (WT) or inactive kAE1 E681Q mutant in inducible inner medullary collecting duct (mIMCD3) cells and assessing their effect on TJ properties. We observed that expression of kAE1 WT but not the inactive mutant kAE1 E681Q, resulted in a decrease in TEER and increased permeability to NaCl, and that this effect was mediated by claudin-4. However, the mechanism by which kAE1 influences claudin-4 and TJ properties remains unknown.

In this manuscript, we hypothesized that kAE1 function affects intracellular Cl^- concentration, which triggers WNK4 kinase regulatory pathway that in turn modulates claudin-4 phosphorylation and activity. Our results show that: *(i)* kAE1 expression and function results in increased phosphorylation of

claudin-4, WNK4, and SPAK; *(ii)* WNK463 inhibits WNK4 kinase activity, and *(iii)* WNK4 inhibition combined with kAE1 expression results in decreased claudin-3 and -4 expression.

4.2 Results

4.2.1 kAE1 expression results in increased claudin-4 phosphorylation

We have previously reported that kAE1 expression affects TJs properties in mIMCD3 cells through claudin-4 and that kAE1 function is essential to this effect[226]. In that manuscript, we also reported that kAE1 expression neither affected claudin-4 abundance nor plasma membrane expression. Based on the fact that claudin-4 phosphorylation alters TJs properties[80,88,89,91,230], we decided to assess the effect of kAE1 WT and inactive kAE1 E681Q mutant expression on claudin-4 phosphorylation. Since anti-phosphorylated claudin-4 antibodies are not available, we used the immobilized iron affinity electrophoresis technique to detect changes in claudin-4 phosphorylation. The principle of this technique is based on the ability of Fe_2Cl_3 to capture phosphorylated proteins because of the negative charge(s) created by the phosphate group(s). This results in disappearance of phosphorylated proteins of interest at the expected molecular weight[232]. By comparing the intensity of the claudin-4 band in the "iron gel" with that in the "normal gel", one can assess the ratio of phosphorylated protein. As shown in **Figure 4.1 A & B**, by calculating the ratio of claudin-4 in $FeCl_3$-containing gel over that of $FeCl_3$-free gel, we found that kAE1 expression resulted in a 21 ± 3% (n=5, ± SEM) increase in claudin-4 phosphorylation. However, kAE1 E681Q expression did not have a similar effect as kAE1 WT (**Figure 4.1 C & D**) as the band density ratio of claudin-4 in the kAE1 E681Q expressing lane was not significantly different from that of the kAE1 E681Q-free lane (-6.8 ± 14.5% (n=6, ± SEM)), indicating that claudin-4 phosphorylation was not affected upon kAE1 E681Q mutant expression. Hence, kAE1 WT, but not kAE1 E681Q, expression increases claudin-4 phosphorylation in mIMCD3 cells. These results indicate that the function of kAE1 is crucial for the effect seen on claudin-4 phosphorylation.

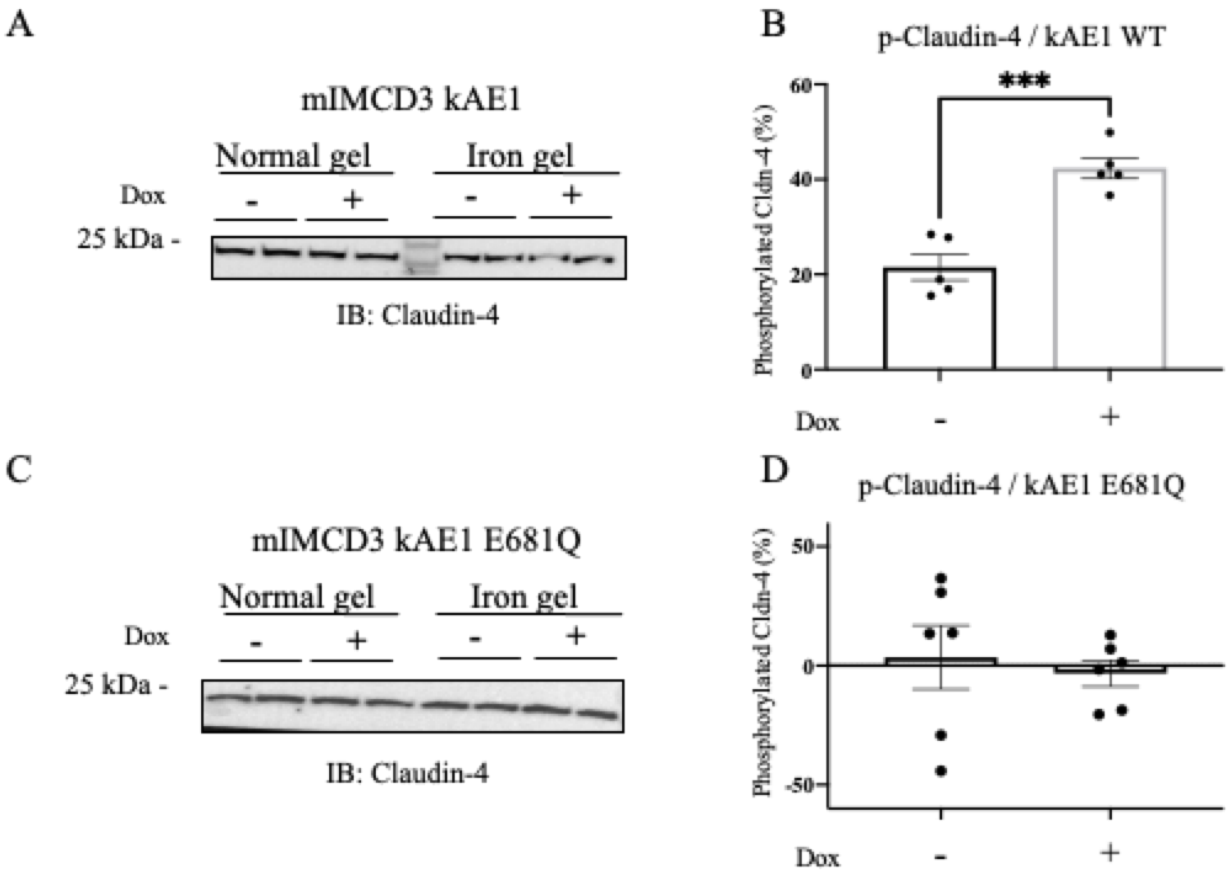

Figure 4.1: Effect of expressing kAE1 WT or E681Q protein on claudin-4 phosphorylation

Representative $FeCl_3$-free or -containing immunoblots showing claudin-4 phosphorylation (p-claudin-4) in the presence or absence of kAE1 WT (A) or E681Q proteins (C). Samples from mIMCD3 cells expressing kAE1 E681Q (Dox) or not (No Dox) were run on 10% acrylamide gels that either contain iron Cl^- or not (See material and Methods for further details). The claudin-4 bands on the "iron gel" represent the non-phosphorylated fraction of claudin-4 in these lysates. **A**, rabbit anti-claudin-4 antibody was used to detect claudin-4 protein in the presence of kAE1 WT. **B**, quantification of phosphorylated claudin-4 normalized to total claudin-4. **C**, rabbit anti-claudin-4 antibody was used to detect claudin-4 protein upon expression of of kAE1 E681Q. **D**, quantification of phosphorylated claudin-4 normalized to total claudin-4. Error bars correspond to means ± SEM, n=5 or 6. No significant (n.s.), ***$P < 0.001$ using a Student's t-test.

4.2.2 kAE1 neither affects ERK 1/2 expression nor its phosphorylation

As claudin-4 is phosphorylated by several kinases, including ERK 1/2 kinases[80,88–91], we decided to investigate the effect of kAE1 expression on ERK 1/2 expression and phosphorylation. Claudin-4 phosphorylation by ERK 1/2 results in the removal of claudin-4 from the TJs and a reduction in TEER[90]. As illustrated in **Figure 4.2 A & B**, kAE1 expression did not alter ERK 1/2 expression levels, as in absence of kAE1 expression, ERK 1/2 to β-actin ratio corresponded to 0.4 ± 0.0 (n=3, ± SEM, normalized to β-actin), a ratio identical to ERK 1/2 abundance in the presence of kAE1 (0.4 ± 0.0, n=3, ± SEM, normalized to β-actin). Likewise, looking at ERK 1/2 phosphorylation using anti-phospho-ERK 1/2 antibodies, kAE1 expression did not cause any effect on ERK 1/2 phosphorylation **(Figure 4.2 C & D**) (No dox 1.4 ± 0.1, Dox 1.3 ± 0.1, n=3, ± SEM, normalized to β-actin). These results indicate that kAE1 neither affects ERK 1/2 expression nor phosphorylation and that claudin-4 phosphorylation upon kAE1 expression is not mediated by ERK 1/2 kinase.

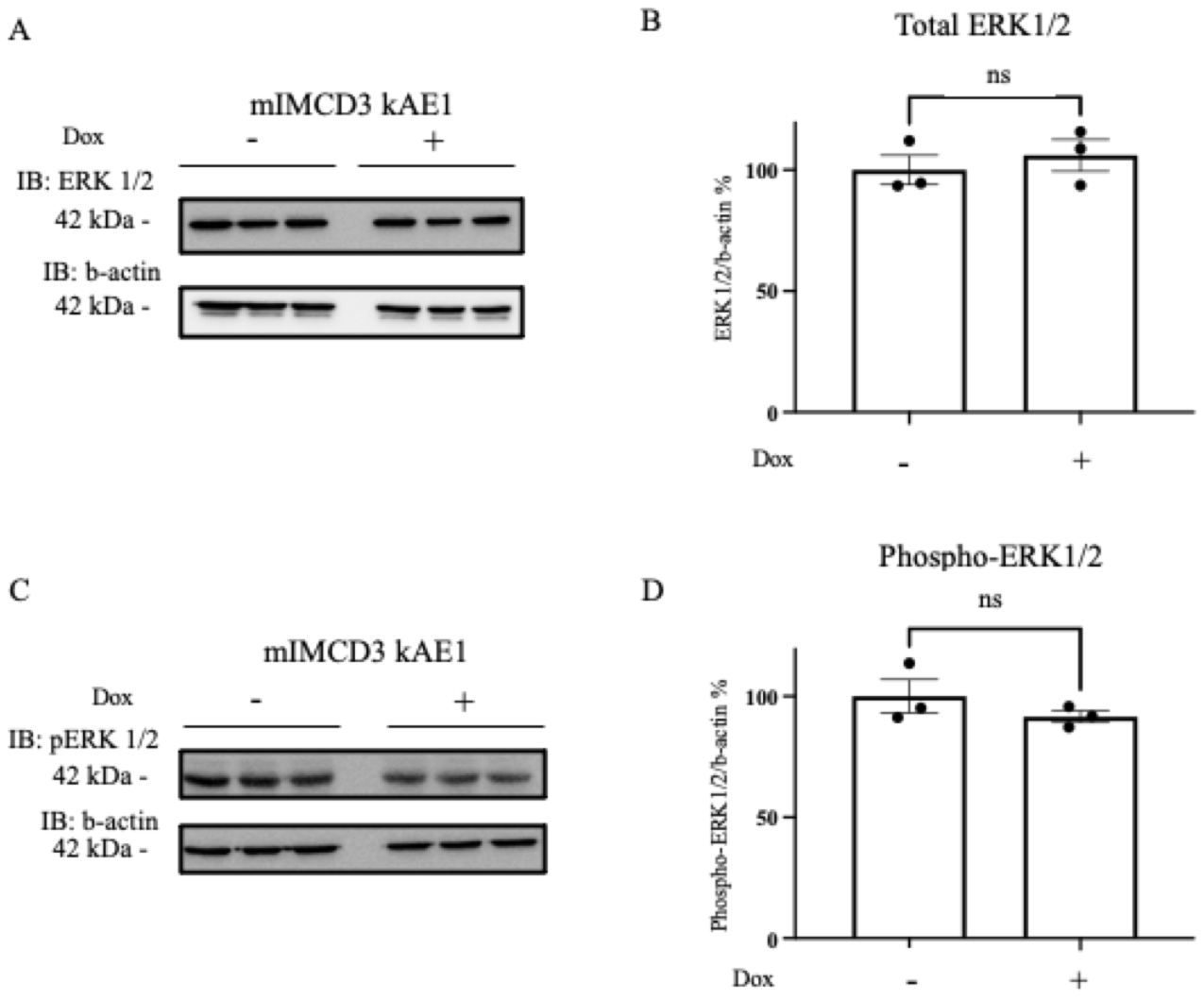

Figure 4.2: kAE1 WT neither affects ERK 1/2 expression nor phosphorylation

mIMCD3 kAE1 WT cells were seeded to 100% confluency and either induced with doxycycline for 24 hours (Dox) or not (No dox) prior to lysis **A**, immunoblot using mouse anti ERK 1/2 and mouse anti β-actin antibodies. **B**, quantification of total ERK 1/2 normalized to β-actin. **C**, immunoblot using mouse anti-phospho-ERK 1/2 and mouse anti-β-actin antibodies. **D**, quantification of phospho-ERK 1/2 normalized to β-actin. Error bars correspond to means ± SEM, n = 3. Not significant (n.s.), using a Student's t-test.

4.2.3 WNK4 is endogenously expressed in mIMCD3 cells and kAE1 affects its phosphorylation and function

As WNK4 is sensitive to Cl^-[98,233], an anion that is a kAE1 substrate, and since kAE1 affects claudin-4 phosphorylation, we hypothesized that WNK4 is involved in kAE1 effect on claudin-4 phosphorylation. We first confirmed that mIMCD3 cells express WNK4 endogenously. Quantitative RT-PCR not only confirmed that mIMCD3 cells express endogenous WNK4, but also L-WNK1 (**Figure 4.3 A**). At the mRNA level, kAE1 expression did not cause any significant change on L-WNK1 mRNA, however, it significantly decreased WNK4 transcript abundance. We confirmed the endogenous expression of WNK4 by immunoblotting for WNK4 protein using rabbit anti-WNK4 antibodies (kind gift from Dr. Maria Chavez-Canales), which showed the expected band at approximately 135 kDa (**Figure 4.3 B**). Based on this finding, we aimed to assess kAE1's effect on WNK4 abundance and phosphorylation state. We quantified the relative amount of WNK4 expression in mIMCD3 cells in presence and absence of kAE1 protein. As shown on **Figure 4.3 B & C**, immunoblot experiments revealed that kAE1 expression had no effect on WNK4 protein abundance. To assess the effect of kAE1 expression on WNK4 phosphorylation, we used rabbit anti-phospho-WNK4 (S1196) antibodies (kind gift from Dr. Maria Chavez-Canales) to detect phosphorylated WNK4. As shown in **Figure 4.3 D & E**, WNK4 phosphorylation increased by 32 ± 8% (n=4, ± SEM) upon kAE1 WT expression in mIMCD3 cells. To determine whether the effect of kAE1 on WNK4 phosphorylation is merely due to kAE1 expression or whether its function is necessary, we assessed WNK4 abundance and phosphorylation upon expression of kAE1 E681Q mutant in mIMCD3 cells. As shown in **Figure 4.4 A & B**, kAE1 E681Q expression neither affected WNK4 abundance nor its phosphorylation in mIMCD3 cells. These results indicate that kAE1 function is required to affect WNK4 phosphorylation level.

To further investigate and confirm kAE1's effect on WNK4, we next determined the phosphorylation status of a known downstream substrate of WNK4, SPAK, by using anti-phospho-SPAK (S373) antibodies. SPAK is phosphorylated by WNK4 and is involved in the regulatory pathway of NCC[228]. As demonstrated in **Figure 4.3 F & G**, kAE1 WT expression resulted in increased phosphorylation of SPAK by 31 ± 12% (n=4, ± SEM), in line with WNK4's increased phosphorylation. However, although SPAK phosphorylation showed an increased trend upon kAE1 E681Q expression, statistical analysis indicated that it is insignificant, (**Figure 4.4 C & D**). Altogether, these results confirm that kAE1 function more than its expression increases WNK4 phosphorylation and phosphorylation of its downstream effector SPAK.

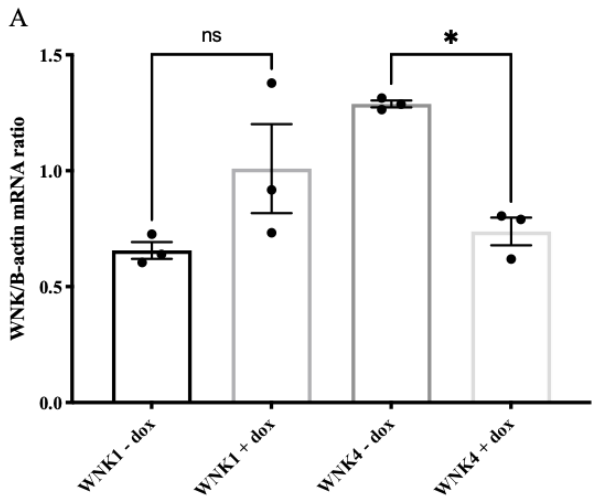
A
ns
*
1.5
1.0
0.5
0.0
WNK/B-actin mRNA ratio
WNK1 - dox
WNK1 + dox
WNK4 - dox
WNK4 + dox

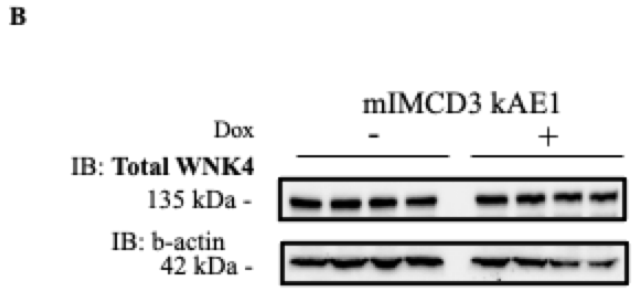
B
mIMCD3 kAE1
Dox
-
+
IB: Total WNK4
135 kDa -
IB: b-actin
42 kDa -

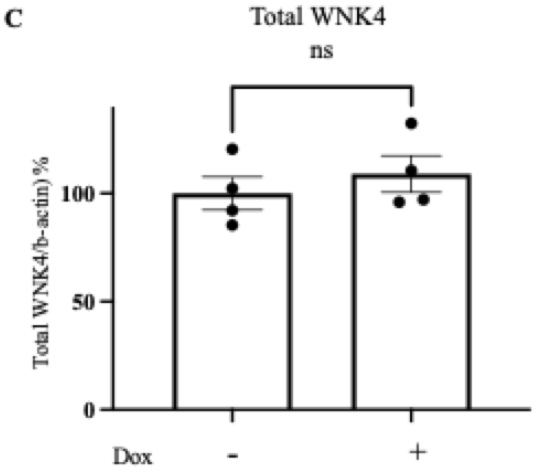
C
Total WNK4
ns
Total WNK4/b-actin) %
100
50
0
Dox
-
+

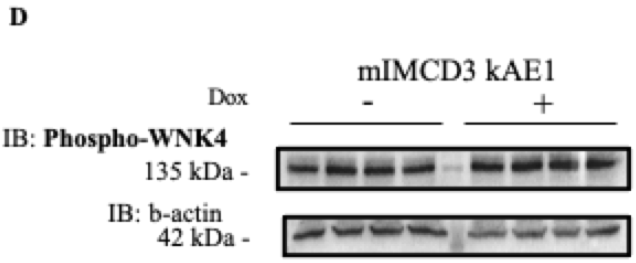
D
mIMCD3 kAE1
Dox
-
+
IB: Phospho-WNK4
135 kDa -
IB: b-actin
42 kDa -

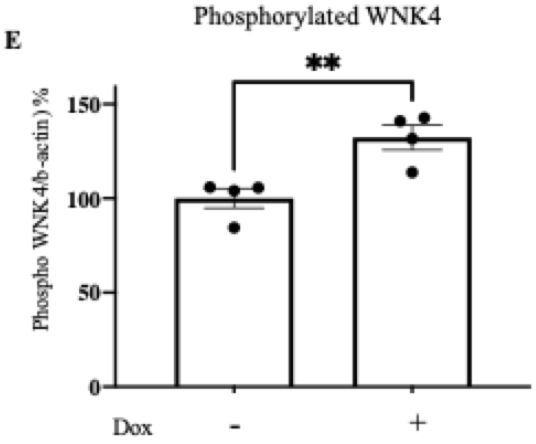
E
Phosphorylated WNK4
**
Phospho WNK4/b-actin) %
150
100
50
0
Dox
-
+

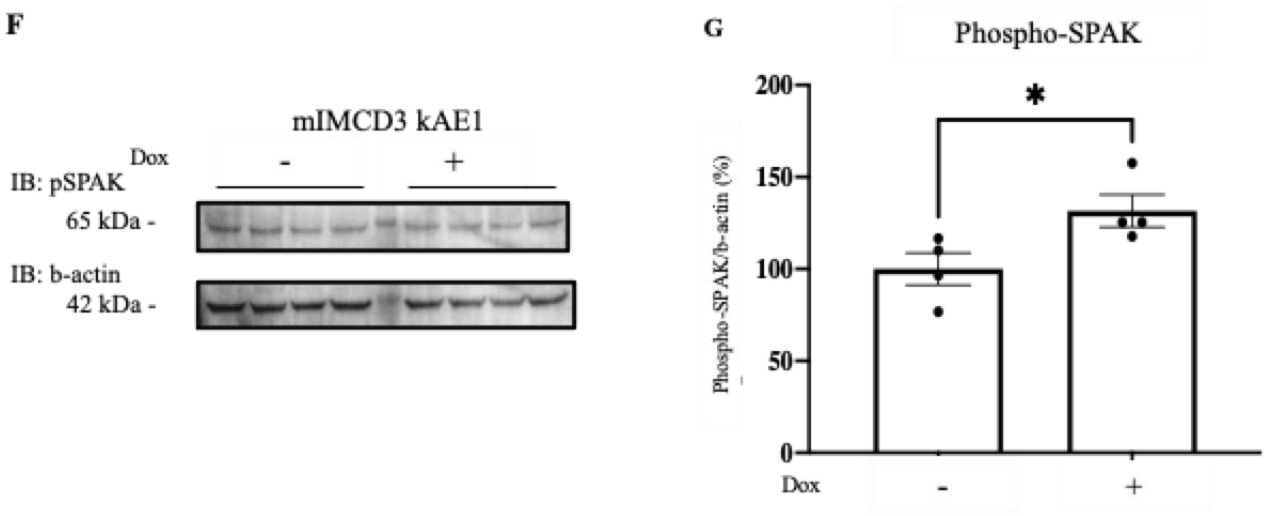

Figure 4.3: mIMCD3 cells express endogenous WNK1/4, and kAE1 protein expression increases WNK4 and SPAK phosphorylation.

A, quantitative RT-PCR analysis of L-WNK1 and WNK4 mRNA abundance in mIMCD3 cells. **B**, Immunoblots using rabbit anti-total WNK4 or mouse anti β-Actin antibodies to detect total WNK4 or β-Actin, respectively, in the presence or absence of kAE1 WT proteins. **C**, quantification of total WNK4 normalized to β-actin. **D**, Immunoblots using rabbit anti-phospho-WNK4 (pWNK4) or mouse anti β-Actin antibodies to detect pWNK4 or β-Actin, respectively, in the presence or absence of kAE1 WT proteins. **E**, quantification of pWNK4 normalized to β-actin. **F**, immunoblots showing phosphorylated SPAK (pSPAK) in the presence or absence of kAE1 WT proteins using sheep anti-phospho-SPAK antibody. **G**, represent quantification of pSPAK normalized to β-actin. Error bars correspond to means ± SEM, n = 3 or 4. Not significant (n.s.), *P < 0.05, **P < 0.01 using one-way ANOVA (A) or a Student's t-test (C, E and G).

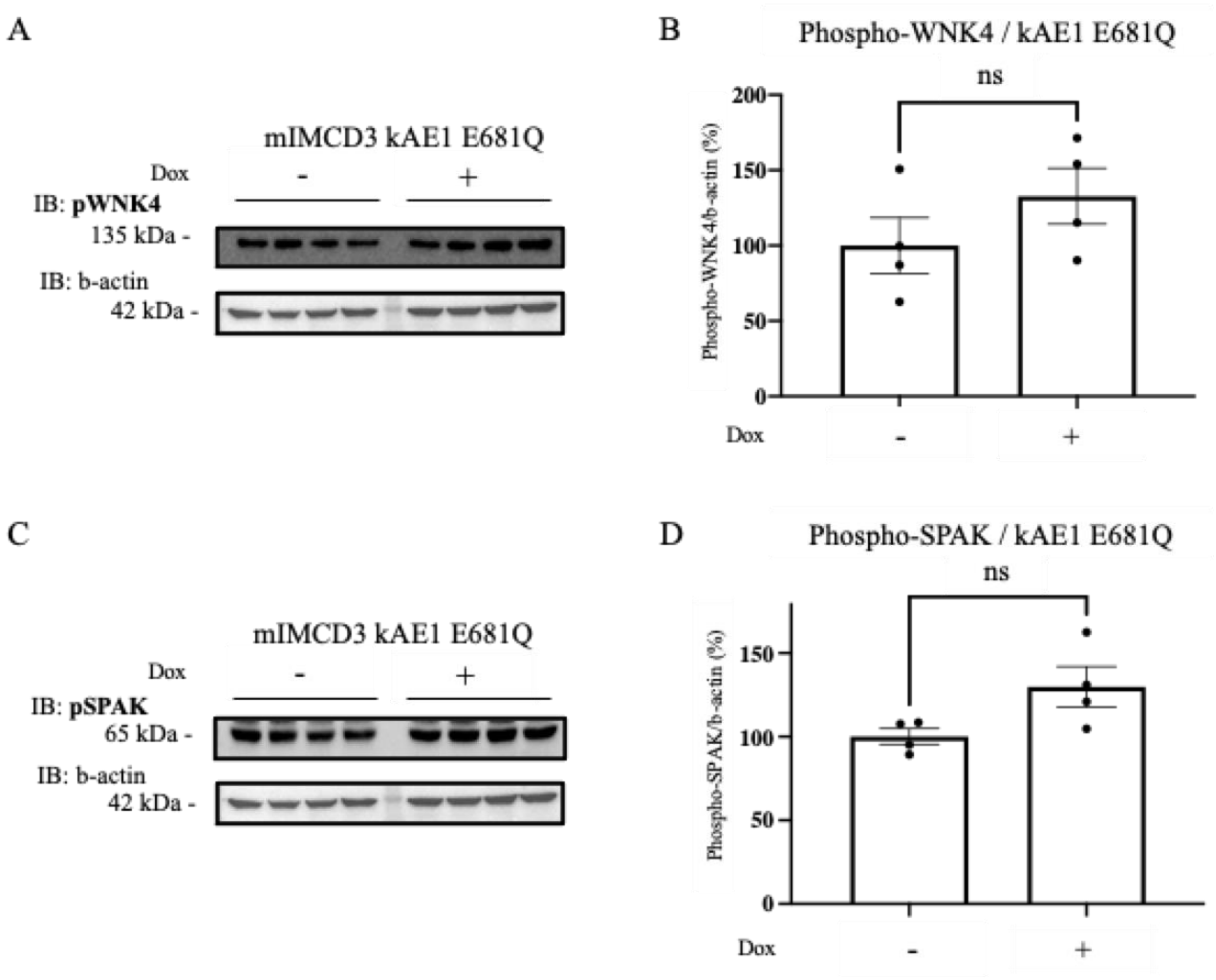

Figure 4.4: kAE1 E681Q protein neither affects WNK4 nor SPAK phosphorylation.

A, rabbit anti phospho-WNK4 or mouse anti-β-actin antibodies were used to detect phospho-WNK4 (pWNK4) or β-actin, respectively, in the presence or absence of kAE1 E681Q proteins. **B**, quantification of pWNK4 normalized to β-actin. **C**, immunoblots showing phosphorylated SPAK (pSPAK) in the presence or absence of kAE1 E681Q proteins using sheep anti phospho-SPAK antibody. **D**, quantification of phospho-SPAK normalized to β-actin. Error bars correspond to means ± SEM, n = 4. Not significant (n.s.) using a Student's t-test.

4.2.4 WNK463 inhibits WNK4 activity

To assess whether claudin-4 phosphorylation is a downstream effect of kAE1 expression/WNK4 phosphorylation cascade, we used WNK463 inhibitor[234] to block WNK4 kinase activity and assess kAE1 effect on tight junction properties and claudin-4 phosphorylation status. Note that this inhibitor is also expected to inhibit WNK1[234]. We first determined the right concentration and incubation time for the optimal inhibitory effect of WNK463. Based on the current literature, mIMCD3 cells were incubated with 4 μM of WNK463 for three different time points: zero hour (negative control), two hours and 24 hours before lysing the cells. Next, we performed an immunoblot to assess total WNK4, phosphorylated WNK4 and phosphorylated SPAK abundance. As illustrated in **Figure 4.5 A to D**, 2 hours incubation time neither caused a significant change in total nor phosphorylated WNK4. However, after a 24 hour incubation time with WNK463, both total and phosphorylated WNK4 increased by 44 ± 7% (n=3, ± SEM) and 84 ± 19% (n=3, ± SEM), respectively, in comparison to the negative control. These results support that a 2 hour incubation time with 4 μM of WNK463 neither affects WNK4 phosphorylation nor its total abundance significantly. However, looking at WNK4 downstream substrate kinase SPAK, we found that its phosphorylation was inhibited by 42 ± 5% (n=3, ± SEM) after 2 hours of incubation with WNK463 (**Figure 4.5 E & F**). The inhibitory effect of WNK463 on WNK4 kinase activity lasted for the 24 hour incubation time, with a decreased phosphorylation level by 47 ± 5% (n=3, ± SEM). These results validate WNK463 as an effective inhibitor for WNK4 kinase activity and provide us with optimal concentration and incubation time for WNK4 inhibition.

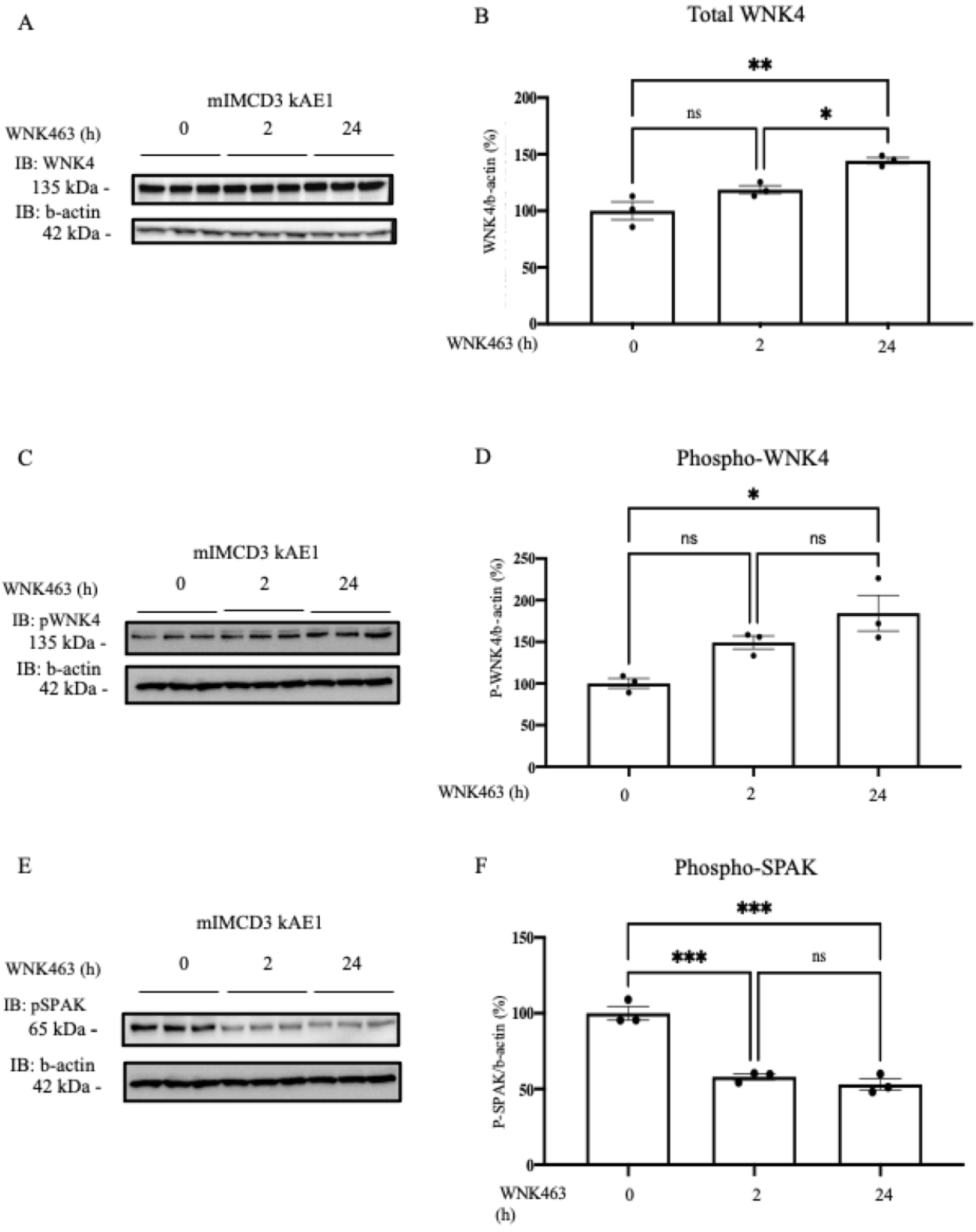
A
mIMCD3 kAE1
WNK463 (h)
0
2
24
IB: WNK4
135 kDa -
IB: b-actin
42 kDa -
B
Total WNK4
**
ns
*
WNK4/b-actin (%)
200
150
100
50
0
WNK463 (h)
0
2
24
C
mIMCD3 kAE1
WNK463 (h)
0
2
24
IB: pWNK4
135 kDa -
IB: b-actin
42 kDa -
D
Phospho-WNK4
*
ns
ns
P-WNK4/b-actin (%)
250
200
150
100
50
0
WNK463 (h)
0
2
24
E
mIMCD3 kAE1
WNK463 (h)
0
2
24
IB: pSPAK
65 kDa -
IB: b-actin
42 kDa -
F
Phospho-SPAK
***
***
ns
P-SPAK/b-actin (%)
150
100
50
0
WNK463
(h)
0
2
24

Figure 4.5: WNK463 inhibits WNK4 kinase activity.

mIMCD3 cells were incubated with 4 μM of WNK463 inhibitor for different incubation times: 0, 2 and 24 hours. **A**, rabbit anti-WNK4 antibody or mouse anti β-Actin antibodies were used to detect total WNK4 or β-Actin proteins, respectively. **B**, Effect of WNK463 on WNK4 total expression at different time points after normalizing to housekeeping protein β-Actin. **C**, rabbit anti-phospho-WNK4 (pWNK4) antibody or mouse anti-β-Actin antibodies were used to detect pWNK4 or β-Actin proteins, respectively. **D**, Effect of WNK463 on WNK4 phosphorylation at different time points after normalization to housekeeping protein β-Actin. **E**, sheep anti-phospho-SPAK or mouse anti-β-Actin antibodies were used to detect pSPAK or β-Actin proteins, respectively. **F**, Effect of WNK463 on SPAK phosphorylation at different time points after normalization to housekeeping protein β-Actin. Error bars correspond to means ± SEM, n = 3. *P < 0.05, **P < 0.01, ***P < 0.001 using one-way ANOVA.

4.2.5 WNK463 inhibitor decreases transepithelial electrical resistance

To assess whether kAE1 effect on TJ properties is mediated by WNK4, we inhibited WNK4 function using WNK463 inhibitor and assessed TJ properties of mIMCD3 cells in the presence or absence of kAE1. We grew confluent mIMCD3 kAE1 WT cells on semi-permeable Transwell filters for 10 days. 24 hours prior to the experiment, we defined 4 experimental conditions based on the presence or absence of *(i)* kAE1 and/or *(ii)* WNK463 inhibitor (see **Table 4.1**). Cells that were neither incubated with doxycycline nor WNK463 were used as negative control (condition A) and the effect of kAE1 expression only (condition B), WNK4 inhibition only (condition C) or both kAE1 expression and WNK4 inhibition (condition D) on TEER was measured. We expected that WNK4 inhibition by WNK463 would attenuate/cancel kAE1 effect on TJ properties.

As illustrated in **Figure 4.6 A** and consistently with our previous observations[226], kAE1 expression decreased the TEER by 40 ± 5% (n=4, ± SEM). Unexpectedly, WNK4 inhibition using WNK463 caused a decrease in TEER by nearly 51 ± 5% (n=4, ± SEM) as well. Furthermore, the combination of both kAE1 expression and WNK4 inhibition resulted in a further decrease in TEER by 88 ± 5% (n=4, ± SEM), indicating an additive effect of kAE1 and WNK inhibition rather than the expected cancellation of kAE1 effect by the WNK inhibitor. The Na^+ to Cl^- absolute permeability ratio was not significantly altered upon incubation with doxycycline (P_{Na}/P_{Cl}: A = 0.97 ± 0.04, B = 0.93 ± 0.04, C = 0.95 ± 0.04, D = 0.89 ± 0.04, n=4, ± SEM, see **Table 4.1**) (**Figure 4.6 B**), however, the absolute permeabilities to both Na^+ and Cl^- increased significantly only with the combined incubation of doxycycline and WNK463 (**Figure 4.6 C & D**). The permeability to Na^+ increased from 0.10 ± 0.30 10^{-4} cm/s to 1.03 ± 0.10 10^{-4} cm/s (n=4, ± SEM) and that of Cl^- increased from 0.105 ± 0.2 10^{-4} cm/s to 1.1 ± 0.1 10^{-4} cm/s (n=4, ± SEM) upon doxycycline and WNK463 incubation. We conclude that WNK463 incubation caused a similar decrease in transepithelial electrical resistance to kAE1 expression. However,

WNK463 inhibitor did not cancel kAE1 effect on TJ properties and instead its incubation in addition to kAE1 expression had a more severe impact on the TEER.

Table 4.1: Experimental conditions used in Figure 4.6

Condition	A	B	C	D
Doxycycline	-	+	-	+
WNK463	-	-	+	+

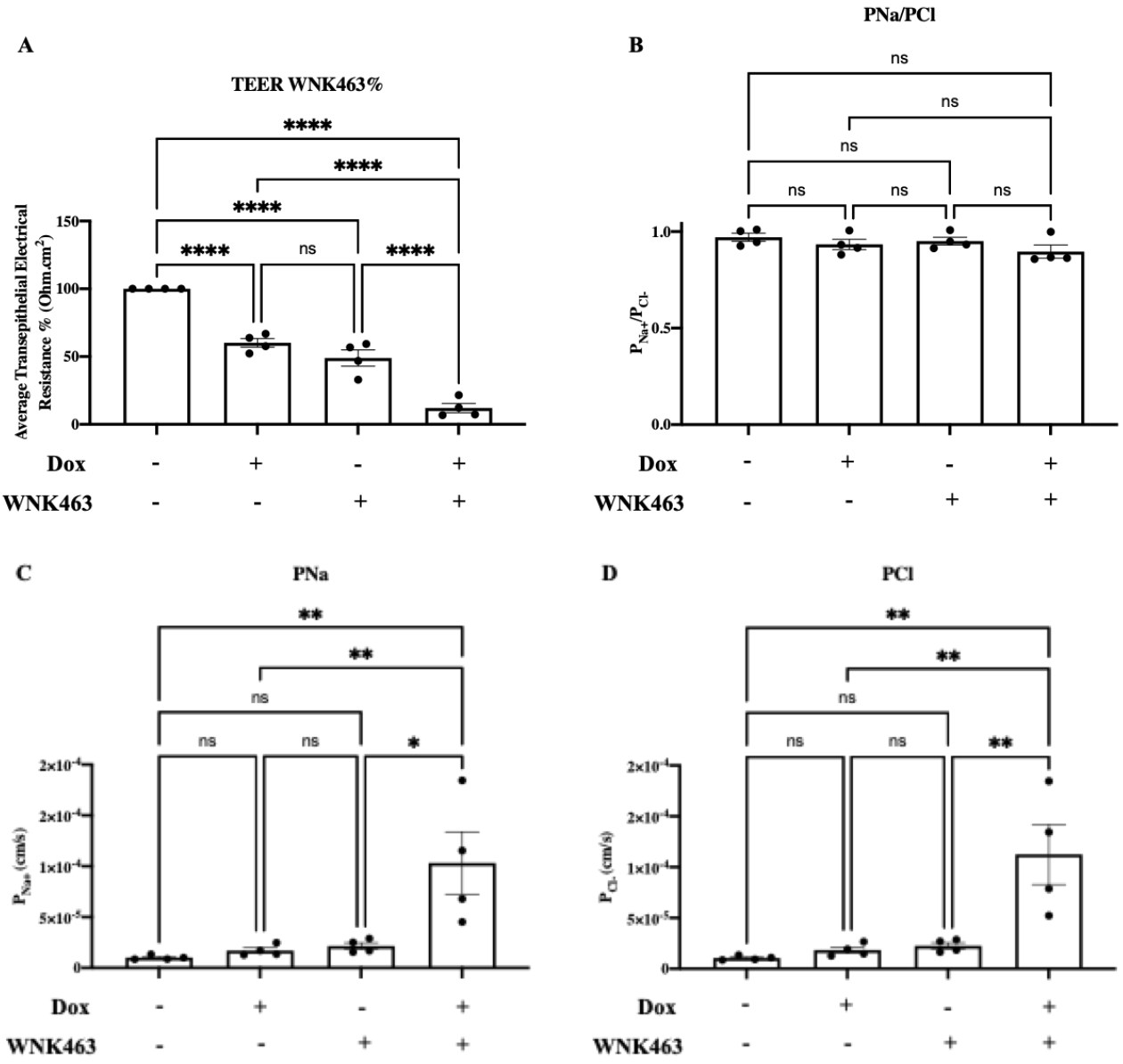

Figure 4.6: WNK463 decreases TEER and its effect is additive to that of kAE1 expression

A, mIMCD3 cells that inducibly express kAE1 WT were seeded on semi-permeable filters for 10 days. 24 hours prior experiment, cells were either induced with doxycycline or not, with or without doxycycline and with or without WNK463 and TEER was measured in Ussing chambers. **B**, P_{Na}/P_{Cl} ratio in the various conditions. **C** and **D**, absolute permeability of the epithelium to $Na^+$and Cl^- in the various conditions. Error bars correspond to means ± SEM, n=4. Not significant (n.s.), *P < 0.05, **P < 0.01, ****P < 0.0001 versus "No Dox/No WNK463" condition using one-way ANOVA.

To assess whether the additive effect of WNK463 and kAE1 expression on TJ was due to an unwanted inhibition of transcellular transporters upon WNK4 inhibition, we repeated the previous experiment in the presence of inhibitors of transcellular transporters[100]: we incubated the cells with 0.1 mM of amiloride from the apical side and 0.1 mM of bumetanide on the basolateral-side to block ENaC and NKCC1, respectively, as previously reported[87]. In the absence of these inhibitors, upon incubation with doxycycline and WNK463 we saw an additive impact on TEER and absolute permeability of Na^+ and Cl^-, however there was no significant effect on the P_{Na}/P_{Cl} ratio. Upon addition of amiloride and bumetanide in the presence or absence of doxycycline/WNK463 (**Table 4.2** and **Figure 4.7 A**), kAE1 expression reduced the TEER by 54 ± 2% (n=6, ± SEM), indicating that transcellular transporters do not significantly contribute to kAE1 effect on TJ properties. WNK4 inhibition reduced the TEER by 72 ± 2% (n=6, ± SEM) compared to 51 ± 5% (n=4, ± SEM) in absence of transcellular inhibitors, indicating that WNK4-sensitive ENac and/or NKCC1 contribute to the overall TEER. Finally, both kAE1 expression and WNK4 inhibition reduced the TEER by 85 ± 1% (n=6, ± SEM), a value similar to TEER in the same condition but in absence of transcellular transporter inhibitors (88 ± 5% (n=4, ± SEM)).

The P_{Na}/P_{Cl} ratio significantly decreased upon addition of doxycycline, WNK463 or combined (P_{Na}/P_{Cl}: A = 1.08 ± 0.8 10^{-2}, B = 1.03 ± 0.01, C = 0.98 ± 0.4 10^{-2} and D = 0.93 ± 0.3 10^{-2} cm/s, n=6, ± SEM, see **Table 4.2**), (**Figure 4.7 B**). The absolute permeabilities to both Na^+ and Cl^- increased significantly with the incubation of WNK463. The permeability to Na^+ increased from A = 0.65 ± 0.30 10^{-5} cm/s to C = 2.2 ± 0.6 10^{-5} cm/s and D = 4.3 ± 0.4 10^{-5} cm/s, (n=6, ± SEM) (**Figure 4.7 C**). The permeability to Cl^- increased from A = 0.6 ± 0.3 10^{-5} cm/s to C = 2.2 ± 0.1 10^{-5} cm/s, and D = 4.6 ± 0.4 10^{-5} cm/s, (n=6, ± SEM) (**Figure 4.7 D**), indicating a slightly larger increase in P_{Cl} than P_{Na} upon WNK463 and doxycycline incubation in the presence of ENaC and NKCC1 inhibitors.

These results suggest that kAE1 effect on TEER is either independent of WNK4 kinase despite its aforementioned effect on WNK4 phosphorylation and activity, or that WNK1/4 inhibition produces additional effects on proteins involved in TJ properties independent of kAE1 expression.

Table 4.2: Experimental conditions used in Figure 4.7

Conditions	A	B	C	D
Doxycycline	-	+	-	+
WNK463	-	-	+	+
Transcellular inhibitors	+	+	+	+

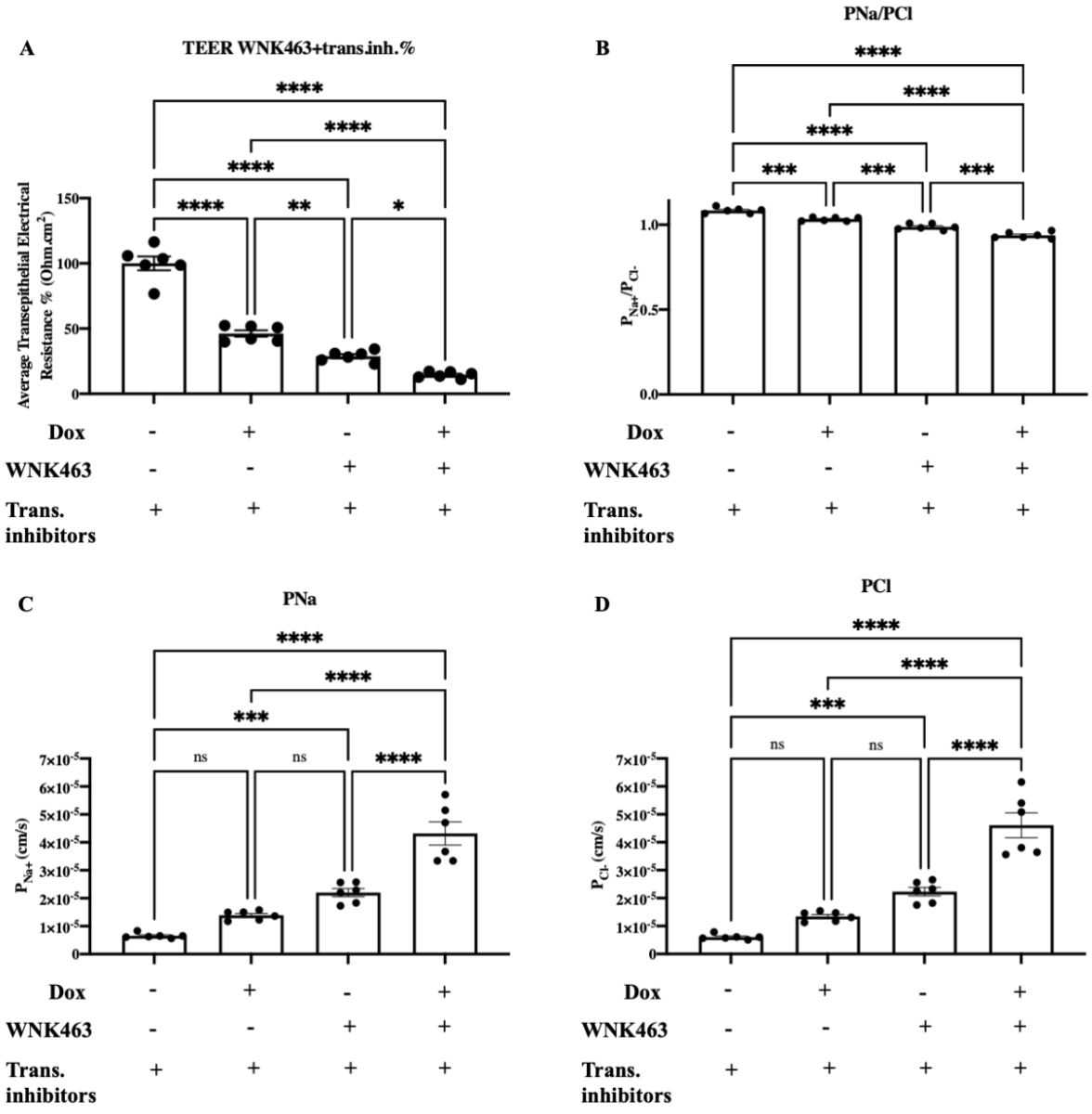

Figure 4.7: Transcellular inhibitors affect TJ properties, but neither reverse kAE1 nor WNK463 effects on TJ properties

A-D Same experimental design as in **Figure 4.6** but with the addition of 0.1 mM amiloride to the apical side and 0.1 mM of bumetanide to the basolateral side at the beginning and during the course of the experiment to inhibit transcellular transporters ENaC and NKCC1, respectively, **A**, TEER, **B**, P_{Na}/P_{Cl}, **C**, P_{Na} and **D**, P_{Cl}. Error bars correspond to means ± SEM, n=6. Not significant (n.s.), *P < 0.05, **P < 0.01, ***P < 0.001****P < 0.0001 versus "No Dox/No Wnk463" condition, using one-way ANOVA.

4.2.6 WNK463 decreases claudin-3 and -4 abundance

To understand the origin of the additive effect of WNK463 combined with kAE1 WT expression, we assessed whether WNK463 inhibitor alters other claudins abundance, since they are major determinants of tight junction integrity. Claudin-3, -4 and -8 are expressed in collecting duct cells[82]. Claudin-4 facilitates paracellular Cl^- flux[82], whereas claudin-3 serves as a general blocker of cations and anions[58]. In our recent publication we demonstrated that mIMCD3 cells express both claudins endogenously[226]. We therefore looked at claudin-3 and -4 total protein abundance upon WNK463 incubation as both claudin-3 and -4 are phosphorylated by WNK4 in MDCK II cells[80]. As illustrated in **Figure 4.8 A & B**, WNK4 inhibition accompanied by kAE1 expression reduced claudin-4 abundance by 42 ± 3%, (n=3, ± SEM), in comparison to the control condition. On the other hand, as shown in **Figure 4.8 C & D**, claudin-3 abundance was reduced by 20 ± 1%, (n=3, ± SEM), upon kAE1 expression, and by 30 ± 4%, (n=3, ± SEM), upon WNK4 inhibition in addition to kAE1 expression. These results, along with the results obtained from Ussing chambers, imply that WNK463 inhibitor in addition to kAE1 expression result in decreased abundance of both claudins, possibly followed by the removal of claudin-3 and -4 from TJs (based on decreased TEER) that may result in their subsequent degradation (decrease in protein abundance).

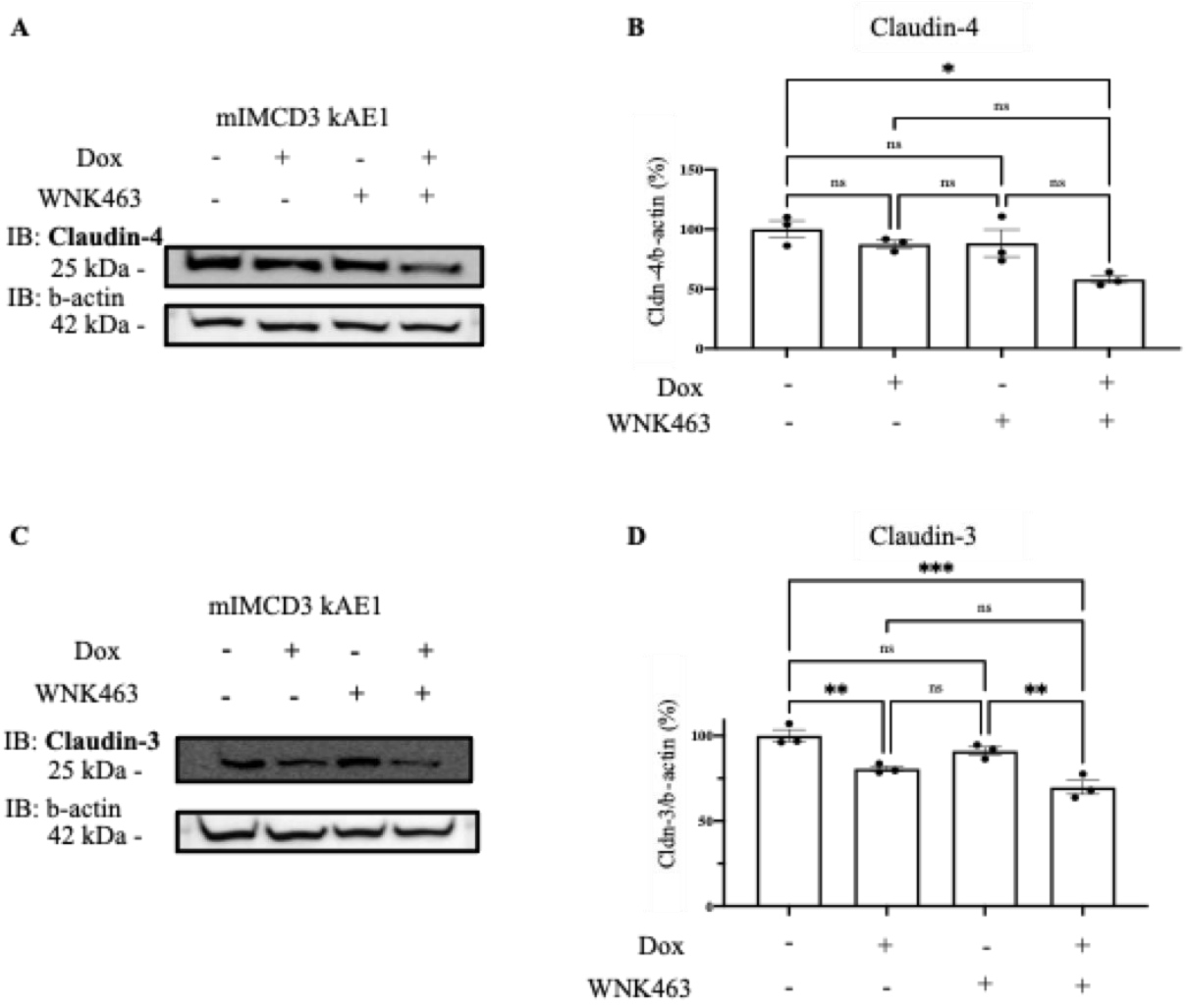

Figure 4.8: WNK463 decreases claudin-3 & -4 expression

mIMCD3 cells were incubated with 4 μM of WNK463 inhibitor 24 hours prior to lysis. **A**, rabbit anti-claudin-4 or mouse anti-β-Actin antibodies were used on this representative immunoblot to detect total claudin-4 or β-Actin proteins, respectively. **B**, Effect of WNK463 on claudin-4 total abundance upon induction of kAE1 expression normalized to housekeeping protein β-Actin. **C**, rabbit anti-claudin-3 or mouse anti-β-Actin antibodies were used on this representative immunoblot to detect claudin-3 or β-Actin proteins, respectively. **D**, Effect of WNK463 on claudin-3 total abundance upon induction of kAE1

expression normalized to housekeeping protein β-Actin. Error bars correspond to means ± SEM, n=3. Not significant (n.s.), *P < 0.05, **P < 0.01, ***P < 0.001, using one-way ANOVA.

4.2.7 dRTA mutants S525F and R589H affect TJ properties

We have previously reported that kAE1 WT modulates TJ properties via claudin-4 using Ussing chambers. *In vivo*, kAE1 is expressed in type-A IC cells in the collecting ducts and mutations in *SLC4A1* gene cause dRTA. Sebastian and colleagues showed that dRTA patients subjected to a low NaCl diet displayed urinary Na^+ and Cl^- loss[191], suggesting that these patients may have a collecting duct epithelium less permeable to these ions. We thus decided to assess the effect of expressing two kAE1 S525F & R589H dRTA mutants on TJ properties. Dominant kAE1 R589H mutant was identified in dRTA patients, and is as active as kAE1 WT[199,235]. kAE1 S525F mutant is a newly identified dRTA mutant whose molecular defect is unknown[236]. We generated mIMCD3 cells that either inducibly express kAE1 S525F or R589H mutant. Both mutants migrated similarly to kAE1 WT on SDS-PAGE as two bands corresponding to high mannose- (lower band) and complex- (upper band) carrying kAE1 proteins (**Figure 4.9 A)**. They were also properly targeted to the basolateral membrane similar to kAE1 WT (**Figure 4.9 B)**. We next assessed the functional activity of these mutants in comparison to kAE1 WT by measuring the initial rate of intracellular alkalization of each mutant upon removal of extracellular chloride. As illustrated in **Figure 4.9 C**, kAE1 S525F mutant showed only 38 ± 6% (n=4, ± SEM) alkalization rate in comparison to kAE1 WT, which was not significantly different from the negative control (No dox) that had an alkalization rate of 11 ± 2% (n=9, ± SEM). On the other hand, R589H mutant showed a similar functional activity as kAE1 WT by displaying 73 ± 17% (n=8, ± SEM) alkalization rate that was not significantly different from kAE1 WT, as previously reported[199] These results indicate that the 2 dRTA mutants are targeted properly to the basolateral membrane, however, they have different exchange rate activities.

Next, we assessed the mutants' effect on TJ properties. We grew kAE1 WT, kAE1 S525F, or kAE1 R589H mutants cells for 10 days on semi-permeable filters and induced kAE1 expression 24 hours prior to starting the experiment. As illustrated in **Figure 4.9 D**, while kAE1 WT expression decreased the TEER by 45 ± 8% (n=4, ± SEM), in agreement with our previous findings, expressing the inactive kAE1 S525H mutant in mIMCD3 cells caused only a 19 ± 1% (n=6, ± SEM) decrease in TEER, compared to cells that were not incubated with doxycycline. Although this effect on TEER was significantly different from the negative control, it was also significantly different from kAE1 WT effect on the TEER. On the other hand, expression of the active kAE1 R589H mutant resulted in 60 ± 3% (n=6, ± SEM) reduction in TEER in comparison to cells that were not incubated with doxycycline. The effect of kAE1 R589H mutant on TEER was not significantly different from that of kAE1 WT. These results indicate that the effect of these mutants' expression on TJ properties is proportional to their functional activities as the most active kAE1 R589H mutant caused the greatest TEER decrease while the inactive kAE1 S525F mutant had only a minor effect on TJ properties. These results are in agreement with our previous observation using the functionally dead kAE1 E681Q engineered mutant.

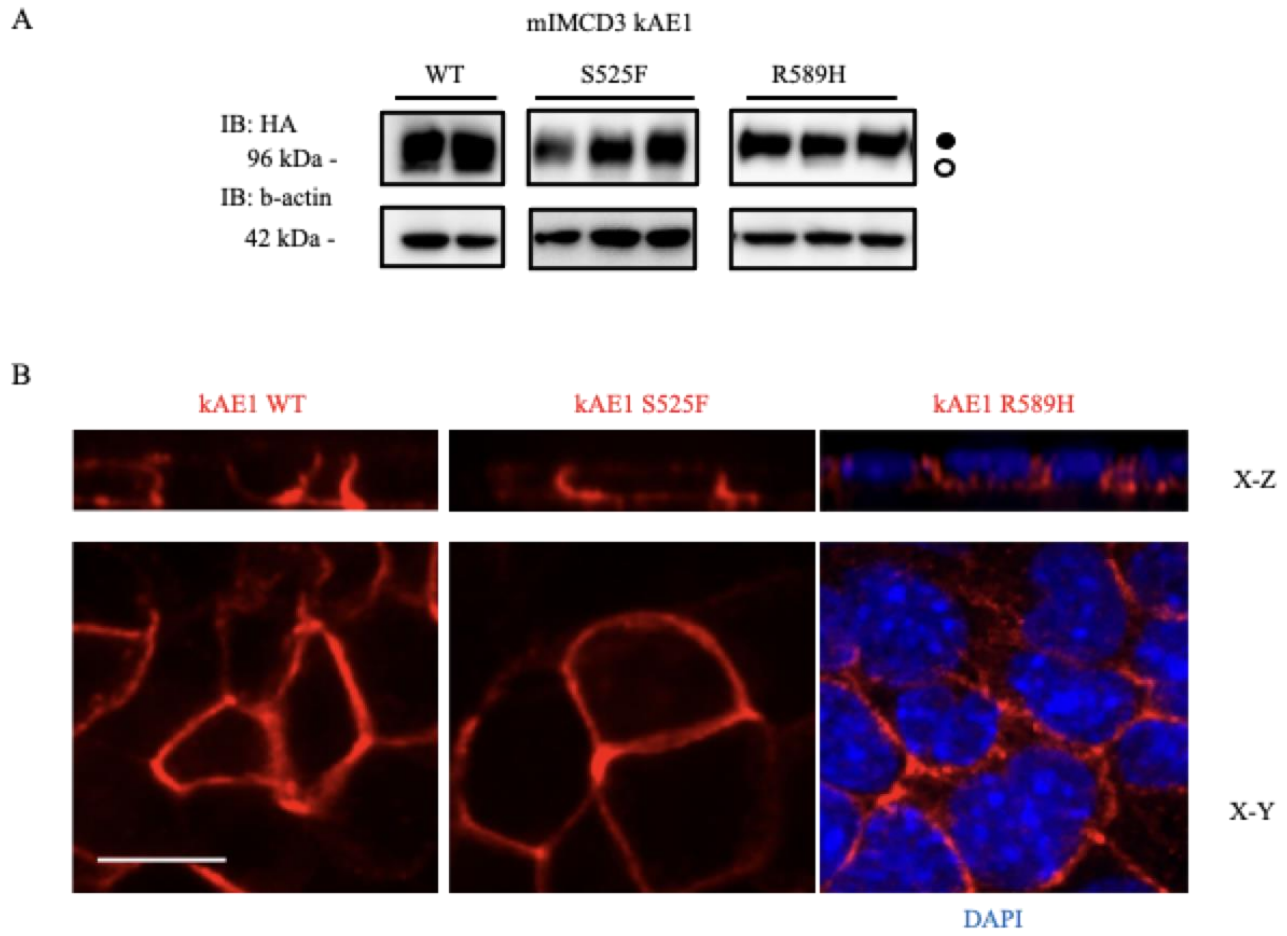
A
mIMCD3 kAE1
WT
S525F
R589H
IB: HA
96 kDa -
IB: b-actin
42 kDa -
B
kAE1 WT
kAE1 S525F
kAE1 R589H
X-Z
X-Y
DAPI
C
dRTA PTI%
Initial rate of intracellular alkalization% (ΔpH/min)
No dox
Dox
S525F
R589H
D
dRTA mutants TEER%
Average Transepithelial Electrical Resistance % (Ohm.cm²)
No dox
Dox
S525F
R589H

Figure 4.9: kAE1 S525F & R589H dRTA mutants affect TJ properties

A, Immunoblot of mIMCD3 cells showing experimental duplicates or triplicates of lysates expressing either kAE1 WT, S525F or R589H mutants. Both mutants are expressed at comparable levels to kAE1 WT and both carry complex (black circle) and high mannose oligosaccharides (white circle)**. B,** mIMCD3 cells stably expressing kAE1 WT, S525F or R589H mutants were grown on semi-permeable filters, fixed, permeabilized and incubated with mouse anti-HA antibody (red). On the kAE1 R589H samples, nuclei were stained with DAPI (blue). X-Y shows a middle section through the cells, X-Z shows a side view of the cells. Bar = 10 μm. **C,** Functional assay using pH-sensitive fluorescent probe BCECF or average transepithelial electrical resistance (**D**) measured on mIMCD3 cells stably expressing either kAE1 WT without doxycycline (No Dox), with doxycycline (Dox), kAE1 S525F with doxycycline (S525F) or kAE1 R589H with doxycycline (R589H). Error bars correspond to means ± SEM, n=4 or 8. *P < 0.05, **P < 0.01, ****P < 0.0001 between indicated conditions. n.s. indicates no significant difference between indicated conditions condition using one-way ANOVA.

4.3 Discussion

In our previous publication[226], we showed that kAE1 physically interacts with claudin-4 in mIMCD3 cells. However, the role of this interaction is still unclear. Interestingly, we also showed that kAE1 function was more important than its physical presence in affecting tight junction properties. Yamauchi and colleagues previously reported that claudin-4 physically interacts with WNK4 in MDCK cells and that this interaction increases claudin-4 phosphorylation[80]. We therefore hypothesized that via its Cl^- transport function, kAE1 alters WNK4 kinase activity, which in turn phosphorylates claudin-4 and results in decreased TEER. In this manuscript, we show that kAE1 WT expression increased phosphorylation of: *(i)* claudin-4, *(ii)* WNK4 and *(iii)* WNK4-downstream effector SPAK. However, inhibition of WNKs with WNK463 did not abolish kAE1 effect on TEER, therefore preventing us from robustly concluding that WNK4 is an intermediate effector in kAE1 effect on TJ properties. It is important to note that given the variability in some of our results, more repetitions are required to provide robust conclusions, especially in data presented in Figures 4.4, 4.3 A and 4.1 D.

4.3.1 Possible effect of kAE1 expression on claudin-4 phosphorylation

In the previous chapter, we reported that although kAE1 expression and function affects TJ properties through claudin-4[226], neither claudin-4 abundance nor plasma membrane expression were affected by kAE1. Thus, the mechanism by which kAE1 affects TJ properties remained unknown. Importantly, we have assessed claudin-4 localization in confluent mIMCD3 cells but did not observe any relocation away from the TJ (**see Chapter 3: Figure 3.5 E & F**). The lack of claudin-4 relocation despite increased phosphorylation has been seen by another research group investigating WNK4 D564A mutant that is related to PHA II disease[80]. Yamauchi and colleagues found that WNK4 WT and D564A mutant increase claudin-4 phosphorylation without affecting its localization at the plasma membrane[80]. Our data,

in agreement with Yamauchi and colleagues' data, suggest that claudin-4 phosphorylation may modify its function at the TJ without altering its targeting to, or removal from the TJs.

In the literature, claudin-4 is reported to undergo several post-transcriptional modifications that affect its function, including phosphorylation[58]. The C-terminus of claudin-4 carries several possible phosphorylation sites by different kinases[74,77]. In MDCK cells, claudin-4 phosphorylation by EphA2 leads to its removal from the TJ, and as a result decreases TEER[88]. Similarly, protein kinase C phosphorylates claudin-4 in ovarian cancer cells which leads to defective barrier function due to claudin-4 delocalization[89]. Comparably, extracellular signal-regulated protein kinase 1 and 2 (ERK 1/2) phosphorylate claudin-4 and leads to its ubiquitination and degradation in rat salivary epithelial cells[90]. However, in keratinocyte cells, claudin-4 phosphorylation by atypical PKC targets claudin-4 to the TJ, which causes a transient increase in TEER during TJ formation[91]. Therefore, conflicting effects of claudin-4 phosphorylation are reported and depend on the expression system used in these studies. It is possible that claudin-4 interaction with other claudins is affected by its kAE1-induced phosphorylation and possibly by its interaction with kAE1. Claudin-4 is known to interact with claudin-8, and together, they form a paracellular Cl^- pore in the collecting ducts[82]. This interaction is crucial for claudin-4 localization into the TJs. It is possible that kAE1-induced phosphorylation of claudin-4 causes a conformational change that may disrupt its interaction with claudin-8, resulting in modified TJ properties. It is also possible that these conformational changes occur within the first extracellular loop leading to a modification in claudin-4 ion selectivity, and subsequently TJ properties. In the absence of kAE1-induced accelerated degradation rate or removal from TJ, we consider that conformational changes in claudin-4 due to kAE1-induced phosphorylation are a reasonable assumption for the effect seen on TJ properties.

Another possibility is that kAE1-induced phosphorylation of claudin-4 increases claudin-4 stability at the TJs as opposed to a relocation to the basolateral membrane as seen in claudin-2 phosphorylation on serine 208[237]. This would not be detectable by cell surface biotinylation, however, our immunofluorescence experiments rejected this possibility as no change in claudin-4 location was detected upon kAE1 expression.

Note that it is possible that claudin-4 behaves differently in the hyper-osmotic environment of the renal medulla which is not fully reflected in the iso-osmotic cell growth conditions in our experiments. In fact, we previously reported that in mouse kidney sections, claudin-4 appears basolaterally located in addition to its expected tight junction localization[226].

4.3.2 Limitations of the IMAEP technique

To assess kAE1 effect on claudin-4 phosphorylation, we used the immobilized metal affinity electrophoresis (IMAEP) technique on lysates from mIMCD3 cells expressing kAE1 WT or E681Q mutant and found that kAE1 WT but not functionally-dead E681Q mutant increased claudin-4 retention in Fe_2Cl_3 -loaded lanes, supporting an increase in claudin-4 phosphorylation. The assay is based on the fact that Fe_2Cl_3 binds and captures the negative charges introduced to proteins by the phosphate group. However, it is possible that changes in the claudin-4 protein charge due to other post-translational modifications, such as glycosylation or palmitoylation might also affect the protein migration. O-linked glycosylation and O-linked palmitoylation of claudin-4 have been predicted to occur at the C-terminus of claudin-4[74]. The addition at the C-terminus of carbohydrate or fatty acid to the serine or threonine by O-linked glycosylation and O-linked palmitoylation respectively, may prevent its further phosphorylation, hence, affect its localization and/or function. In our IMAEP experiments, we observed that kAE1 WT expression increases claudin-4 phosphorylation. However, in agreement with our previous observations that kAE1 E681Q mutant does not affect TJ properties, this mutant's expression had no

effect on claudin-4 phosphorylation. These data indicate that the effect seen on TJ properties is due to kAE1 increasing claudin-4 phosphorylation. However, the results obtained by IMAEP are yet to be confirmed by another assay. Due to the lack of anti-phospho-claudin-4 and the poor performance of anti-phospho amino acids antibodies, our attempts to confirm our findings by coimmunoprecipitation have not been successful. Also an attempt to confirm our IMAEP results by mass spectrometry has not been successful either.

4.3.3 Role of WNK4 on kAE1-induced decrease in TEER and limitations to the use of WNK463 inhibitor

Changes in intracellular Cl^- concentration influence the function of the protein kinase WNK family[98]. All members of the WNK family (1 to 4) contain a Cl^- binding site that is located in the highly conserved kinase domain in WNK family members[95,99]. Cl^- bound to WNK1 inhibits its autophosphorylation, thus, inhibits its kinase activity[99]. *In vitro* kinase assays showed that WNK4, WNK1 and WNK3 are inhibited by a serial increase in Cl^- concentration[98]. WNK4 kinase activity responds to Cl^- concentration variations ranging from 0 to 40 mmol[98], which are within the physiological range of epithelial cells. These findings were further confirmed by *in vivo* studies that identified WNK4 as a physiological intracellular Cl^- sensor[233]. As kAE1 utilizes Cl^- in its exchange activity, we hypothesized that kAE1 transport influences WNK4 activity, and subsequently, claudin-4 phosphorylation. WNK4 inhibition with WNK463 inhibitor resulted in increased WNK4 phosphorylation and total expression. This increase in WNK4 phosphorylation and total expression is most likely a cellular regulatory response to compensate for the absence of inhibited-WNK4 downstream regulatory pathways. However, we found that despite an efficient WNK inhibition with WNK463, the TEER was further decreased upon the combination of kAE1 expression and WNK4 inhibition compared with kAE1 expression alone, supporting that WNK inhibition does not abolish kAE1 effect but is rather

additive. One possible conclusion from these experiments is that WNK4 is not an intermediate player in kAE1 effect on the TEER in mIMCD3 cells, and that our hypothesis of WNK4's role may be wrong. However, our results may be explained by 4 other mechanisms:

(i) the increased activity of transcellular transporters, which are inhibited by WNK1 and WNK4 activities: ENaC, NKCC1, NCC and ROMK may also play a significant role in the effect of WNK inhibition on the TEER. WNK4 inhibits the activities of these transporters by reducing their surface expression at the plasma membrane[100–102]. We speculate that inhibiting WNK4 via WNK463 inhibitor results in increased transport activities of these transcellular transporters, resulting in a lower TEER. To test this hypothesis, we repeated Ussing chambers experiments using inhibitors of the transcellular pathway, specifically using ENaC inhibitor amiloride and NKCC1 inhibitor bumetanide as previously reported[82]. Our results showed that blocking the transcellular transporters ENaC and NKCC1 did not reverse the effect of WNK463 (**Figure 4.7 A**). In fact, blocking these transporters resulted in further decrease in the TEER, indicating that the activity of these transporters is somehow contributing to maintenance of the TJ integrity. Sassi and colleagues recently found that claudin-8 expression is regulated by ENaC γ-subunit[238]. ENaC γ-subunit silencing resulted in a decrease in claudin-8 expression. This observation was confirmed in kidney tubule-specific knockout mice. Mice lacking ENaC γ-subunit, but not α- and β- subunits, had a lower abundance of claudin-8. Interestingly, claudin-8 reduction resulted in a significant decrease in TEER and increased Na^+ permeability *in vitro*[238]. Their finding aligns with our results where ENaC inhibition resulted in further decrease in TEER and increased paracellular flux of Na^+ and Cl^-. Further, the application of amiloride at the apical side not only inhibited ENaC, but also likely inhibited the Na^+/H^+ exchanger 1 (NHE1)[239], consequently affecting intracellular pH and cytosolic Na^+ concentration. Similarly, NKCC1 inhibition by bumetanide likely affected the transcellular transport of Cl^-, which in turn is expected to impact intracellular Cl^- concentration. Therefore, experiments

conducted with transcellular inhibitors further complicated rather than simplified the interpretation of our results.

(ii) Another possibility is that WNK4 inhibition may impact other claudins' phosphorylation or function, such as claudin-3. In many epithelial cell types, claudin-3 is considered a strong barrier and has been reported to be phosphorylated by WNK4[58,80]. We have previously confirmed that claudin-3 is expressed in mIMCD3 cells, however, it does not physically interact with kAE1 in these cells **(Figure 3.4 B)**. We therefore speculated that WNK4 inhibition may affect the barrier function of claudin-3 possibly resulting in a further decrease in TEER independently of kAE effect on TEER. To test this second hypothesis, we assessed claudin-3 expression and found that claudin-3 total abundance is significantly decreased not only by WNK4 inhibition, but also by kAE1 expression itself (**Figure 4.8**). The combination of kAE1 expression and WNK463 inhibitor added their individual effect on TEER. This observation explains the reduction seen in the TEER since claudin-3 is considered as a general blocker.

(iii) A third explanation may be that the effect of kAE1 on claudin-4 phosphorylation is modulated through a different kinase, possibly ERK 1/2. In keratinocytes, ERK 1/2 increased claudin-4 phosphorylation and reduced the TEER[90]. However, these effects were accompanied by a reduction in claudin-4 membrane expression, in disagreement with our data. To test this hypothesis, we performed an immunoblot assessing ERK 1/2 expression and phosphorylation status upon kAE1 expression. We found that kAE1 expression neither altered ERK 1/2 expression nor its phosphorylation, eliminating ERK 1/2 as a possible candidate for increased claudin-4 phosphorylation.

(iv) a last possible explanation is that WNK463 inhibits both WNK4 and WNK1 (and possibly WNK3, although we have no evidence of its expression in IMCD3 cells). In such case, the impact of WNK463 on TEER and increased permeability may reflect WNK1 and 4 inhibition. Further, WNK463

may switch off the regulatory pathways that involve all WNK family members leading to a more dramatic effect on TJ properties than inhibition of WNK4 only, thus confounding our results. We have not tested this hypothesis.

Overall, our results show that kAE1 expression triggers claudin-4, WNK4 and SPAK phosphorylation, however a robust conclusion on the involvement of WNK4 in kAE1 effect on TJ properties could not be reached in these experiments. Our results also show that kAE1 dRTA mutants expression affect TJ properties in a manner proportional to their transport activity, indicating that the urinary loss of sodium and chloride in dRTA patients is unlikely due to an effect of kAE1 mutants on TJ properties.

5. Chapter 5: Summary, Proposed Model & Future Directions

5.1 Summary

The objective of this thesis was to investigate the relationship between the tight junction protein claudin-4 and the basolateral membrane protein kidney anion exchanger 1. The first evidence of their relationship was provided to us by Dr. Reithmeier from the University of Toronto. Screening for kAE1 interactors using the membrane yeast two hybrid assay, Dr. Reithmeier's lab found that kAE1 physically interacts with claudin-4 protein.

In this thesis, we aimed to: *(i)* confirm the interaction in mammalian cells, *(ii)* explore the effect of expressing kAE1 protein on claudin-4 function, and *(iii)* investigate the mechanism by which kAE1 affects claudin-4 function.

5.1.1 Limitations of our work due to cell line models and viral transfection strategies

5.1.1.1 Cell line models

The preliminary data of this project were generated using MDCK cells. MDCK cells are epithelial cells that were derived from canine kidney cells and have been used to study the characterization of different proteins and their mutations, including kAE1[197], claudin-4[240] and WNK4[231]. However, this cell line was not ideal for our study for two reasons: *(i)* it was derived from the whole kidney[241], and *(ii)* kAE1 dRTA mutants have a different phenotype when they are expressed in MDCK cells compared to animal models and more physiologically relevant mIMCD3 cells[197,199]. For example, kAE1 R589H mutant was retained in the endoplasmic reticulum in MDCK cells[197], whereas it reached the plasma membrane and functioned normally in mIMCD3 and kAE1 R607H knockin mouse model[199].

As a result, we switched to mIMCD3 cells, another immortalized cell line derived from the mouse inner medullary collecting duct cells. In addition to being derived from the collecting ducts, these cells express endogenous claudin-4 and WNK4 but not kAE1. Because these cells do not express endogenous

kAE1, but have the machinery for kAE1 normal trafficking, they were the perfect model to test the effect of kAE1 expression on claudin-4 abundance and function.

5.1.1.2 Constitutive vs Inducible Viral Expression systems

In order to study the effect of kAE1 expression on claudin-4, we first stably expressed kAE1 using the retroviral constitutive expression plasmid pFB-Neo EV, kAE1 WT or mutants. This expression system was not optimal because: *(i)* the transfection efficiency differs between experiments, *(ii)* viral transfection affects TJ properties, and most importantly, *(iii)* the cells lose kAE1 expression within 14 days even in the continuous presence of selecting antibiotics. Therefore, using this approach for kAE1 expression had its limitations, as at least 8 to 10 days after seeding the cells are required to obtain fully polarized cells, leaving only a week to perform experiments before expression was lost.

As an alternative strategy, we switched to the lentiviral inducible-expression system pLVX-Tet3G (regulator-plasmid), and pLVX-TRE3G kAE1 WT, S525F, R589H, or E681Q mutants (response-plasmids). Upon incubation with doxycycline, the transfected cells express kAE1 WT or mutants. Using this approach allowed us to overcome the issues faced with the constitutive retroviral expression system as we were able to: *(i)* re-use the same batch of cells generated by a single lentiviral infection and eliminate the problem of variability in transfection efficiency between experiments, *(ii)* correct the effect of the viral transfection on TJ properties in our control condition, and *(iii)* optimize expression levels of kAE1 protein by inducing its expression within 24 to 48 prior to experiment time.

5.1.2 The kidney anion exchanger 1 affects tight junction properties via claudin-4

5.1.2.1 kAE1 & claudin-4 interaction in mammalian cells

After successfully generating mIMCD3 cells that inducibly express kAE1 proteins, we first wanted to confirm the interaction between kAE1 and claudin-4 in our model. In Chapter 3 we presented strong evidence that kAE1 interacts with claudin-4 by co-immunoprecipitation assay. In that experiment,

kAE1 failed to co-immunoprecipitate with claudin-3 and irrelevant IgG indicating some specific interaction between the two proteins. To eliminate any possibility that this interaction occurred during cell lysis preparation, we confirmed this proximity in intact cells by performing proximity ligation assay. In this assay, the two proteins were found to be within 20-40 nm of distance in polarized and non-polarized mIMCD3 cells (**Figure 3.4 D**). Additionally, immunohistochemistry of kidney section showed that the two proteins colocalize at the basolateral membrane of type-A IC cells. The localization of claudin-4 to the basolateral membrane is most likely due to the hyperosmotic environment of the inner medulla in the kidney as was shown for other claudins[242], a condition that is not present in our *in vitro* experiments. Altogether, these data confirm that the two proteins interact and colocalize in mammalian cells *in vivo*.

5.1.2.2 kAE1 modulates TJ properties via claudin-4

In Chapter 3 we concluded that kAE1 expression modulates TJ properties via claudin-4 using different approaches and experimental designs, but mainly relying on the Ussing chamber experimental set-up. This experiment is based on measuring voltage deflection relative to current induction, from which we can calculate the transepithelial electrical resistance, TEER. Furthermore, using the same settings we can also conduct dilution potential studies at the end of the experiment from which we can determine the absolute permeability of the epithelium to Na^+ and Cl^- using the Goldman-Hodgkin Katz and Kimizuka Koketsu equations[186,187].

kAE1 expression resulted in a decrease in TEER and increased Na^+ and Cl^- permeability. These results were due to kAE1 function as kAE1 E681Q mutant neither had an effect on TEER nor on Na^+ and Cl^- permeability. Similarly, knocking down claudin-4 resulted in decreased TEER and increased Na^+ and Cl^- permeability. However, inducing kAE1 expression in claudin-4 knock-down cells did not cause further change in tight junction integrity. Overall, these results indicated that kAE1 effect on TJ

properties was through claudin-4 protein. Although kAE1 effect on TJ properties was similar to the effect of knocking down claudin-4, we neither found an effect of kAE1 on claudin-4 expression nor on its plasma membrane abundance.

This last observation, along with the fact that kAE1 function was crucial for its effect on TJ properties, laid the foundation of the research hypothesis presented in Chapter 4 that kAE1 regulates claudin-4 function by modulating its phosphorylation, most likely through WNK4.

5.1.3 kAE1 expression affects tight junction properties proportionally to its function and via a claudin-4 phosphorylation pathway

5.1.3.1 kAE1 expression results in claudin-4 phosphorylation

In Chapter 4 we explored how kAE1 affects claudin-4 function. Looking at claudin-4 phosphorylation we found that kAE1 expression increases claudin-4 phosphorylation. As for its effect on TEER, kAE1 function is required for its effect on claudin-4 phosphorylation. The drop in TEER resulting from increased claudin-4 phosphorylation is linked to WNK4 kinase activity, but is neither due to a decrease in claudin-4 abundance nor plasma membrane localization. Looking at WNK4 and its downstream effectors SPAK/OSR1 kinases, we found that kAE1 function increases their phosphorylation. The effect of kAE1 was not extended to ERK 1/2 as there was no effect on abundance or phosphorylation of this kinase.

Nevertheless, WNK463 inhibitor impacted the TEER to a similar extent as kAE1 expression. Interestingly, WNK inhibition in addition to kAE1 expression resulted in a further decrease in TEER. Inhibition of transcellular ENaC and NKCC1 transporters did not abolish the TEER decrease caused by WNK4 inhibition. Instead, it caused a further decrease in TEER when combined with WNK463. The additive effect caused by WNK inhibition and kAE1 expression on TEER could be explained by the

decrease in claudin-3 and -4 expression. As claudin-3 is a general blocker, a decrease in claudin-3 expression could explain the drop in the TEER and the increased flux of both Na^+ and Cl^-.

5.1.3.2 dRTA mutants and tubular physiology of the collecting ducts

In Chapter 4 we explored the effect of expressing dRTA-causing kAE1 S525F & R589H mutants on TJ properties. Although the kAE1 mutants had a similar profile as the kAE1 WT in terms of expression level and localization, the functional assay showed that kAE1 S525F mutant had a significantly lower exchange activity compared to kAE1 WT and R589H mutant. Examining their effect on the TJ properties, we observed that the inactive kAE1 S525F mutant had less impact on TEER compared to fully active kAE1 WT or R589H mutant. Altogether, along with the results from Chapter 3 using inactive kAE1 E681Q mutant, we concluded that kAE1 effect on TJ properties is proportional to its function (exchange rate).

5.2 Proposed model

In this Thesis, we show that kAE1 function alters tight junction properties via WNK4-, SPAK- and claudin-4 phosphorylation. Based on these findings, we propose that by its chloride/bicarbonate exchange activity, kAE1 function contributes to the efficient pairing of urinary acidification with Na^+ reabsorption in the CD. Indeed, the aldosterone sensitive nephron is responsible for fine tuning NaCl reabsorption and acid secretion. Aldosterone regulates key proteins that are involved in these functions, such as ENaC[30], claudin-4[33], and the V-H^+ ATPase pump[34]. Unlike principal cells, type-A IC cells are energized by the V-H^+ ATPase[243]. The V-H^+ ATPase pumping rate is regulated by luminal pH and electrical charge[244]. We propose that upon aldosterone stimulation, NaCl reabsorption is increased by the function of ENaC in PC and claudin-4 phosphorylation paracellularly. Claudin-4 not only facilitates Cl^- reabsorption paracellularly, but also prevents the back flux of Na^+ into the lumen. Its phosphorylation may inhibit its function, resulting in less Na^+ barrier. In type-A IC, the V-H^+ ATPase pump secretes H^+

to acidify the urine and promotes HCO_3^- exchange with Cl^- into the blood through kAE1. An increase in intracellular [Cl^-] inhibits WNK4 activity that leads to changes in claudin-4, and possibly -3, phosphorylation. These changes in phosphorylation of claudin-4, and possibly -3, may lead to decreased TJ integrity and impaired paracellular Na^+ blockage. The increased back flux of Na^+ would then result in reduced transepithelial voltage difference, increased luminal voltage, and as a result would attenuate ATPase-mediated H^+ secretion rate as a reset point for these cells. In this model, kAE1 activity would link the ability of the CD epithelium to efficiently reabsorb Na^+ while acidifying the urine pH.

5.3 Limitations and Future directions

5.3.1 Confirmation of Claudin-4 phosphorylation

Although we showed that claudin-4 phosphorylation increases upon kAE1 expression, it is yet to be confirmed by another approach. One of the main future directions for completion of this project is to confirm claudin-4 phosphorylation using a different technique, and, consecutively, the position of the phosphorylated amino acid. Several experimental approaches could be used to confirm claudin-4 phosphorylation. For example, radio-labeled ^{32}[P]orthophosphate could be used to measure the level of claudin-4 phosphorylation upon kAE1 expression.

Another approach would be to use mass spectrometry. Using mass spectrometry not only can provide information about the level of claudin-4 phosphorylation, but it could also provide us with the position of the phosphorylated amino acid. We have started looking into this approach, however, more troubleshooting is required before we can draw any conclusions.

5.3.2 kAE1 & claudin-4 interaction & possibly WNK4 complex

In this thesis, we showed that kAE1 physically interacts with claudin-4. However, the role of this interaction remains obscure. To investigate the importance of this interaction in kAE1 effect on TJ properties, we would first need to determine the amino acid sequence involved in this interaction on both

proteins. Preliminary results using peptide spot assay of kAE1 amino acid sequence indicated that claudin-4 interacts with the third and fourth extracellular loops, and the N-terminus of kAE1 protein. This experiment would need to be repeated in order to confirm these findings, and this finding would further need to be validated using other approaches such as a GST pull down, surface plasmon resonance using purified proteins/peptides and generation of truncated proteins on the potential binding sites.

A reciprocal approach, in which peptides covering claudin-4 amino acids sequence would be spotted on a cellulose membrane in a peptide spot assay would determine the interaction sequence of claudin-4. It is also important to note that both proteins contain PDZ-binding domains[69,140], which might contribute to their interaction.

Based on the fact that claudin-4 interacts with kAE1 in mIMCD3 cells, and that it also interacts with WNK4 in MDCK cells[80], it is possible that the three proteins may form a protein complex. kAE1-induced changes of $[Cl^-]$ in the microenvironment of this complex (rather than whole cell $[Cl^-]$ change) may trigger an effect on WNK4 kinase activity and subsequently claudin-4 phosphorylation and TJ properties. To test this hypothesis we could perform a co-immunoprecipitation using anti-kAE1, anti-claudin-4 and anti-WNK4 antibodies and identify their co-immunoprecipitated partners. All three proteins would be co-immunoprecipitated if in the same protein complex. This experiment could be performed *in vitro*, using mIMCD3 kAE1 cells, or *ex vivo*, using a mouse kidney lysate.

5.3.3 Cl^- insensitive WNK4 mutant

In Chapter 4 we generated our hypothesis that kAE1 modulates claudin-4 phosphorylation through WNK4. We developed this hypothesis based on the fact that WNK4 kinase activity is sensitive to intracellular $[Cl^-]$ and that Cl^- is a substrate of kAE1. To test our hypothesis we used WNK463 to inhibit WNK4 activity. Although WNK463 indeed inhibited WNK4 kinase activity, we were unable to

reach a robust conclusion as WNK463 is not specific to WNK4 only, but likely inhibits all WNK kinase family members, thus confounding our results.

The optimal way to robustly validate our hypothesis would be to repeat Ussing chambers experiments after expression of the Cl^- insensitive double mutant WNK4 L319F/L321F[233] in mIMCD3 cells in the presence or absence of kAE1. In this experimental setting, as WNK4 would be the only WNK family member to be constitutively active, we would be able to assess whether this protein is a downstream effector of kAE1 on TJ properties. We would expect that expression of this mutant would decrease transepithelial electrical resistance and that kAE1 expression or claudin-4 knockout would not cause a further decrease in TEER.

Lastly, as WNK4 activity is modulated by L-WNK1[102], and L-WNK1 activity is regulated by KS-WNK1[96], it would be important to assess the effect of kAE1 expression on L-WNK1 and KS-WNK1 mRNA, and total and phosphorylated protein expression in mIMCD3 cells by qRT-PCR and immunoblot, respectively.

5.3.4 Collecting duct micro-perfusion

Our experiments have been performed *in vitro*. This allowed us to manipulate kAE1 and claudin-4 expression at will to test our hypothesis. However, our results would need to be validated *in vivo*. To decipher the role of kAE1 and claudin-4 in acid/base balance and electrolyte homeostasis in the collecting duct, and the effect of one on the other's function, we would need to conduct electrophysiological micro-perfusion studies on isolated collecting ducts from different animal models that are currently available to us: *(i)* wild type mice, *(ii)* type-A IC- specific claudin-4 knockout mice, and *(iii)* dRTA kAe1 R607H or L919X knock-in mice.

In summary, our work has revealed and dissected the modulation of tight junction properties by the function of a chloride/bicarbonate exchanger in collecting duct cells. This finding has improved our

understanding of the functional relationship between tight junction proteins and transporters in the collecting duct and may be relevant for the future design of new therapeutic approaches to treat dRTA or hypertension.

Bibliography

1. Wolff, G. E., Crosby, R. D., Roberts, J. A. & Wittrock, D. A. Differences in daily stress, mood, coping, and eating behavior in binge eating and nonbinge eating college women. Addictive Behaviors **25**, 205–216 (2000).
2. Brenner, B. M. & Rector, F. C. Brenner & Rector's the kidney. (Saunders Elsevier, 2008).
3. Saxén, L. & Sariola, H. Early organogenesis of the kidney. Pediatric Nephrology **1**, 385–392 (1987).
4. Capel, B., Albrecht, K. H., Washburn, L. L. & Eicher, E. M. Migration of mesonephric cells into the mammalian gonad depends on Sry. Mech. Dev. **84**, 127–131 (1999).
5. Brenner, B. M. & Rector, F. C. Brenner & Rector's The Kidney. (Saunders Elsevier, 2008).
6. Chen, L. et al. Transcriptomes of major renal collecting duct cell types in mouse identified by single-cell RNA-seq. Proc. Natl. Acad. Sci. U. S. A. **114**, E9989–E9998 (2017).
7. Kriz, W. & Kaissling, B. Structural organization of the mammalian kidney. in 595–691 (Elsevier, 2013).
8. Park, J. et al. Single-cell transcriptomics of the mouse kidney reveals potential cellular targets of kidney disease. Science (80-.). eaar2131 (2018).
9. Loffing, J. et al. Differential subcellular localization of ENaC subunits in mouse kidney in response to high- and low-Na diets. Am. J. Physiol. - Ren. Physiol. **279**, F252-8 (2000).
10. Obermuller, N. et al. Expression of the thiazide-sensitive Na-Cl cotransporter in rat and human kidney. Am. J. Physiol. - Ren. Fluid Electrolyte Physiol. **269**, (1995).
11. Mistry, A. C. et al. The sodium chloride cotransporter (NCC) and epithelial sodium channel (ENaC) associate. Biochem. J. **473**, 3237–3252 (2016).
12. Koeppen, B. M. & Stanton, B. A. Renal physiology. (Mosby, 2007).
13. Kloth, S., Aigner, J., Brandt, E., Moll, R. & Minuth, W. W. Histochemical markers reveal an unexpected heterogeneous composition of the renal embryonic collecting duct epithelium. Kidney Int. **44**, 527–536 (1993).
14. Madsen, K. M. & Tisher, C. C. Structural-functional relationships along the distal nephron. American Journal of Physiology - Renal Fluid and Electrolyte Physiology **250**, (1986).
15. Madsen, K. M., Verlander, J. W. & Tisher, C. C. Relationship between structure and function in distal tubule and collecting duct. J. Electron Microsc. Tech. **9**, 187–208 (1988).
16. Schuster, V. L. Function and regulation of collecting duct intercalated cells. Annu. Rev. Physiol. **55**, 267–88 (1993).
17. Teng-umnuay, P., Verlander, J. W., Yuan, W., Tisher, C. C. & Madsen, K. M. Identification of distinct subpopulations of intercalated cells in the mouse collecting duct. J. Am. Soc. Nephrol. **7**, 260–74 (1996).
18. Roy, A., Al-bataineh, M. M. & Pastor-Soler, N. M. Collecting duct intercalated cell function and regulation. Clin. J. Am. Soc. Nephrol. **10**, 305–24 (2015).
19. Trepiccione, F. et al. A fate-mapping approach reveals the composite origin of the connecting tubule and alerts on "single-cell"-specific KO model of the distal nephron. Am. J. Physiol. Physiol. **311**, F906 (2016).
20. van Adelsberg, J., Edwards, J. C., Takito, J., Kiss, B. & al-Awqati, Q. An induced extracellular matrix protein reverses the polarity of band 3 in intercalated epithelial cells. Cell **76**, 1053–1061 (1994).
21. Gao, X. et al. Deletion of hensin/DMBT1 blocks conversion of - to -intercalated cells and induces

distal renal tubular acidosis. Proc. Natl. Acad. Sci. **107**, 21872–21877 (2010).
22. Park, J. et al. Single-cell transcriptomics of the mouse kidney reveals potential cellular targets of kidney disease. Science (80-.). **360**, 758–763 (2018).
23. Kim, J., Kim, Y. H., Cha, J. H., Tisher, C. C. & Madsen, K. M. Intercalated cell subtypes in connecting tubule and cortical collecting duct of rat and mouse. J Am Soc Nephrol **10**, 1–12 (1999).
24. Chen, L. et al. Transcriptomes of major renal collecting duct cell types in mouse identified by single-cell RNA-seq. Proc. Natl. Acad. Sci. U. S. A. **114**, E9989–E9998 (2017).
25. Sebastian, A., McSherry, E. & Morris Jr., R. C. Impaired renal conservation of sodium and chloride during sustained correction of systemic acidosis in patients with type 1, classic renal tubular acidosis. J Clin Invest **58**, 454–469 (1976).
26. Gueutin, V. et al. Renal beta-intercalated cells maintain body fluid and electrolyte balance. J Clin Invest **123**, 4219–4231 (2013).
27. Souma, T., Suzuki, N. & Yamamoto, M. Renal erythropoietin-producing cells in health and disease. Front. Physiol. **6**, 167 (2015).
28. Ohyama, Y. & Shinki, T. Calcitriol. Handb. Horm. 548-e97A-5 (2016).
29. Fountain, J. H. & Lappin, S. L. Physiology, Renin Angiotensin System. StatPearls (StatPearls Publishing, 2018).
30. Frindt, G., Ergonul, Z. & Palmer, L. G. Surface expression of epithelial Na channel protein in rat kidney. J. Gen. Physiol. **131**, 617–627 (2008).
31. Li, C. et al. Molecular mechanisms of angiotensin II stimulation on aquaporin-2 expression and trafficking. Am. J. Physiol. - Ren. Physiol. **300**, 1255–1261 (2011).
32. Terzic, A. et al. Channelopathies of cardiac inwardly rectifying potassium channels. Electrical Diseases of the Heart: Genetics, Mechanisms, Treatment, Prevention (2008).
33. Le Moellic, C. et al. Aldosterone and tight junctions: Modulation of claudin-4 phosphorylation in renal collecting duct cells. Am. J. Physiol. - Cell Physiol. **289**, C1513-21 (2005).
34. Wagner, C. A. et al. Renal vacuolar H+-ATPase. Physiol. Rev. **84**, 1263–1314 (2004).
35. Mark, P. B., Stevens, K. K. & Jardine, A. G. Electrolytes: Acid-Base Balance. Encycl. Hum. Nutr. **2**–**4**, 139–145 (2012).
36. Goel, N. & Calvert, J. Understanding blood gases/acid-base balance. Paediatr. Child Health (Oxford). **22**, 142–148 (2012).
37. Poupin, N., Calvez, J., Lassale, C., Chesneau, C. & Tomé, D. Impact of the diet on net endogenous acid production and acid-base balance. Clin. Nutr. **31**, 313–321 (2012).
38. Boron, W. F. Acid-base transport by the renal proximal tubule. J. Am. Soc. Nephrol. **17**, 2368–2382 (2006).
39. Unwin, R. J., Shirley, D. G. & Capasso, G. Urinary acidification and distal renal tubular acidosis. J. Nephrol. **15**, S142-50 (2002).
40. Biemesderfer, D. et al. NHE3: A Na+/H+ exchanger isoform of renal brush border. Am. J. Physiol. - Ren. Fluid Electrolyte Physiol. **265**, (1993).
41. Kurtz, I. Molecular mechanisms and regulation of urinary acidification. Compr. Physiol. **4**, 1737–1774 (2014).
42. Pereira, P., Miranda, D., Oliveira, E. & Simoes e Silva, A. Molecular Pathophysiology of Renal Tubular Acidosis. Curr. Genomics **10**, 51–59 (2009).
43. Wagner, C. A. & Geibel, J. P. Acid-base transport in the collecting duct. J. Nephrol. **15**, S112-27 (2002).
44. Alper, S. L. Genetic diseases of acid-base transporters. Annu. Rev. Physiol. **64**, 899–923 (2002).

45. Alper, S. L., Natale, J., Gluck, S., Lodish, H. F. & Brown, D. Subtypes of intercalated cells in rat kidney collecting duct defined by antibodies against erythroid band 3 and renal vacuolar H+-ATPase. Proc. Natl. Acad. Sci. U. S. A. **86**, 5429–5433 (1989).
46. Wagner, C. A. et al. Renal vacuolar H+-ATPase. Physiological Reviews **84**, 1263–1314 (Physiol Rev, 2004).
47. FARQUHAR, M. G. & PALADE, G. E. Junctional complexes in various epithelia. J. Cell Biol. **17**, 375–412 (1963).
48. Acharya, P. et al. Distribution of the tight junction proteins ZO-1, occludin, and claudin-4, -8, and -12 in bladder epithelium. Am. J. Physiol. - Ren. Physiol. **287**, (2004).
49. Martìn-Padura, I. et al. Junctional adhesion molecule, a novel member of the immunoglobulin superfamily that distributes at intercellular junctions and modulates monocyte transmigration. J. Cell Biol. **142**, 117–127 (1998).
50. Itoh, M. et al. Junctional adhesion molecule (JAM) binds to PAR-3: A possible mechanism for the recruitment of PAR-3 to tight junctions. J. Cell Biol. **154**, 491–497 (2001).
51. Furuse, M. et al. Occludin: A novel integral membrane protein localizing at tight junctions. J. Cell Biol. **123**, 1777–1788 (1993).
52. Ikenouchi, J. et al. Tricellulin constitutes a novel barrier at tricellular contacts of epithelial cells. J. Cell Biol. **171**, 939–945 (2005).
53. Steed, E., Rodrigues, N. T. L., Balda, M. S. & Matter, K. Identification of MarvelD3 as a tight junction-associated transmembrane protein of the occludin family. BMC Cell Biol. **10**, (2009).
54. Raleigh, D. R. et al. Tight junction-associated MARVEL proteins marvelD3, tricellulin, and occludin have distinct but overlapping functions. Mol. Biol. Cell **21**, 1200–1213 (2010).
55. Saitou, M. et al. Complex phenotype of mice lacking occludin, a component of tight junction strands. Mol. Biol. Cell **11**, 4131–4142 (2000).
56. Cording, J. et al. In tight junctions, claudins regulate the interactions between occludin, tricellulin and marvelD3, which, inversely, modulate claudin oligomerization. J. Cell Sci. **126**, 554–564 (2013).
57. Furuse, M., Sasaki, H. & Tsukita, S. Manner of interaction of heterogeneous claudin species within and between tight junction strands. J. Cell Biol. **147**, 891–903 (1999).
58. Günzel, D. & Yu, A. S. L. Claudins and the modulation of tight junction permeability. Physiol. Rev. **93**, 525–569 (2013).
59. Loh, Y. H., Christoffels, A., Brenner, S., Hunziker, W. & Venkatesh, B. Extensive expansion of the claudin gene family in the teleost fish, Fugu rubripes. Genome Res. **14**, 1248–57 (2004).
60. Krause, G. et al. Structure and function of claudins. Biochimica et Biophysica Acta - Biomembranes **1778**, 631–645 (2008).
61. Yu, A. S. L. Claudins and the kidney. Journal of the American Society of Nephrology **26**, 11–19 (2013).
62. Suzuki, H. et al. Crystal structure of a claudin provides insight into the architecture of tight junctions. Science (80-.). **344**, 304–307 (2014).
63. Van Itallie, C. M. & Anderson, J. M. Claudins and epithelial paracellular transport. Annual Review of Physiology **68**, 403–429 (2006).
64. Cukierman, L., Meertens, L., Bertaux, C., Kajumo, F. & Dragic, T. Residues in a Highly Conserved Claudin-1 Motif Are Required for Hepatitis C Virus Entry and Mediate the Formation of Cell-Cell Contacts. J. Virol. **83**, 5477–5484 (2009).
65. Colegio, O. R., Van Itallie, C. M., McCrea, H. J., Rahner, C. & Anderson, J. M. Claudins create charge-selective channels in the paracellular pathway between epithelial cells. Am. J. Physiol. -

Cell Physiol. **283**, C142–C147 (2002).
66. Piorntek, J. et al. Formation of tight junction: determinants of homophilic interaction between classic claudins. FASEB J. **22**, 146–158 (2008).
67. Katahira, J. et al. Clostridium perfringens enterotoxin utilizes two structurally related membrane proteins as functional receptors in vivo. J. Biol. Chem. **272**, 26652–26658 (1997).
68. Katahira, J., Inoue, N., Horiguchi, Y., Matsuda, M. & Sugimoto, N. Molecular cloning and functional characterization of the receptor for Clostridium perfringens enterotoxin. J. Cell Biol. **136**, 1239–1247 (1997).
69. Itoh, M. et al. Direct binding of three tight junction-associated MAGUKs, ZO-1, ZO-2, and ZO-3, with the COOH termini of claudins. J. Cell Biol. **147**, 1351–1363 (1999).
70. Rüffer, C. & Gerke, V. The C-terminal cytoplasmic tail of claudins 1 and 5 but not its PDZ-binding motif is required for apical localization at epithelial and endothelial tight junctions. Eur. J. Cell Biol. **83**, 135–144 (2004).
71. Arabzadeh, A., Troy, T.-C. & Turksen, K. Role of the Cldn6 Cytoplasmic Tail Domain in Membrane Targeting and Epidermal Differentiation In Vivo. Mol. Cell. Biol. **26**, 5876–5887 (2006).
72. Müller, D., Kausalya, P. J., Meij, I. C. & Hunziker, W. Familial hypomagnesemia with hypercalciuria and nephrocalcinosis: Blocking endocytosis restores surface expression of a novel Claudin-16 mutant that lacks the entire C-terminal cytosolic tail. Hum. Mol. Genet. **15**, 1049–1058 (2006).
73. Van Itallie, C. M., Colegio, O. R. & Anderson, J. M. The cytoplasmic tails of claudins can influence tight junction barrier properties through effects on protein stability. J. Membr. Biol. **199**, 29–38 (2004).
74. Butt, A. M. et al. Role of post translational modifications and novel crosstalk between phosphorylation and O-beta-GlcNAc modifications in human claudin-1, -3 and -4. Mol. Biol. Rep. **39**, 1359–1369 (2012).
75. Shigetomi, K. & Ikenouchi, J. Regulation of the epithelial barrier by post-translational modifications of tight junction membrane proteins. Journal of Biochemistry **163**, 265–272 (2018).
76. Van Itallie, C. M., Gambling, T. M., Carson, J. L. & Anderson, J. M. Palmitoylation of claudins is required for efficient tight-junction localization. J. Cell Sci. **118**, 1427–1436 (2005).
77. González-Mariscal, L., Garay, E. & Quirós, M. Regulation of Claudins by Posttranslational Modifications and Cell-Signaling Cascades. Current Topics in Membranes **65**, (2010).
78. Ikari, A. et al. Phosphorylation of paracellin-1 at Ser217 by protein kinase A is essential for localization in tight junctions. J. Cell Sci. **119**, 1781–1789 (2006).
79. D'Souza, T., Agarwal, R. & Morin, P. J. Phosphorylation of Claudin-3 at threonine 192 by cAMP-dependent protein kinase regulates tight junction barrier function in ovarian cancer cells. J. Biol. Chem. **280**, 26233–26240 (2005).
80. Yamauchi, K. et al. Disease-causing mutant WNK4 increases paracellular chloride permeability and phosphorylates claudins. Proc. Natl. Acad. Sci. U. S. A. **101**, 4690–4694 (2004).
81. Tatum, R. et al. WNK4 phosphorylates ser206 of claudin-7 and promotes paracellular Cl- permeability. FEBS Lett. **581**, 3887–3891 (2007).
82. Hou, J., Renigunta, A., Yang, J. & Waldegger, S. Claudin-4 forms paracellular chloride channel in the kidney and requires claudin-8 for tight junction localization. Proc. Natl. Acad. Sci. U. S. A. **107**, 18010–18015 (2010).
83. Van Itallie, C. M., Fanning, A. S. & Anderson, J. M. Reversal of charge selectivity in cation or anion-selective epithelial lines by expression of different claudins. Am. J. Physiol. - Ren. Physiol.

285, F1078–F1084 (2003).
84. Hou, J., Gomes, A. S., Paul, D. L. & Goodenough, D. A. Study of claudin function by RNA interference. J. Biol. Chem. **281**, 36117–36123 (2006).
85. Van Itallie, C. M., Mitic, L. L. & Anderson, J. M. Claudin-2 forms homodimers and is a component of a high molecular weight protein complex. J. Biol. Chem. **286**, 3442–3450 (2011).
86. Fujita, H., Hamazaki, Y., Noda, Y., Oshima, M. & Minato, N. Claudin-4 Deficiency Results in Urothelial Hyperplasia and Lethal Hydronephrosis. PLoS One **7**, e52272 (2012).
87. Gong, Y. et al. The Cap1-claudin-4 regulatory pathway is important for renal chloride reabsorption and blood pressure regulation. Proc. Natl. Acad. Sci. U. S. A. **111**, E3766–E3774 (2014).
88. Tanaka, M., Kamata, R. & Sakai, R. EphA2 phosphorylates the cytoplasmic tail of claudin-4 and mediates paracellular permeability. J. Biol. Chem. **280**, 42375–42382 (2005).
89. D'Souza, T., Indig, F. E. & Morin, P. J. Phosphorylation of claudin-4 by PKCε regulates tight junction barrier function in ovarian cancer cells. Experimental Cell Research **313**, (Academic Press Inc., 2007).
90. Cong, X. et al. Claudin-4 is required for modulation of paracellular permeability by muscarinic acetylcholine receptor in epithelial cells. J. Cell Sci. **128**, 2271–2286 (2015).
91. Aono, S. & Hirai, Y. Phosphorylation of claudin-4 is required for tight junction formation in a human keratinocyte cell line. Exp. Cell Res. **314**, 3326–3339 (2008).
92. Xu, B. E. et al. WNK1, a novel mammalian serine/threonine protein kinase lacking the catalytic lysine in subdomain II. J. Biol. Chem. **275**, 16795–16801 (2000).
93. O'Reilly, M., Marshall, E., Speirs, H. J. L. & Brown, R. W. WNK1, a gene within a novel blood pressure control pathway, tissue-specifically generates radically different isoforms with and without a kinase domain. J. Am. Soc. Nephrol. **14**, 2447–2456 (2003).
94. Lenertz, L. Y. et al. Properties of WNK1 and implications for other family members. J. Biol. Chem. **280**, 26653–26658 (2005).
95. Xu, B. e. et al. Regulation of WNK1 by an autoinhibitory domain and autophosphorylation. J. Biol. Chem. **277**, 48456–48462 (2002).
96. Subramanya, A. R., Yang, C. L., Zhu, X. & Ellison, D. H. Dominant-negative regulation of WNK1 by its kidney-specific kinase-defective isoform. Am. J. Physiol. - Ren. Physiol. **290**, 619–624 (2006).
97. Wilson, F. H. et al. Human hypertension caused by mutations in WNK kinases. Science (80-.). **293**, 1107–1112 (2001).
98. Terker, A. S. et al. Unique chloride-sensing properties of WNK4 permit the distal nephron to modulate potassium homeostasis. Kidney Int. **89**, 127–134 (2016).
99. Piala, A. T. et al. Chloride sensing by WNK1 involves inhibition of autophosphorylation. Sci. Signal. **7**, ra41 (2014).
100. Ring, A. M. et al. WNK4 regulates activity of the epithelial Na+ channel in vitro and in vivo. Proceedings of the National Academy of Sciences of the United States of America **104**, (2007).
101. Kahle, K. T. et al. WNK4 regulates the balance between renal NaCl reabsorption and K + secretion. Nat. Genet. **35**, 372–376 (2003).
102. Yang, C. L., Angell, J., Mitchell, R. & Ellison, D. H. WNK kinases regulate thiazide-sensitive Na-Cl cotransport. J. Clin. Invest. **111**, 1039–1045 (2003).
103. Romero, M. F., Chen, A. P., Parker, M. D. & Boron, W. F. The SLC4 family of bicarbonate (HCO3-) transporters. Molecular Aspects of Medicine **34**, 159–182 (2013).
104. Passow, H. Molecular aspects of band 3 protein-mediated anion transport across the red blood cell membrane. Reviews of physiology, biochemistry and pharmacology **103**, 61–203 (1986).

105. Fairbanks, G., Steck, T. L. & Wallach, D. F. H. Electrophoretic Analysis of the Major Polypeptides of the Human Erythrocyte Membrane. Biochemistry **10**, 2606–2617 (1971).
106. Tanner, M. J. A., Martin, P. G. & High, S. The complete amino acid sequence of the human erythrocyte membrane anion-transport protein deduced from the cDNA sequence. Biochem. J. **256**, 703–712 (1988).
107. Jennings, M. L. Proton fluxes associated with erythrocyte membrane anion exchange. J. Membr. Biol. **28**, 187–205 (1976).
108. Knauf, P. A. Erythrocyte Anion Exchange and the Band 3 Protein: Transport Kinetics and Molecular Structure. Curr. Top. Membr. Transp. **12**, 249–363 (1979).
109. Jennings, M. L. Transport of H2S and HS- across the human red blood cell membrane: Rapid H2S diffusion and AE1-mediated Cl-/HS- exchange. Am. J. Physiol. - Cell Physiol. **305**, (2013).
110. Grinstein, S., Ship, S. & Rothstein, A. Anion transport in relation to proteolytic dissection of band 3 protein. BBA - Biomembr. **507**, 294–304 (1978).
111. Steck, T. L., Ramos, B. & Strapazon, E. Proteolytic Dissection of Band 3, the Predominant Transmembrane Polypeptide of the Human Erythrocyte Membrane. Biochemistry **15**, 1154–1161 (1976).
112. Arakawa, T. et al. Crystal structure of the anion exchanger domain of human erythrocyte band 3. Science (80-.). **350**, 680–684 (2015).
113. Chang, S. H. & Low, P. S. Identification of a critical ankyrin-binding loop on the cytoplasmic domain of erythrocyte membrane band 3 by crystal structure analysis and site-directed mutagenesis. J. Biol. Chem. **278**, 6879–6884 (2003).
114. Low, P. S. Structure and function of the cytoplasmic domain of band 3: center of erythrocyte membrane-peripheral protein interactions. BBA - Reviews on Biomembranes **864**, 145–167 (1986).
115. Campanella, M. E., Chu, H. & Low, P. S. Assembly and regulation of a glycolytic enzyme complex on the human erythrocyte membrane. Proc. Natl. Acad. Sci. U. S. A. **102**, 2402–2407 (2005).
116. Ercolani, L., Brown, D., Stuart-Tilley, A. & Alper, S. L. Colocalization of GAPDH and band 3 (AE1) proteins in rat erythrocytes and kidney intercalated cell membranes. Am. J. Physiol. - Ren. Fluid Electrolyte Physiol. **262**, (1992).
117. Lux, S. E., John, K. M., Kopito, R. R. & Lodish, H. F. Cloning and characterization of band 3, the human erythrocyte anion-exchange protein (AE1). Proc. Natl. Acad. Sci. U. S. A. **86**, 9089–9093 (1989).
118. Kollert-Jons, A., Wagner, S., Hubner, S., Appelhans, H. & Drenckhahn, D. Anion exchanger 1 in human kidney and oncocytoma differs from erythroid AE1 in its NH2 terminus. Am. J. Physiol. - Ren. Fluid Electrolyte Physiol. **265**, F813–F821 (1993).
119. Cordat, E. & Casey, J. R. Bicarbonate transport in cell physiology and disease. Biochem. J. **417**, 423–439 (2009).
120. Kopito, R. R. & Lodish, H. F. Primary structure and transmembrane orientation of the murine anion exchange protein. Nature **316**, 234–238 (1985).
121. Pasternack, G. R., Anderson, R. A., Leto, T. L. & Marchesi, V. T. Interactions between protein 4.1 and band 3. An alternative binding site for an element of the membrane skeleton. J. Biol. Chem. **260**, 3676–3683 (1985).
122. Rogalski, A. A., Steck, T. L. & Waseem, A. Association of glyceraldehyde-3-phosphate dehydrogenase with the plasma membrane of the intact human red blood cell. J. Biol. Chem. **264**, 6438–6446 (1989).

123. Pries, A. R., Secomb, T. W. & Gaehtgens, P. Biophysical aspects of blood flow in the microvasculature. Cardiovasc. Res. **32**, 654–667 (1996).
124. Sterling, D., Reithmeier, R. A. F. & Casey, J. R. A transport metabolon: Functional interaction of carbonic anhydrase II and chloride/bicarbonate exchangers. J. Biol. Chem. **276**, 47886–47894 (2001).
125. Cordat, E. & Reithmeier, R. A. F. Structure, function, and trafficking of SLC4 and SLC26 anion transporters. Curr. Top. Membr. **73**, 1–67 (2014).
126. Sahr, K. E., Taylor, W. M., Daniels, B. P., Rubin, H. L. & Jarolim, P. The structure and organization of the human erythroid anion exchanger (AE1) gene. Genomics **24**, 491–501 (1994).
127. Eladari, D. & Kumai, Y. Renal acid-base regulation: new insights from animal models. Pflugers Archiv European Journal of Physiology **467**, 1623–1641 (2015).
128. Wu, F. et al. Anion exchanger 1 interacts with nephrin in podocytes. J. Am. Soc. Nephrol. **21**, 1456–1467 (2010).
129. Keskanokwong, T. et al. Interaction of integrin-linked kinase with the kidney chloride/bicarbonate exchanger, kAE1. J. Biol. Chem. **282**, 23205–23218 (2007).
130. Genetet, S., Ripoche, P., Le Van Kim, C., Colin, Y. & Lopez, C. Evidence of a structural and functional ammonium transporter RhBG·anion exchanger 1·ankyrin-G complex in kidney epithelial cells. J. Biol. Chem. **290**, 6925–6936 (2015).
131. Sorrell, S. L., Golder, Z. J., Johnstone, D. B. & Karet Frankl, F. E. Renal peroxiredoxin 6 interacts with anion exchanger 1 and plays a novel role in pH homeostasis. Kidney Int. **89**, 105–112 (2016).
132. Matte, A. et al. Membrane association of peroxiredoxin-2 in red cells is mediated by the N-terminal cytoplasmic domain of band 3. Free Radic. Biol. Med. **55**, 27–35 (2013).
133. Tristan, C., Shahani, N., Sedlak, T. W. & Sawa, A. The diverse functions of GAPDH: Views from different subcellular compartments. Cell. Signal. **23**, 317–323 (2011).
134. Su, Y. et al. Glyceraldehyde 3-phosphate dehydrogenase is required for band 3 (anion exchanger 1) membrane residency in the mammalian kidney. Am. J. Physiol. - Ren. Physiol. **300**, F157-66 (2011).
135. Su, Y. et al. Physical and functional links between anion exchanger-1 and sodium pump. J. Am. Soc. Nephrol. **26**, 400–409 (2015).
136. Sawasdee, N. et al. Human kidney anion exchanger 1 interacts with adaptor-related protein complex 1 μ1A (AP-1 mu1A). Biochem. Biophys. Res. Commun. **401**, 85–91 (2010).
137. Almomani, E. Y. et al. Adaptor protein 1 complexes regulate intracellular trafficking of the kidney anion exchanger 1 in epithelial cells. Am. J. Physiol. - Cell Physiol. **303**, C554-66 (2012).
138. Junking, M. et al. Role of Adaptor Proteins and Clathrin in the Trafficking of Human Kidney Anion Exchanger 1 (kAE1) to the Cell Surface. Traffic **15**, 788–802 (2014).
139. Almomani, E. Y., Touret, N. & Cordat, E. Adaptor protein 1 B mu subunit does not contribute to the recycling of kAE1 protein in polarized renal epithelial cells. Mol. Membr. Biol. **34**, 50–64 (2017).
140. Su, Y. et al. PDLIM5 links kidney anion exchanger 1 (kAE1) to ILK and is required for membrane targeting of kAE1. Sci. Rep. **7**, 39701 (2017).
141. Mohebbi, N. & Wagner, C. A. Pathophysiology, diagnosis and treatment of inherited distal renal tubular acidosis. J. Nephrol. **31**, 511–522 (2018).
142. Cordat, E. & Casey, J. R. Bicarbonate transport in cell physiology and disease. Biochem J **417**, 423–439 (2009).
143. Bruce, L. J. et al. Familial distal renal tubular acidosis is associated with mutations in the red cell anion exchanger (Band 3, AE1) gene. J. Clin. Invest. **100**, 1693–707 (1997).

144. Karet, F. E. et al. Mutations in the chloride-bicarbonate exchanger gene AE1 cause autosomal dominant but not autosomal recessive distal renal tubular acidosis. Proc Natl Acad Sci U S A **95**, 6337–6342 (1998).
145. Jarolim, P. et al. Autosomal dominant distal renal tubular acidosis is associated in three families with heterozygosity for the R589H mutation in the AE1 (band 3) Cl-/HCO3- exchanger. J. Biol. Chem. **273**, 6380–8 (1998).
146. Karet, F. E. et al. Mutations in the gene encoding B1 subunit of H +-ATPase cause renal tubular acidosis with sensorineural deafness. Nat. Genet. **21**, 84–90 (1999).
147. Lewis, S. E., Erickson, R. P., Barnett, L. B., Venta, P. J. & Tashian, R. E. N-ethyl-N-nitrosourea-induced null mutation at the mouse Car-2 locus: an animal model for human carbonic anhydrase II deficiency syndrome. Proc Natl Acad Sci U S A **85**, 1962–1966 (1988).
148. Trepiccione, F. et al. New Findings on the Pathogenesis of Distal Renal Tubular Acidosis. Kidney Dis. (Basel, Switzerland) **3**, 98–105 (2017).
149. Zhang, Z. et al. Identification of Two Novel Mutations in the SLC4A1 Gene in Two Unrelated Chinese Families with Distal Renal Tubular Acidosis. Arch. Med. Res. **43**, 298–304 (2012).
150. Fry, A. C. et al. Mutation conferring apical-targeting motif on AE1 exchanger causes autosomal dominant distal RTA. J. Am. Soc. Nephrol. **23**, 1238–49 (2012).
151. Cordat, E. & Reithmeier, R. A. F. Structure, Function, and Trafficking of SLC4 and SLC26 Anion Transporters. in 1–67 (2014).
152. Park, E. et al. Genotype–Phenotype Analysis in Pediatric Patients with Distal Renal Tubular Acidosis. Kidney Blood Press. Res. **43**, 513–521 (2018).
153. Devonald, M. A. J., Smith, A. N., Poon, J. P., Ihrke, G. & Karet, F. E. Non-polarized targeting of AE1 causes autosomal dominant distal renal tubular acidosis. Nat. Genet. **33**, 125–127 (2003).
154. Toye, A. M., Banting, G. & Tanner, M. J. A. Regions of human kidney anion exchanger 1 (kAE1) required for basolateral targeting of kAE1 in polarised kidney cells: mis-targeting explains dominant renal tubular acidosis (dRTA). J. Cell Sci. **117**, 1399–410 (2004).
155. Cordat, E. et al. Dominant and recessive distal renal tubular acidosis mutations of kidney anion exchanger 1 induce distinct trafficking defects in MDCK cells. Traffic **7**, 117–128 (2006).
156. Mumtaz, R. et al. Intercalated Cell Depletion and Vacuolar H+-ATPase Mistargeting in an Ae1 R607H Knockin Model. J. Am. Soc. Nephrol. **28**, 1507–1520 (2017).
157. Merkulova, M. et al. Mapping the H (V)-ATPase interactome: identification of proteins involved in trafficking, folding, assembly and phosphorylation. Sci. Rep. **5**, 14827 (2015).
158. Merkulova, M. et al. Targeted Deletion of the Ncoa7 Gene Results in Incomplete Distal Renal Tubular Acidosis in Mice. Am. J. Physiol. Physiol. (2018).
159. Laing, C. M., Toye, A. M., Capasso, G. & Unwin, R. J. Renal tubular acidosis: developments in our understanding of the molecular basis. Int J Biochem Cell Biol **37**, 1151–1161 (2005).
160. Ring, T., Frische, S. & Nielsen, S. Clinical review: Renal tubular acidosis–a physicochemical approach. Crit. Care **9**, 573 (2005).
161. Krishnan, D. et al. Deficiency of Carbonic anhydrase II results in a urinary concentrating defect. Front. Physiol. **8**, 1108 (2018).
162. Wilson, F. H. et al. Human hypertension caused by mutations in WNK kinases. Science (80-.). **293**, 1107–1112 (2001).
163. Uawithya, P., Pisitkun, T., Ruttenberg, B. E. & Knepper, M. A. Transcriptional profiling of native inner medullary collecting duct cells from rat kidney. Physiol. Genomics **32**, 229–53 (2008).
164. Webb, T. N. et al. Cell-specific regulation of L-WNK1 by dietary K. Am. J. Physiol. Renal Physiol. **310**, F26 (2016).

165. Terker, A. S. et al. Unique chloride-sensing properties of WNK4 permit the distal nephron to modulate potassium homeostasis. Kidney Int. **89**, 127–134 (2016).
166. Ring, A. M. et al. An SGK1 site in WNK4 regulates Na channel and K channel activity and has implications for aldosterone signaling and K homeostasis. Proc. Natl. Acad. Sci. **104**, 4025–4029 (2007).
167. Boyden, L. M. et al. Mutations in kelch-like 3 and cullin 3 cause hypertension and electrolyte abnormalities. Nature **482**, 98–102 (2012).
168. Louis-Dit-Picard, H. et al. KLHL3 mutations cause familial hyperkalemic hypertension by impairing ion transport in the distal nephron. Nat. Genet. **44**, 456–460 (2012).
169. Gong, Y. et al. KLHL3 regulates paracellular chloride transport in the kidney by ubiquitination of claudin-8. Proc. Natl. Acad. Sci. **112**, 4340–4345 (2015).
170. Sohara, E. & Uchida, S. Kelch-like 3/Cullin 3 ubiquitin ligase complex and WNK signaling in salt-sensitive hypertension and electrolyte disorder. Nephrol. Dial. Transplant. **31**, 1417–1424 (2016).
171. Hou, J., Renigunta, A., Yang, J. & Waldegger, S. Claudin-4 forms paracellular chloride channel in the kidney and requires claudin-8 for tight junction localization. Proc. Natl. Acad. Sci. U. S. A. **107**, 18010–5 (2010).
172. Susa, K. et al. Impaired degradation of WNK1 and WNK4 kinases causes PHAII in mutant KLHL3 knock-in mice. Hum. Mol. Genet. **23**, 5052–5060 (2014).
173. Hadj-Rabia, S. et al. Claudin-1 gene mutations in neonatal sclerosing cholangitis associated with ichthyosis: A tight junction disease. Gastroenterology **127**, 1386–1390 (2004).
174. Wilcox, E. R. et al. Mutations in the gene encoding tight junction claudin-14 cause autosomal recessive deafness DFNB29. Cell **104**, 165–172 (2001).
175. Thorleifsson, G. et al. Sequence variants in the CLDN14 gene associate with kidney stones and bone mineral density. Nat. Genet. **41**, 926–30 (2009).
176. Simon, D. B. et al. Paracellin-1, a renal tight junction protein required for paracellular Mg2+ resorption. Science (80-.). **285**, 103–106 (1999).
177. Konrad, M. et al. Mutations in the tight-junction gene claudin 19 (CLDN19) are associated with renal magnesium wasting, renal failure, and severe ocular involvement. Am. J. Hum. Genet. **79**, 949–957 (2006).
178. Bürgel, N. et al. Mechanisms of diarrhea in collagenous colitis. Gastroenterology **123**, 433–443 (2002).
179. Oshima, T., Miwa, H. & Joh, T. Changes in the expression of claudins in active ulcerative colitis. in Journal of Gastroenterology and Hepatology (Australia) **23**, (2008).
180. Lanigan, F. et al. Increased claudin-4 expression is associated with poor prognosis and high tumour grade in breast cancer. Int. J. Cancer **124**, 2088–2097 (2009).
181. Satake, S. et al. Cdx2 transcription factor regulates claudin-3 and claudin-4 expression during intestinal differentiation of gastric carcinoma. Pathol. Int. **58**, 156–163 (2008).
182. Szabó, I., Kiss, A., Schaff, Z. & Sobel, G. Claudins as diagnostic and prognostic markers in gynecological cancer. Histology and Histopathology **24**, 1607–1615 (2009).
183. Boireau, S. et al. DNA-methylation-dependent alterations of claudin-4 expression in human bladder carcinoma. Carcinogenesis **28**, 246–258 (2007).
184. Karanjawala, Z. E. et al. New markers of pancreatic cancer identified through differential gene expression analyses: Claudin 18 and annexin A8. Am. J. Surg. Pathol. **32**, 188–196 (2008).
185. Tzelepi, V. N., Tsamandas, A. C., Vlotinou, H. D., Vagianos, C. E. & Scopa, C. D. Tight junctions in thyroid carcinogenesis: Diverse expression of claudin-1, claudin-4, claudin-7 and occludin in

thyroid neoplasms. Mod. Pathol. **21**, 22–30 (2008).
186. Borovac, J. et al. Claudin-4 forms a paracellular barrier, revealing the interdependence of claudin expression in the loose epithelial cell culture model opossum kidney cells. Am. J. Physiol. - Cell Physiol. **303**, C1278-91 (2012).
187. Kimizuka, H. & Koketsu, K. Ion transport through cell membrane. J. Theor. Biol. **6**, 290–305 (1964).
188. Cordat, E. & Reithmeier, R. A. F. Structure, function, and trafficking of SLC4 and SLC26 anion transporters. Curr. Top. Membr. **73**, 1–67 (2014).
189. Vince, J. W. & Reithmeier, R. A. F. Carbonic anhydrase II binds to the carboxyl terminus of human band 3, the erythrocyte Cl-/HCO3/- exchanger. J. Biol. Chem. **273**, 28430–28437 (1998).
190. Cordat, E., Li, J. & Reithmeier, R. A. F. Carboxyl-terminal truncations of human anion exchanger impair its trafficking to the plasma membrane. Traffic **4**, 642–651 (2003).
191. Sebastian, A., McSherry, E. & Morris, R. C. Impaired renal conservation of sodium and chloride during sustained correction of systemic acidosis in patients with type 1, classic renal tubular acidosis. J. Clin. Invest. **58**, 454–469 (1976).
192. Quilty, J. A., Cordat, E. & Reithmeier, R. A. F. Impaired trafficking of human kidney anion exchanger (kAE1) caused by hetero-oligomer formation with a truncated mutant associated with distal renal tubular acidosis. Biochem. J. **368**, 895–903 (2002).
193. Ungsupravate, D. et al. Impaired trafficking and intracellular retention of mutant kidney anion exchanger 1 proteins (G701D and A858D) associated with distal renal tubular acidosis. Mol. Membr. Biol. **27**, 92–103 (2010).
194. Toye, A. M., Banting, G. & Tanner, M. J. A. Regions of human kidney anion exchanger 1 (kAE1) required for basolateral targeting of kAE1 in polarized kidney cells: Mis-targeting explains dominant renal tubular acidosis (dRTA). J. Cell Sci. **117**, 1399–1410 (2004).
195. Rungroj, N. et al. A Novel Missense Mutation in AE1 Causing Autosomal Dominant Distal Renal Tubular Acidosis Retains Normal Transport Function but Is Mistargeted in Polarized Epithelial Cells. J. Biol. Chem. **279**, 13833–13838 (2004).
196. Kittanakom, S., Cordat, E., Akkarapatumwong, V., Yenchitsomanus, P. T. & Reithmeier, R. A. F. Trafficking defects of a novel autosomal recessive distal renal tubular acidosis mutant (S773P) of the human kidney anion exchanger (kAE1). J. Biol. Chem. **279**, 40960–40971 (2004).
197. Cordat, E. et al. Dominant and recessive distal renal tubular acidosis mutations of kidney anion exchanger induce distinct trafficking defects in MDCK cells. Traffic **7**, 117–128 (2006).
198. Vichot, A. A. et al. Loss of kAE1 expression in collecting ducts of end-stage kidneys from a family with SLC4A1 G609R-associated distal renal tubular acidosis. Clin. Kidney J. **10**, 135–140 (2017).
199. Mumtaz, R. et al. Intercalated Cell Depletion and Vacuolar H+-ATPase Mistargeting in an Ae1 R607H Knockin Model. J. Am. Soc. Nephrol. **28**, 1507–1520 (2017).
200. Chu, C. et al. Band 3 Edmonton I, a novel mutant of the anion exchanger 1 causing spherocytosis and distal renal tubular acidosis. Biochem. J. **426**, 379–388 (2010).
201. Cordat, E. & Casey, J. R. Bicarbonate transport in cell physiology and disease. Biochem. J. **417**, 423–439 (2009).
202. Jennings, M. L. & Smith, J. S. Anion-proton cotransport through the human red blood cell band 3 protein. Role of glutamate 681. J. Biol. Chem. **267**, 13964–13971 (1992).
203. Chernova, M. N. et al. Electrogenic sulfate/chloride exchange in Xenopus oocytes mediated by murine AE1 E699Q. J. Gen. Physiol. **109**, 345–360 (1997).
204. Sonoda, N. et al. Clostridium perfringens enterotoxin fragment removes specific claudins from tight junction strands: Evidence for direct involvement of claudins in tight junction barrier. J. Cell

Biol. **147**, 195–204 (1999).
205. Gong, Y. et al. The Cap1-claudin-4 regulatory pathway is important for renal chloride reabsorption and blood pressure regulation. Proc. Natl. Acad. Sci. U. S. A. **111**, E3766–E3774 (2014).
206. Popov, M. & Reithmeier, R. A. F. Calnexin interaction with N-glycosylation mutants of a polytopic membrane glycoprotein, the human erythrocyte anion exchanger 1 (band 3). J. Biol. Chem. **274**, 17635–17642 (1999).
207. Hou, J., Renigunta, A., Yang, J. & Waldegger, S. Claudin-4 forms paracellular chloride channel in the kidney and requires claudin-8 for tight junction localization. Proc. Natl. Acad. Sci. U. S. A. **107**, 18010–18015 (2010).
208. Lanaspa, M. A., Andres-Hernando, A., Rivard, C. J., Dai, Y. & Berl, T. Hypertonic stress increases claudin-4 expression and tight junction integrity in association with MUPP1 in IMCD3 cells. Proc. Natl. Acad. Sci. U. S. A. **105**, 15797–15802 (2008).
209. Kiuchi-Saishin, Y. et al. Differential expression patterns of claudins, tight junction membrane proteins, in mouse nephron segments. J. Am. Soc. Nephrol. **13**, 875–886 (2002).
210. Fujita, H., Hamazaki, Y., Noda, Y., Oshima, M. & Minato, N. Claudin-4 Deficiency Results in Urothelial Hyperplasia and Lethal Hydronephrosis. PLoS One **7**, e52272 (2012).
211. Conner, S. D. & Schmid, S. L. Regulated portals of entry into the cell. Nature **422**, 37–44 (2003).
212. Le Moellic, C. et al. Aldosterone and tight junctions: Modulation of claudin-4 phosphorylation in renal collecting duct cells. Am. J. Physiol. - Cell Physiol. **289**, C1513-21 (2005).
213. Gong, Y. et al. KLHL3 regulates paracellular chloride transport in the kidney by ubiquitination of claudin-8. Proc. Natl. Acad. Sci. U. S. A. **112**, 4340–4345 (2015).
214. Hou, J. et al. Claudin-16 and claudin-19 interact and form a cation-selective tight junction complex. J. Clin. Invest. **118**, 619–628 (2008).
215. Hou, J. et al. Claudin-16 and claudin-19 interaction is required for their assembly into tight junctions and for renal reabsorption of magnesium. Proc. Natl. Acad. Sci. U. S. A. **106**, 15350–15355 (2009).
216. Inai, T., Sengoku, A., Hirose, E., Iida, H. & Shibata, Y. Claudin-7 expressed on lateral membrane of rat epididymal epithelium does not form aberrant tight junction strands. Anat. Rec. **290**, 1431–1438 (2007).
217. Westmoreland, J. J. et al. Dynamic distribution of claudin proteins in pancreatic epithelia undergoing morphogenesis or neoplastic transformation. Dev. Dyn. **241**, 583–594 (2012).
218. Pasternak, J. A., Kent-Dennis, C., Van Kessel, A. G. & Wilson, H. L. Claudin-4 undergoes age-dependent change in cellular localization on pig jejunal villous epithelial cells, independent of bacterial colonization. Mediators Inflamm. **2015**, 263629 (2015).
219. Cordat, E., Li, J. & Reithmeier, R. A. F. Carboxyl-terminal truncations of human anion exchanger impair its trafficking to the plasma membrane. Traffic **4**, 642–651 (2003).
220. Satchwell, T. J., Hawley, B. R., Bell, A. J., Leticia Ribeiro, M. & Toye, A. M. The cytoskeletal binding domain of band 3 is required for multiprotein complex formation and retention during erythropoiesis. Haematologica **100**, 133–142 (2015).
221. Angelow, S., Kim, K. J. & Yu, A. S. L. Claudin-8 modulates paracellular permeability to acidic and basic ions in MDCK II cells. J. Physiol. **571**, 15–26 (2006).
222. Gueutin, V. et al. Renal β-intercalated cells maintain body fuid and electrolyte balance. J. Clin. Invest. **123**, 4219–4231 (2013).
223. Mineta, K. et al. Predicted expansion of the claudin multigene family. FEBS Lett. **585**, 606–612 (2011).
224. Wu, J., Helftenbein, G., Koslowski, M., Sahin, U. & Tureci, Ö. Identification of New claudin

family members by a novel PSI-BLAST based approach with enhanced specificity. Proteins Struct. Funct. Genet. **65**, 808–815 (2006).
225. Kiuchi-Saishin, Y. et al. Differential expression patterns of claudins, tight junction membrane proteins, in mouse nephron segments. Journal of the American Society of Nephrology **13**, 875–886 (2002).
226. Lashhab, R. et al. The kidney anion exchanger 1 affects tight junction properties via claudin-4. Sci. Rep. **9**, 3099 (2019).
227. Wilson, F. H. et al. Human hypertension caused by mutations in WNK kinases. Science **293**, (2001).
228. Alessi, D. R. et al. The WNK-SPAK/OSR1 pathway: Master regulator of cation-chloride cotransporters. Science Signaling (2014).
229. Yang, C.-L., Zhu, X., Wang, Z., Subramanya, A. R. & Ellison, D. H. Mechanisms of WNK1 and WNK4 interaction in the regulation of thiazide-sensitive NaCl cotransport. J. Clin. Invest. **115**, 1379–1387 (2005).
230. Ohta, A. et al. Overexpression of human WNK1 increases paracellular chloride permeability and phosphorylation of claudin-4 in MDCKII cells. Biochem. Biophys. Res. Commun. **349**, 804–808 (2006).
231. Kahle, K. T. et al. Paracellular Cl- permeability is regulated by WNK4 kinase: Insight into normal physiology and hypertension. Proc. Natl. Acad. Sci. U. S. A. **101**, 14877–14882 (2004).
232. Lee, B. S., Lasanthi, G. D., Jayathilaka, P., Huang, J. S. & Gupta, S. Immobilized metal affinity electrophoresis: A novel method of capturing phosphoproteins by electrophoresis. J. Biomol. Tech. **19**, 106–108 (2008).
233. Chen, J. C. et al. WNK4 kinase is a physiological intracellular chloride sensor. Proc. Natl. Acad. Sci. U. S. A. **116**, 4502–4507 (2019).
234. Yamada, K. et al. Small-molecule WNK inhibition regulates cardiovascular and renal function. Nat. Chem. Biol. **12**, 896–898 (2016).
235. Bruce, L. J. et al. Familial distal renal tubular acidosis is associated with mutations in the red cell anion exchanger (band 3, AE1) gene. J. Clin. Invest. **100**, 1693–1707 (1997).
236. Bertocchio, J. P. et al. Red Blood Cell AE1/Band 3 Transports in Dominant Distal Renal Tubular Acidosis Patients. Kidney Int. Reports **5**, 348–357 (2020).
237. Van Itallie, C. M. et al. Phosphorylation of claudin-2 on serine 208 promotes membrane retention and reduces trafficking to lysosomes. J. Cell Sci. **125**, 4902–4912 (2012).
238. Sassi, A. et al. Interaction between epithelial sodium channel γ-subunit and claudin-8 modulates paracellular sodium permeability in renal collecting duct. J. Am. Soc. Nephrol. **31**, 1009–1023 (2020).
239. Pedersen, S. F., King, S. A., Nygaard, E. B., Rigor, R. R. & Cala, P. M. NHE1 Inhibition by Amiloride- and Benzoylguanidine-type Compounds: INHIBITOR BINDING LOCI DEDUCED FROM CHIMERAS OF NHE1 HOMOLOGUES WITH ENDOGENOUS DIFFERENCES IN INHIBITOR SENSITIVITY. J. Biol. Chem. **282**, 19716–19727 (2007).
240. Tanos, B. E. et al. IQGAP1 controls tight junction formation through differential regulation of claudin recruitment. J. Cell Sci. **128**, 853–862 (2015).
241. Gaush, C. R., Hard, W. L., Smith, T. F. & Read, W. O. Characterization of an Established Line of Canine Kidney Cells (MDCK). Proc. Soc. Exp. Biol. Med. **122**, 931–935 (1966).
242. Lanaspa, M. A., Andres-Hernando, A., Rivard, C. J., Dai, Y. & Berl, T. Hypertonic stress increases claudin-4 expression and tight junction integrity in association with MUPP1 in IMCD3 cells. Proc. Natl. Acad. Sci. U. S. A. **105**, 15797–15802 (2008).

243. Chambrey, R. et al. Renal intercalated cells are rather energized by a proton than a sodium pump. Proc. Natl. Acad. Sci. U. S. A. **110**, 7928–7933 (2013).
244. Andersen, O. S., Silveira, J. E. N. & Steinmetz, P. R. Intrinsic characteristics of the proton pump in the luminal membrane of a tight urinary epithelium: The relation between transport rate and ΔμH. J. Gen. Physiol. **86**, 215–234 (1985).

Appendices

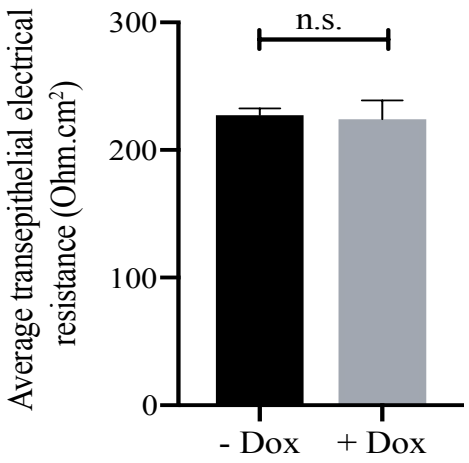

Supplementary Figure 1: Doxycycline incubation does not alter transepithelial electrical resistance.

Non-infected polarized mIMCD3 cells were kept un-induced or induced for 24 hours with doxycycline and Ussing chamber experiments were performed as described in the Methods section. Error bars correspond to means ± SEM, n=3-4, there was no significant (n.s.) difference between - Dox and + Dox conditions.

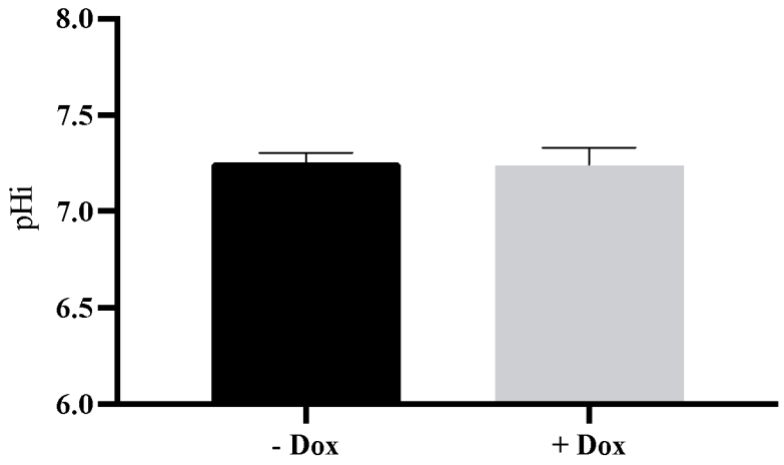

Supplementary Figure 2: kAE1 E681Q expression does not alter cytosolic pH.

Initial cytosolic pH was measured for the 20 seconds before switching from a Cl^--containing to a Cl^--free Ringer's perfusion solution in mIMCD3 kAE1 cells kept un-induced or induced for 24 hours with doxycycline. Error bars correspond to means ± SEM, n=3-7.

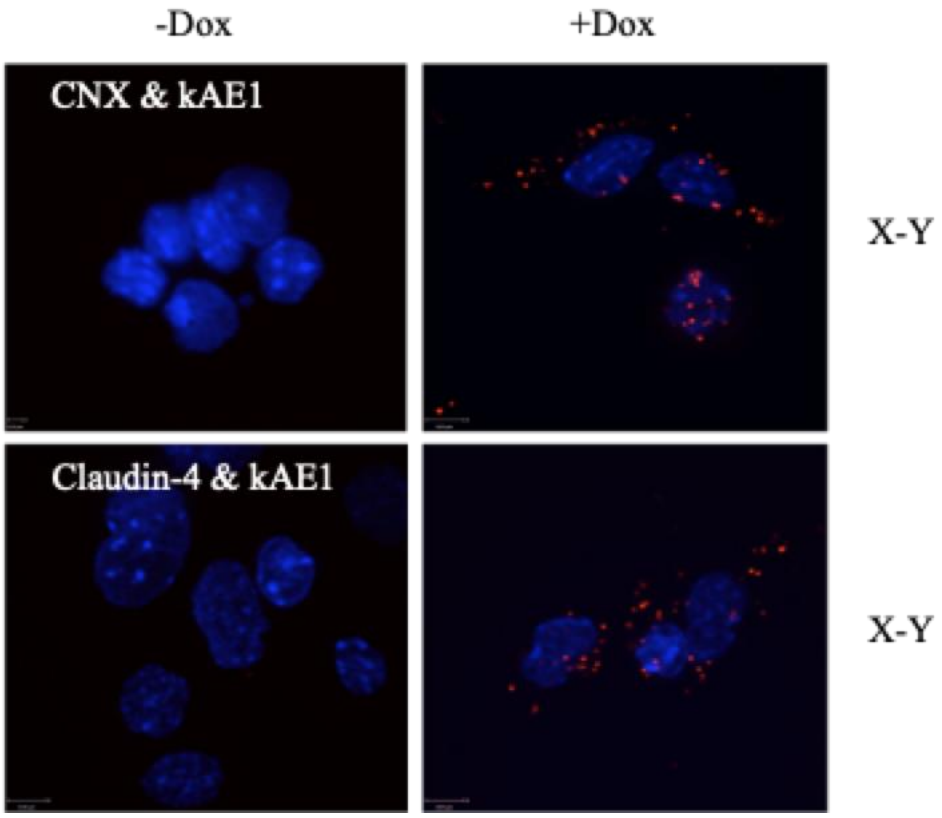

Supplementary Figure 3: kAE1 is in close proximity with claudin-4 in non-polarized mIMCD3 cells.

Proximity ligation assay was performed on non-polarized mIMCD3 cells stably expressing kAE1 grown on coverslips. CNX, corresponding to calnexin, was used as a positive control[194]. Cells were examined under a confocal microscope using a 63 X objective and top views (X-Y) are shown. Red signal indicates that the 2 proteins labeled are within 30 to 40 nm of distance from each other in non-polarized mIMCD3 cells. Nuclear staining is shown in blue as DAPI staining.